

Electronics and Computer Science
Faculty of Engineering and Physical Sciences
University of Southampton

Jonah Foley
August 24, 2024

**Implementation, Evaluation and Simulation of OFDM for
Dual-Mode Index Modulated Systems in Multi-Path Fading
Channels**

Project supervisor: Professor Sheng Chen
Second examiner: Professor Kees De Groot

A project report submitted for the award of
MEng Electronic Engineering

Abstract

A rigorous treatment of orthogonal-frequency-division-multiplexing (OFDM) is presented, based on an analysis of the wireless channel derived from first principles. We show its ability to combat inter-symbol-interference at a detection complexity and bandwidth lower than that of single-carrier systems. Performance metrics such as bit-error-rate and peak-to-average-power-ratio (PAPR) are quantified via MATLAB simulation, demonstrating the PAPR problem which restricts the feasibility of OFDM on the uplink. To resolve this problem we present a theory of frequency-domain index-modulation (IM), a novel transmission scheme which assigns each OFDM subcarrier into one of two modes, active or inactive, enabling implicit transmission of information in terms of the subcarrier activity. By setting a subset of the available subcarriers to inactive we can show that the PAPR is reduced, with the IM scheme mitigating the throughput losses incurred through an underutilisation of the available subcarriers. For each IM scheme investigated, we present an LLR detection strategy which achieves near maximum-likelihood (ML) performance, at a considerably lower complexity. We then investigate how the techniques of IM-OFDM can be applied to the state-of-the-art dual-mode (DM) OFDM, which utilises two constellation modes to enhance throughput beyond that of conventional OFDM.

Statement of Originality

- I have read and understood the [ECS Academic Integrity](#) information and the University's [Academic Integrity Guidance for Students](#).
- I am aware that failure to act in accordance with the [Regulations Governing Academic Integrity](#) may lead to the imposition of penalties which, for the most serious cases, may include termination of programme.
- I consent to the University copying and distributing any or all of my work in any form and using third parties (who may be based outside the EU/EEA) to verify whether my work contains plagiarised material, and for quality assurance purposes.

I have acknowledged all sources, and identified any content taken from elsewhere.

I have not used any resources produced by anyone else.

I did all the work myself, or with my allocated group, and have not helped anyone else.

The material in the report is genuine, and I have included all my data/code/designs.

I have not submitted any part of this work for another assessment.

My work did not involve human participants, their cells or data, or animals.

Acknowledgements

Thank you to my supervisor, Professor Sheng Chen, for being attentive to my every question along the way and encouraging me to pursue challenging ideas.

Thank you to my parents who have continuously supported my academic journey and enabled me to pursue my interests.

Contents

1	Introduction	6
1.1	Overview of Technologies	6
1.2	Approach	7
2	SISO Channels	10
2.1	Outdoor SISO Wireless Channel Modelling	10
2.1.1	Single Path Propagation with Fixed Antennas	10
2.1.2	Single Path Propagation with a Moving Antenna	11
2.1.3	Two-path Propagation with Fixed Antennas	11
2.1.4	Two-path Propagation with a Moving Antenna	13
2.1.5	Deriving a Channel Model	13
2.2	Channel Characterisation	16
2.2.1	Doppler Spread & Coherence Time	16
2.2.2	Delay Spread & Coherence Bandwidth	16
2.3	A Statistical Channel Model	17
3	Multi-Carrier Modulation	19
3.1	Principles of Multi Carrier Modulation	20
3.1.1	Multi-Carrier Modulation with Non-overlapping Subchannels .	21
3.1.2	Multi-carrier Modulation With Overlapping Subchannels .	22
3.1.3	Multi-carrier Detection With Overlapping Subchannels .	24
3.2	Multi-Carrier Modulation Using the FFT	24
3.2.1	OFDM Modulation	25
3.2.2	OFDM Demodulation	27
3.3	Performance of OFDM	27
3.3.1	Bit Error Rate	27
3.3.2	Peak to Average Power Ratio	28
4	Index Modulation Aided OFDM	31
4.1	Single Mode Index Modulation	31
4.1.1	GSIM-OFDM (IM-OFDM)	32
4.1.1.1	Modulation	32

4.1.1.2	Detection	33
4.1.1.3	Performance	34
4.1.2	EGSIM-OFDM	40
4.1.2.1	Modulation	40
4.1.2.2	Detection	42
4.1.2.3	Performance	43
4.2	Multi Mode Index Modulation	45
4.2.1	DM-OFDM	45
4.2.1.1	Modulation	46
4.2.1.2	Detection	48
4.2.1.3	Performance	49
5	Conclusions	53
5.1	Review of Findings	53
5.2	Future Work	54
A	Baseband Discrete-in-time Channel Input-Output Relationship	62
B	Derivation of the Distribution of the Channel Path Gain	66
C	Matrix Representation of OFDM	68
D	OFDM PAPR Derivation	71
E	GSIM-OFDM LLR Closed Form Derivation	74
F	GSIM-OFDM Subcarrier Mapping Policy	77
G	LLR Error Correction Algorithm	79
H	EGSIM-OFDM Subcarrier Mapping Policy	81
I	Single Mode IM-OFDM Complexity Comparison	84
J	DM-OFDM LLR Closed Form Derivation	85
K	Complexity Analysis	87
L	Project Directory Structure	89
M	Risk Assessment & Project Brief	91

1 | Introduction

1.1 Overview of Technologies

Due to the ever increasing demand of higher data-rate wireless communications, multicarrier modulation schemes such as orthogonal-frequency-division-multiplexing (OFDM) have pervaded past and upcoming wireless standards such as; 802.11a/g [1], WiMAX [2], Long Term Evolution (LTE) [3] and now 5G [4]. Multi-carrier modulation schemes offer an approach to wireless transmission which is resilient to frequency-selective fading by subdividing the channel into a set of subchannels, each which experience relatively flat fading, permitting one-tap equalisation at the receiver. This has a considerably lower complexity than the multi-tap FIR filters typically used in single-carrier equalisation schemes [5] enabling use of higher order constellations, and thus data rates. While OFDM was initially conceived in the 1960s [6], its wide-spread adoption arose as a result of an efficient digital implementation using the fast-fourier-transform (FFT) [7, 8], and the advent of low cost digital signal processors with sufficiently low delay for real time use.

Despite its advantages, OFDM presents multiple challenges in its implementation. The primary challenge which this report will investigate is its high peak-to-average-power-ratio (PAPR), the effects of which will be considered in section 3.3. A host of PAPR reduction techniques have been proposed in the existing literature [9], however this project will focus on an algorithm-level approach called index modulation (IM).

Index modulation is a general philosophy which can be applied to systems which have an enumerable physical quantity. For example, multi-input-multiple-output systems which utilise multiple transmit and receive antennas can implement spatial-domain IM (SD-IM) [10, 11] by enumerating the set of antennas, while OFDM naturally facilitates enumeration of the subcarrier indices leading to frequency-domain IM (FD-IM or IM-OFDM). Consistent to all approaches is that each element of the enumerated resource is assigned to a separate mode, such as active or inactive, which enables us to implicitly convey information by encoding message data into the activation pattern. We may therefore tackle the PAPR problem of OFDM by transmitting data

on a subset of the available subcarriers while transmitting a zero amplitude signal on the remaining and employing IM to mitigate the throughput losses.

However, as the size of the constellation alphabet increases, the capability of the index bits to make up for the throughput loss incurred using index modulation is decreased. This limitation of single-mode IM-OFDM will therefore motivate our investigation into dual-mode (DM) index-modulation which attempts to apply the techniques learned from single mode IM-OFDM to a system in which *all* subcarriers are active and instead distinguished by which constellation their symbol belongs to. This increases throughput beyond that of conventional OFDM, regardless of constellation size, at the cost of PAPR.

To conclude this chapter we will set out our approach to developing and comparing simulations. In chapter 2 we shall use ray-tracing analysis to derive baseband discrete-in-time model of the channel favourable for simulation purposes. Chapter 3 will motivate the use of multi-carrier modulation and then show how it can be efficiently implemented in the discrete-time domain using the FFT. We shall then draw conclusions about OFDM, quantifying the BER performance and demonstrating the PAPR issue using analytical and statistical methods. Chapter 4 will develop a theory of index-modulation starting with single mode schemes and then moving onto dual-mode schemes, each of which will see a rigorous performance analysis. Finally, chapter 5 will summarise our findings and present directions for future work. Supplementary materials are found in appendices A-K with a risk assessment found in Appendix M.

1.2 Approach

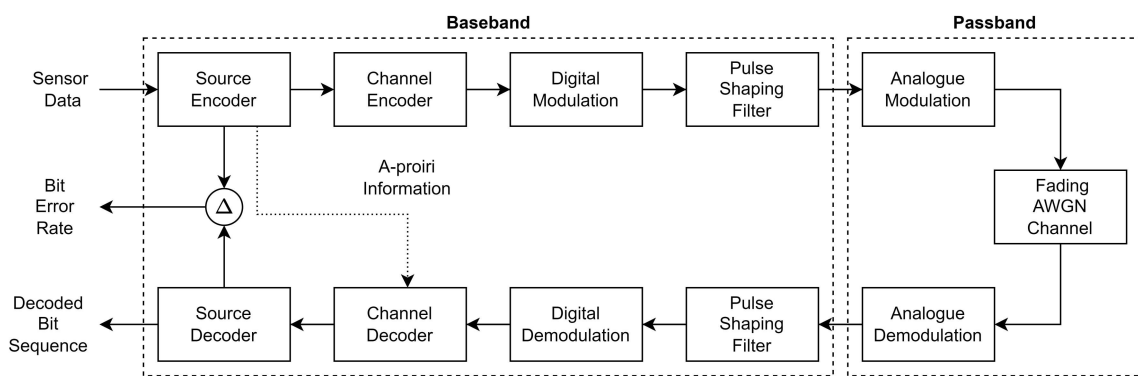


Figure 1.1: Block diagram of the shannonian transceiver, recreated from [12]

Figure 1.1 shows the block diagram of the shannonian transceiver which represents digital communication at a high level. This project will consider only the role of the digital modulator/demodulator. In order to do so we make the following assumptions; (1) the bit stream input to the modulator is uniformly distributed, (2) passband

effects such as frequency/phase offset, carrier/clock recovery and doppler shift will not be considered, and, (3) the channel impulse response will be known at the receiver. In doing so, we will be able to analyse the performance contribution of solely the modulator/demodulator pair, where our algorithms will be implemented.

The approach taken will be to develop a model of the transmission scheme under test in MATLAB and use Monte-Carlo methods to obtain numerical results which quantify the performance of the system. A state machine representation of the approach is shown in Figure 1.2. By repeating this loop until a minimum number of bit errors has been reached, we can then measure the bit error rate at a given bit-power-to-noise-power-ratio (E_b/N_0) as

$$\text{BER} = \frac{\text{Minimum Number of Bit Errors}}{\text{Number of Bits Transmitted}} \quad (1.1)$$

This process will be repeated for each value of the E_b/N_0 over the range of 0 to 30dB, which will enable us to make deductions about the transmission schemes performance over a range of channel conditions.

Aside from BER metrics, we will need to measure quantities such as PAPR, spectral efficiency and complexity. Spectral efficiency is a measure of the bits per OFDM subcarrier - a quantity that can be calculated directly with an equation. Complexity will be measured as a function of the number of complex multiplications, represented using 'big-O' notation. PAPR is a statistical quantity since it varies depending on the data being modulated. Therefore, the standard approach is to plot the complementary cumulative distribution function (CCDF) of the PAPR which plots the probability that the PAPR is greater than a certain threshold, for each value of the threshold.

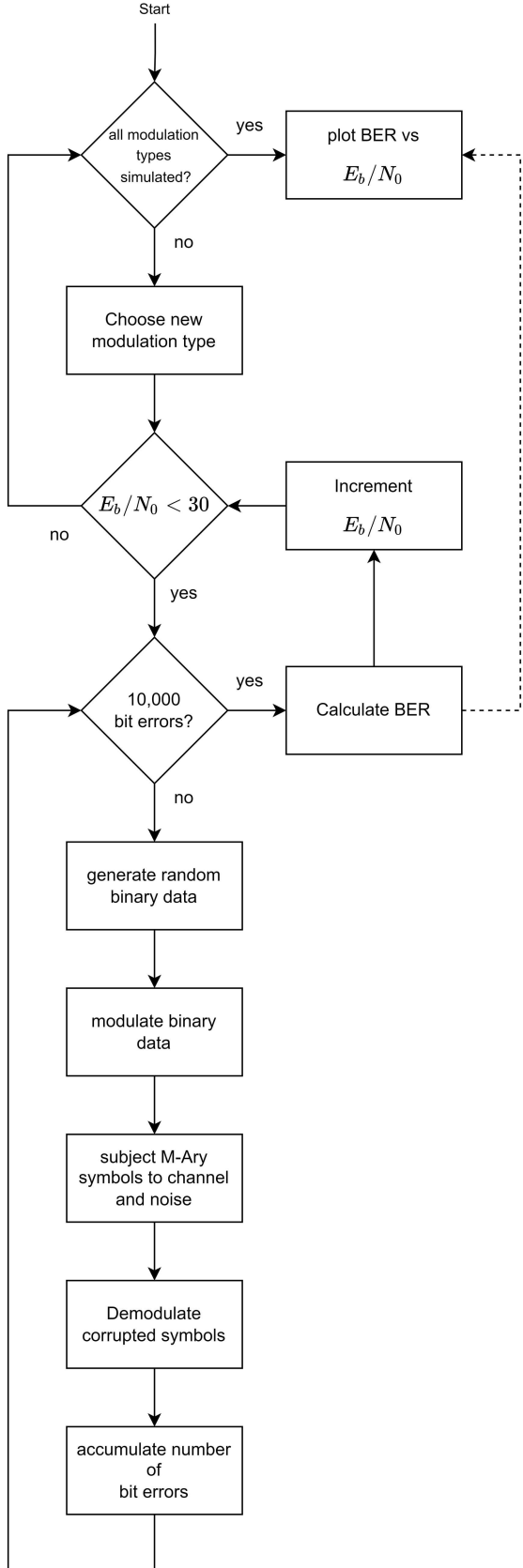


Figure 1.2: Generic state machine for simulating the BER of a modulation scheme using Monte-Carlo methods

2 | SISO Channels

2.1 Outdoor SISO Wireless Channel Modelling

Our first goal is to build and justify a wireless channel model which we can subject our transmission schemes to in order to simulate the effect of wireless transmission. When transmitting a signal in a busy urban environment there are many factors which degrade signal quality such as propagation path-loss, reflection, diffraction and scattering. These effects generate reflected copies of the transmitted signal, leading to multi-path propagation [13].

As a result of this multi-path propagation, the receive antenna is excited by the superposition of multiple copies of the transmitted symbol, each from a path of differing length. Due to the differing path lengths, each copy of the received signal will arrive with a different amplitude and phase. In the worse case, the received copies of the transmitted signal destructively cancel out leading to incorrect demodulation, and ultimately bit errors. This is unless we can develop an approach for 'undoing' the effect of fading, which may be possible provided we can model the effect of the channel on our signal with sufficient accuracy. Such a model will now be developed following a treatment laid out in [14].

2.1.1 Single Path Propagation with Fixed Antennas

If we consider a single stationary antenna transmitting a signal $\cos(2\pi ft)$ into the far-field region, the electric field at any point, in the direction of signal transmission is given by

$$E(f, t, (r, \phi, \gamma)) = \frac{\alpha_s(\phi, \gamma, s) \cos(2\pi f(t - r/c))}{r} \quad (2.1)$$

where, (r, ϕ, γ) is a position in space, \mathbf{u} , which is displacement r from the receive antenna at vertical and horizontal angles (ϕ, γ) to \mathbf{u} . $\alpha_s(\phi, \gamma, s)$ is the radiation pattern of the transmit antenna transmitting at the carrier frequency, f , and angle (ϕ, γ) . The phase at \mathbf{u} is offset r/c as a result of the time it takes an EM wave at the speed of light to travel a distance, r . Now introducing a receive antenna at the point

$\mathbf{u} = (r, \theta, \gamma)$, we may write the received signal's electric field as

$$E_r(f, t, \mathbf{u}) = \frac{\alpha(\theta, \gamma, f) \cos(2\pi f(t - r/c))}{r} \quad (2.2)$$

with $\alpha(\theta, \gamma, f)$ being the sum of the radiation patterns of the transmit and receive antennas.

2.1.2 Single Path Propagation with a Moving Antenna

A common scenario is the presence of movement of one of the antennas, such as a mobile phone's antenna as a car moves along the road. To consider such a scenario we assume that the receive antenna location varies with time, t as $\mathbf{u}(t) = (r(t), \theta, \gamma)$, where $r(t) = r_0 + vt$ for a body travelling at speed v . We may now re-write the electric field at the receive antenna as

$$E(f, t, (r_0 + vt)) = \frac{\alpha_s(\theta, \gamma, f) \cos(2\pi f(t - r_0 v - vt/c))}{r_0 + vt} \quad (2.3)$$

By rewriting, $f(t - r_0 v - vt/c)$ as $f(1 - v/c)t - fr_0/c$, we can see there is a new oscillation given by, $\cos(2\pi(f(1 - v/c)t - fr_0/c)) = \cos(2\pi f(1 - v/c)t - 2\pi fr_0/c)$. That is, there has been a *doppler shift* of $D = f(1 - v/c) - f = -fv/c$.

2.1.3 Two-path Propagation with Fixed Antennas

Now assume a transmission model in which a stationary transmit antenna is transmitting towards a stationary receive antenna a horizontal distance r away, in front of a wall, offset a distance $d > r$ in front of the transmit antenna. We assume the transmitted wave, of form $\cos(2\pi ft)$ reflects perpendicularly off the back wall and superposes with the signal which travelled along the direct path at the receive antenna. Equally, assume that the reflected wave has intensity of a wave which has travelled the distance to the wall and back to the receive antenna, $2d - r$, and finally that the sum of radiation patterns at the receiver, α , is the same for both signals. We can then say that the electric field at the receiver is denoted

$$E_r(f, t) = \frac{\alpha \cos(2\pi f(t - r/c))}{r} - \frac{\alpha \cos(2\pi f(t - (2d - r)/c))}{2d - r} \quad (2.4)$$

Note, they are subtracted due to the change in direction of propagation of the reflected electric field at the wall. We know that if the two waves superpose in anti-phase then destructive interference occurs. Therefore, first calculating the phase difference we see that

$$\Delta\theta = \left| \left(-\frac{2\pi f(2d - r)}{c} + \pi \right) \right| - \left| \left(-\frac{2\pi fr}{c} \right) \right| = \frac{4\pi f}{c}(d - r) + \pi \quad (2.5)$$

An additional phase shift of π is introduced to the reflected wave as it experience a phase reversal at the wall. Setting $\Delta\theta$ to an odd integer multiple of π , i.e. the

anti-phase condition, we see that destructive interference occurs when

$$\pi(2n + 1) = \frac{4\pi f}{c}(d - r) + \pi \quad (2.6)$$

$$2n = \frac{4f}{c}(d - r) \quad (2.7)$$

$$\implies d - r = \frac{cn}{2f} \quad n = 0, 1, \dots \quad (2.8)$$

Correspondingly the constructive interference condition is $d - r = \frac{c}{4f}(2n - 1)$, such that we see an interference pattern of alternating nodes and anti-nodes. The distance between a node and anti-node is the *coherence distance* given by

$$\begin{aligned} \Delta x_c &= \frac{cn}{2f} - \frac{c}{4f}(2n - 1) \\ &= \frac{c}{4f} \\ &= \frac{\lambda}{4} \end{aligned} \quad (2.9)$$

Similarly, we can formulate Equation 2.8 as a function of frequency for a fixed r to yield

$$f = \frac{cn}{2(d - r)} \quad n = 0, 1, \dots \quad (2.10)$$

and correspondingly for the in-phase condition

$$f = \frac{c}{4(d - r)}(2n - 1) \quad n = 0, 1, \dots \quad (2.11)$$

such that the change in frequency which causes transition from node to anti-node at a fixed distance is

$$\Delta f_c = \frac{cn}{2(d - r)} - \frac{c}{4(d - r)}(2n - 1) \quad (2.12)$$

$$= \frac{1}{2} \left(\frac{2d - r}{c} - \frac{r}{c} \right)^{-1} \quad (2.13)$$

Based on this formulation, we denote

$$T_d = \frac{2d - r}{c} - \frac{r}{c} \quad (2.14)$$

as the *delay spread* of the channel, corresponding to the maximum propagation delays between two paths in a multi-path environment. We then define the *coherence bandwidth*, $B_c = 1/T_d$ as a measure of the channel 'richness' in the frequency domain. If B_c is very large it means that the channel's frequency domain response is 'flat' over a large range of frequencies such that our transmitted signal experiences approximately equal attenuation over all its constituent frequencies, provided the signal bandwidth, B , satisfies $B < B_c$. The harsher the wireless environment the greater the number of paths to the Rx antenna and therefore the greater the delay spread and the smaller the coherence bandwidth. In such scenarios it is unlikely our transmitted signal would have $B < B_c$ and therefore the experienced attenuation is frequency-selective. This is called *multipath fading*.

2.1.4 Two-path Propagation with a Moving Antenna

Recalling the distance between two minima and maxima is $\lambda/4$, the fading therefore occurs on the time scale of $T_c = \lambda/4v$, which we call the coherence time. Assuming now a two-path propagation in which the Rx antenna moves with $r(t) = r_0 + vt$, we may write the electric field at the receive antenna as

$$E_r(f, t) = \frac{\alpha \cos(2\pi f((1 - v/c)t - r_0/c))}{r_0 + vt} - \frac{\alpha \cos(2\pi f((1 + v/c)t + (r_0 - 2d)/c))}{2d - r_0 - vt} \quad (2.15)$$

The first term has Doppler shift, $D_1 = -fv/c$ while the second has doppler shift $D_2 = fv/c$, yielding a *doppler spread*,

$$D_s = D_2 - D_1 = \frac{2fv}{c} = \frac{2v}{\lambda} \quad (2.16)$$

The doppler spread determines the rate of traversal of the pattern of nodes and anti-nodes, and is inversely proportional to the coherence time, i.e. $D_s \propto 1/T_c$. The effect of the receive antenna moving through the field of nodes and anti-nodes is most obvious when the Rx antenna is closer to the reflecting wall than to the Tx antenna. In such a case the attenuation of the direct and reflected paths are approximately equal and we may approximate $d \approx r_0 + vt$ which yields an expression for the receive antenna electric field

$$E_r(f, t) \approx \frac{\alpha \cos(2\pi f((1 - v/c)t - r_0/c)) - \alpha \cos(2\pi f((1 + v/c)t + (r_0 - 2d)/c))}{r_0 + vt} \quad (2.17)$$

$$= \frac{2\alpha \sin(2\pi f(t - d/c)) \sin(2\pi f((v/c)t + (r_0 - d)/c))}{r_0 + vt} \quad (2.18)$$

We can see that under this approximation, $E_r(f, t)$ is composed of two sinusoids, one at the natural carrier frequency, on the order of GHz, and one at fv/c , on the order of 50 – 100Hz. Figure 2.1 shows the observed effect; as time proceeds the received signal energy oscillates between minima and maxima, at a rate of $D_s/2$. When the difference in path lengths is a multiple of $\lambda/4$ the direct and reflected paths are in anti-phase and the Rx antenna finds itself in an anti-node, such that the signal value is lost. This occurs on the order of milliseconds, whereas the attenuation as a result of the denominator of Equation 2.18 occurs on the order of seconds such that it is effectively constant over the period of detection.

2.1.5 Deriving a Channel Model

Figure 2.2 shows the ray diagram of a time evolving scenario involving a stationary transmit and a moving receive antenna. At each time step the rays superpose at the receiver, with each ray subject to an attenuation factor $\alpha_i(t)$. Each ray has a

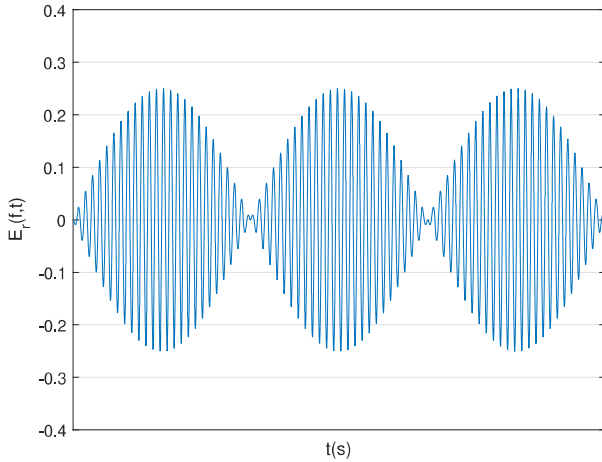


Figure 2.1: Variation of the electric field at the receive antenna under the condition the non-stationary receiver is between the reflecting wall and the Tx antenna.

different path length, so we assign each ray a delay, $\tau_i(t)$, denoting the time delay from transmit to receive antenna over the i th path. We assume we are transmitting over frequency bands narrow relative to the carrier frequency such that we can assume frequency independence of $\alpha(\cdot)$ and $\tau(\cdot)$. Note however, while individual paths may not be frequency dependent, the overall system is frequency dependent due to the differing delays of each path. Under the principle of superposition, the received signal may be thus written as

$$y(t) = \sum_i \alpha_i(t) x(t - \tau_i(t)) \quad (2.19)$$

This equation is linear such that we can quantify the overall effect of the channel as the convolution of the input signal at a delay $(t - \tau)$ with a channel impulse response (CIR), $h(t, \tau)$

$$y(t) = \int_{-\infty}^{\infty} h(t, \tau) x(t - \tau) d\tau \quad (2.20)$$

By comparison of Equation 2.19 and Equation 2.20, we can derive an expression for the channel impulse response

$$h(\tau, t) = \sum_i \alpha_i(t) \delta(\tau - \tau_i(t)) \quad (2.21)$$

from which we see we may classify the time varying channel as a series of delayed impulse impulses scaled by their attenuation factor. Equally, we may define the channel frequency response (CFR), $H(f; t)$, as the Fourier transform of the CIR

$$\begin{aligned} H(f; t) &= \int_{-\infty}^{\infty} h(\tau, t) e^{-j2\pi f t \tau} d\tau \\ &= \int_{-\infty}^{\infty} \sum_i \alpha_i(t) \delta(\tau - \tau_i(t)) e^{-j2\pi f t \tau} d\tau \end{aligned}$$

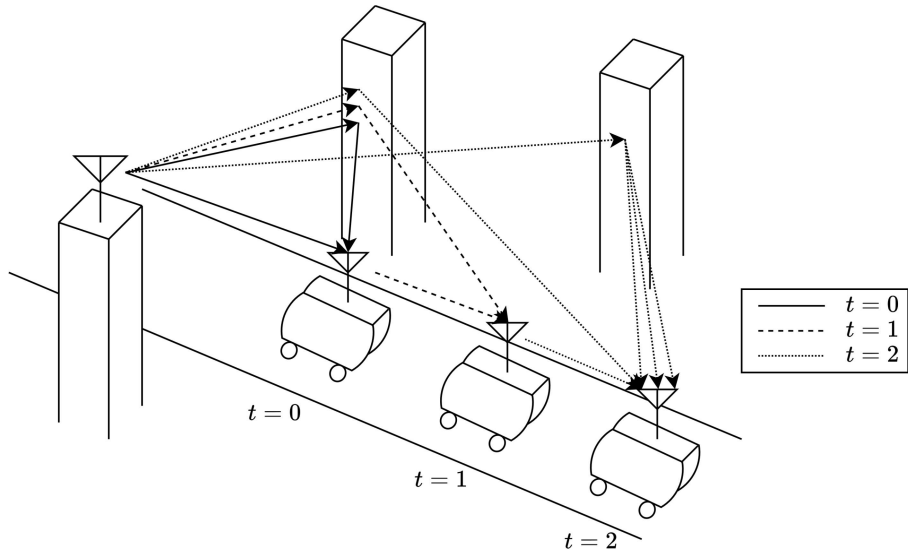


Figure 2.2: A multipath city environment showing the direct, reflected and scattered rays from a base station to a moving receiver as time evolves. Not all rays are included in this diagram.

$$\begin{aligned}
 &= \sum_i \alpha_i(t) \int_{-\infty}^{\infty} \delta(\tau - \tau_i(t)) e^{-j2\pi f t \tau} d\tau \\
 &= \sum_i \alpha_i(t) e^{-j2\pi f \tau_i(t)}
 \end{aligned} \tag{2.22}$$

It is useful to visualise the channel as multiplicative attenuation of each signal frequency by an amount equal to $H(f; t)$. The CFR varies in time much slower (on the order of milliseconds) than the delay spread of the channel (on the order of microseconds). If such a channel is also constant in frequency for a range greater than its doppler spread, then it is classified as *underspread*. Most wireless channels are underspread [15] which in simulation means we can assume that the CIR remains constant (in time) but varying in frequency over the symbol period of a signal.

While equation 2.20 describes the input-output relationship of the system, its continuous-in-time relationship and the CIR, $h(t, \tau)$, models a *passband* channel. We would rather consider only baseband signal processing in a discrete-time scenario. Therefore, following a derivation shown in Appendix A, we can derive a discrete in time input-output relationship of the channel

$$\mathbf{y}[n] = \sum_l \mathbf{h}_l[n] \mathbf{x}[n-l] + \mathbf{v}[n] \quad n = 0, 1, \dots \tag{2.23}$$

where $\mathbf{h}_l[n]$ is a complex variable denoting the l th tap of the discrete baseband CIR. Furthermore, $\mathbf{v}[n]$ is the discrete in time noise sequence said to be a complex *circularly-symmetric gaussian* random variable distributed as $v \sim \mathcal{CN}(0, N_0/2)$, and limited to a bandwidth $B/2$.

2.2 Channel Characterisation

2.2.1 Doppler Spread & Coherence Time

We may characterise the channel as *fast fading* or *slow fading* depending on how fast the channel taps, $\mathbf{h}_l[n]$ change. We begin by recalling (from Appendix A)

$$\begin{aligned}\mathbf{h}_l[n] &= \sum_i \alpha_i^b(n/B) \operatorname{sinc}(l - B\tau_i(n/B)) \\ &= \sum_i \alpha_i(n/B) e^{-j2\pi f_c \tau_i(n/B)} \operatorname{sinc}(l - B\tau_i(n/B))\end{aligned}\quad (2.24)$$

where f_c is the carrier frequency, and noticing that there are three terms, $\alpha_i(n/B)$, $e^{-j2\pi f_c \tau_i(n/B)}$ and $\operatorname{sinc}(l - B\tau_i(n/B))$ which impact the rate of change of $\mathbf{h}_l[n]$. $\alpha_i(n/B)$ is a quantity which changes slowly with time so it has little impact, and the sinc term is scaled by B which is comparatively much smaller than f_c , which scales the phase term. This means changes to $\mathbf{h}_l[n]$ occur primarily as a result of significant phase changes in the exponential term. The rate at which they change can be quantified in terms of the doppler shift. Extending the two-path case to the multi-path case, the doppler shift is given as $D_i = fv_i/c = D_i = f\tau'_i(t)$, such that the doppler spread, D_s can be more generally defined

$$D_s = \max_{i,j \forall i \neq j} \{f_c |\tau'_i(t) - \tau'_j(t)|\} \quad (2.25)$$

This means significant changes to $\mathbf{h}_l[n]$ occur (in the worst case) every

$$T_c = \lambda/4v \approx 1/(4D_s) \quad (2.26)$$

seconds [16], which we define as the coherence time of the channel.

Based on this model we define *fast fading* as a channel in which the symbol period, T_s is greater than T_c such that $B < D_s$. Equally, *slow fading* occurs when the symbol rate, T_s is *much* less than T_c . In such case $B \gg D_s$. The key takeaway is that the harsher the environment, the greater the doppler spread, the smaller the coherence time and the faster the rate at which the channel taps change, increasing the likelihood multiple fades occur per symbol period. In our case, we shall assume slow fading such that the CIR remains constant over the symbol period.

2.2.2 Delay Spread & Coherence Bandwidth

The delay spread, T_d , may be defined as the difference in propagation time between the longest and shortest paths in an environment, considering only those paths with significant energy so as to effect the received symbol significantly, i.e.

$$T_d = \max_{i,j} \{|\tau_i(t) - \tau_j(t)|\} \quad (2.27)$$

As the number of Tx antennas in an environment increases the delay spread becomes shorter, and typically a wireless channel is *underspread* meaning, $T_d \ll T_c$. Typically, T_d is on the order of a few microseconds for a non ultra-wide-band applications, which means we can model the CIR with $L \approx 5 - 8$ taps. Furthermore, as the demand for higher data rates grows, cell coverage becomes smaller, instead favouring a greater quantity of cells which further reduces T_d , validating the underspread assumption.

The delay spread also dictates the *frequency coherence* of the channel. This is a measure of how quickly the channel changes over frequency. We recall that the CFR is given by

$$H(f; t) = \sum_i \alpha_i(t) e^{-j2\pi f \tau_i(t)} \quad (2.28)$$

In the multipath case, ($i > 0$), the phase of $H(f; t)$ is dependent on the sum of each of the $\tau_i(t)$ terms leading to *frequency selective* fading where each frequency component in the transmitted signal experiences a different level of attenuation. Therefore, the received electric field changes not only in time with $1/(4D_s)$ but also as the baseband signal frequency, f , changes by $1/(2T_d)$. We define this quantity the *coherence bandwidth*, B_c .

$$B_c = \frac{1}{2T_d} \quad (2.29)$$

When $B \ll B_c$ the channel is said to be *frequency flat* such that all signal frequencies experience similar fading and thus we can represent the channel with a single tap. On the contrary, a frequency selective channel occurs when $B > B_c$, which must be represented by a multi-tap CIR, which we shall assume proceeding.

2.3 A Statistical Channel Model

Doppler spread, coherence spread, and multi-path ray tracing analysis provide us with a characterisation of the channel for a particular configuration of antennas, at a particular relative speed and time. While useful in developing a model, we are more interested in a characterisation which models the channel over a wide range of scenarios. Proceeding we will determine the statistical distribution which models a fast fading environment, which will be the basis for our simulatory model.

We begin by assuming that fast fading can be quantified by a complex channel gain, $\mathbf{h}_l[m] = \alpha_i + j\alpha_q$. The path gain has a magnitude $\alpha = \sqrt{\alpha_i^2 + \alpha_q^2}$ and phase, $\phi = \arctan(\alpha_q/\alpha_i)$. From Equation 2.24 we can see that the phase of the i th path is $2\pi f_c \tau_i \pmod{2\pi}$. For the i th path of length d_i , we may write $f_c \tau_i = d_i/\lambda$. Here, λ is the carrier wavelength, so it is sufficient to assume $d_i \gg \lambda$, from which we can say that the phase is uniformly distributed over $[0, 2\pi]$ and independent from one

sample to the next. We can further assume that each channel gain characterises the sum of many different path gains, as was written in Equation A.14. Therefore, the central limit theorem suggests that the distribution of α_i and α_q tends towards a normal gaussian distribution regardless of the distribution of each multi-path gain [17], such that $\mathbf{h}_l[m]$ is distributed as $\sim \mathcal{CN}(0, \sigma_l^2)$. This is sufficient knowledge for our simulation purposes - a 5-8 tap channel with circularly-symmetric gaussian coefficients is a simple model which captures the described behaviour, however, for completeness a derivation for the distribution of α is listed in Appendix B.

3 | Multi-Carrier Modulation

Multi-carrier modulation, or, frequency-division-multiplexing, is a technique employed to overcome the effects of frequency-selective fading channels [18]. Its initial use dates back almost a century, where frequency-division-multiplexed telegraph lines transmitted parallel data using multiple non-orthogonal subcarriers. One of the earliest military applications was in 1957 with the Kineplex system [19].

Prior to the realisation of OFDM as an industry standard, the typical approach to communication over frequency selective channels were single carrier schemes with time-domain equalisation. One such approach would be to consider a length k sequence of sequentially transmitted complex M -Ary symbols, which has a finite number of realisations, given by M^k . The receiver could consider each of the M^k sequence realisations and calculate the mean square error (MSE) metric by squaring the difference between the received sequence of symbols and the test sequence subject to the CIR. By choosing the length k sequence with the lowest MSE metric, we have a maximum likelihood (ML) detection algorithm [20]. [21] presents an implementation for a time-domain ML sequence detector using the Viterbi algorithm with a reduced complexity, proportional to M^L where L is the length of the CIR. This is a problem due to the ever increasing data rate requirements which calls for higher order modulation schemes such as QAM-256, which, with $L = 8$ would require an unfeasible $256^8 \approx 1.8 \times 10^{19}$ complex computations. Furthermore, it is difficult to accurately maintain and update a large number of taps for an equaliser in a rapidly time varying channel [16]. This motivates the use of sub-optimal linear equalisers such as the zero forcing (ZF) or minimum-mean-square-error (MMSE) equaliser which approach ML performance at a reduced complexity. The ZF approach requires inversion of the CIR, but since we view the channel as a finite-duration FIR filter, its inversion is an infinite duration IIR filter [5]. This is unrealisable and therefore must be truncated at the cost of accuracy. MMSE equalisers achieve a better balance of avoiding noise enhancement while eliminating ISI, however are ultimately realised as multi-tap FIR filters which introduces a non-ideal delay to the system.

Comparatively, provided that the channel is underspread, meaning that it is approximately time-invariant over the symbol period, we may achieve much simpler

equalisation in the frequency domain. In fact, we will show that multi-carrier modulation facilitates the use of a single tap zero-forcing equaliser at the receiver which is both easy to maintain and scales linearly in complexity with the sequence length. This makes multi-carrier techniques particularly advantageous in environments with large delay spreads where the signal bandwidth is highly likely to exceed the channel coherence bandwidth.

3.1 Principles of Multi Carrier Modulation

Consider a linearly modulated, single carrier signal with symbol rate f_s and bandwidth B_s . We can assume the use of a pulse-shaping filter to reduce the signals bandwidth. One common choice would be the root-raise-cosine (RRC) filter, which balances the trade off between spectral-leakage and bandwidth by a roll-off factor, $0 \leq \alpha \leq 1$. In such a case, the linearly modulated signal has bandwidth $B_s = f_s(1 + \alpha)$. To better visualise this, Figure 3.1 shows the power spectral density (PSD) plot of such a signal, transmitting complex QAM-16 symbols at a rate of 8Hz with $\alpha = 0.2$, modulated onto a 1KHz carrier. We can see the bandwidth is 9.6Hz as expected.

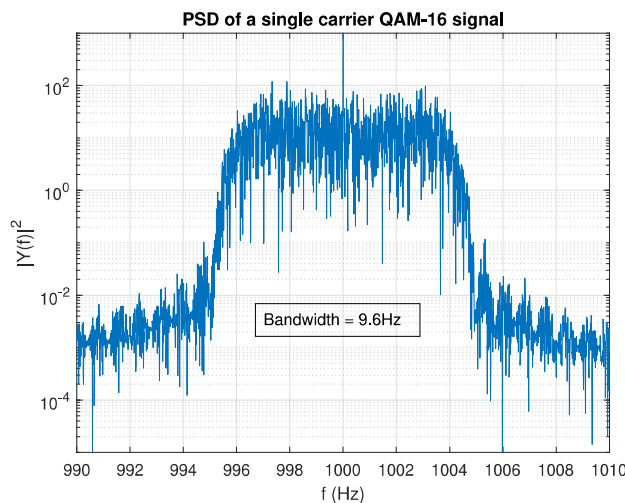


Figure 3.1: PSD of a single carrier QAM-16 signal, transmitting data at a symbol rate, $f_s = 8\text{Hz}$

The coherence bandwidth for the channel is assumed to be $B_c < B_s$, so the signal experiences frequency selective fading. The basic premise of multi-carrier modulation is to break this wideband system into N linearly modulated parallel subsystems, each with subchannel bandwidth $B_n = B_s/N$ and data rate $f_n \approx f_s/N = N/T_s$. For N sufficiently large, the subchannel bandwidth $B_n = B_s/N \ll B_c$ which ensures relatively flat fading on each subchannel. This is illustrated in Figure 3.2.

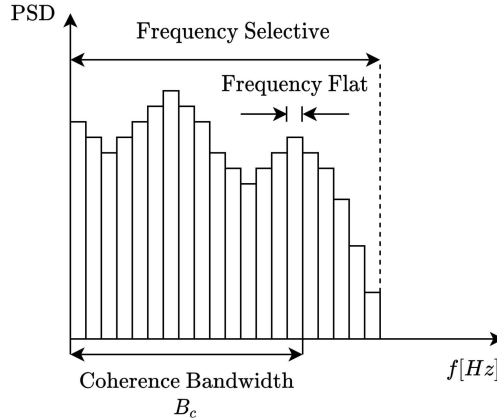


Figure 3.2: The frequency spectrum of a signal with bandwidth, $B_s > B_c$ split into $N = 20$ subchannels each with $B_n = B_s/N \ll B_c$ to achieve flat fading across each subcarrier.

3.1.1 Multi-Carrier Modulation with Non-overlapping Sub-channels

To formulate this idea more rigorously, the transmitted signal of a multi-carrier (MC) modulation scheme with N subcarriers may generally be represented as:

$$x(t) = \sum_{i=0}^{N-1} s_i \cdot g(t) \cdot \cos(2\pi f_i t + \phi_i) \quad (3.1)$$

where $s_i \in \mathcal{M} = \{s_1, s_2, \dots, s_M\}$ the M -ary constellation alphabet, ϕ_i is the phase offset by the i th sub-carrier, f_i is the modulating frequency of the i th sub-carrier and $g(t)$ is the transmit pulse-shaping filter.

As a result of the fact that the RRC does not have a brick-wall frequency response, there is spectral leakage of the complex symbols modulated at each subcarrier, which we can observe in Figure 3.1. The magnitude of the leakage frequencies decays as you move away from the main spectral lobe, which, for our multi-carrier system indicates that the closer we space our subcarriers, the more inter-carrier-interference (ICI) there will be. A reasonable approach is to modulate each symbol at a frequency $f_i = f_0 + i \cdot B_n$ for $i = 1, 2, \dots, N - 1$, which is shown in Figure 3.3. It is important to note, the sampling frequency is equal to the single carrier case at 8Hz, however since 4 complex symbols are transmitted in parallel, the symbol rate is now reduced by a factor of 4 to 2Hz, maintaining an equivalent bit-rate. As a result, the bandwidth of each subchannel is reduced by a factor of 4, and thus the signal bandwidth is equivalent to that of the single-carrier scheme.

In this scenario, demodulation requires an ideal band-pass filter at the receiver in order to select each subchannel which can be unfeasible to realise at a reasonable complexity. Furthermore, this system requires N independent oscillators which is

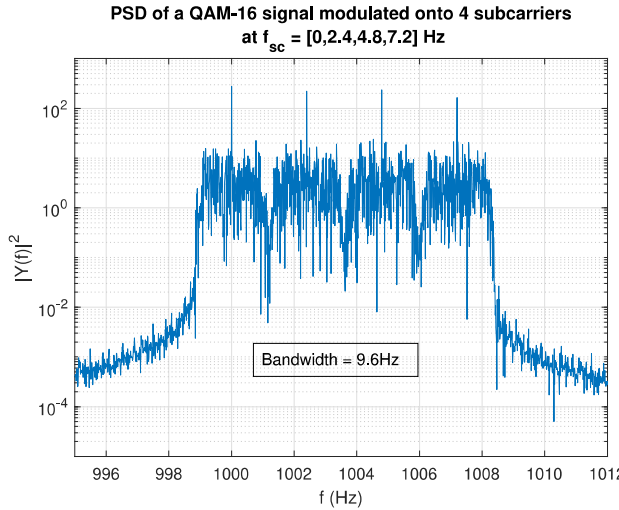


Figure 3.3: PSD of a non-orthogonal multi-carrier QAM-16 signal with 4 subcarriers, transmitting at a symbol rate, $f_s = 8\text{Hz}$

large in size and power inefficient. We will now show that we can use overlapping orthogonal subcarriers to resolve many of these issues while making better use of the spectrum, beyond that of even single carrier systems.

3.1.2 Multi-carrier Modulation With Overlapping Subchannels

Multi-carrier modulation with overlapping subchannels (OFDM) was first introduced in 1966 [6]. It operates based on the principle that the subcarriers $\cos(2\pi(f_0 + i/T_n)t + \phi_i)$ for $i = 1, 2, \dots$ form a set of approximately orthogonal basis vectors on the interval $[0, T_n]$ for any set of phase offsets ϕ_i , and symbol period T_n . This can be shown by taking their inner product as follows

$$\begin{aligned} & \frac{1}{T_n} \int_0^{T_n} \cos\left(2\pi\left(f_0 + \frac{i}{T_n}\right)t + \phi_i\right) \cos\left(2\pi\left(f_0 + \frac{j}{T_n}\right)t + \phi_j\right) dt \\ &= \frac{1}{2T_n} \int_0^{T_n} \cos\left(2\pi\frac{(i-j)t}{T_n} + \phi_i - \phi_j\right) dt + \\ & \quad \frac{1}{2T_n} \int_0^{T_n} \cos\left(2\pi\left(2f_0 + \frac{i+j}{T_n}\right)t + \phi_i + \phi_j\right) dt \end{aligned} \quad (3.2)$$

Carrying out the integration for the second term in Equation 3.2 yields

$$\begin{aligned} & \frac{1}{2T_n} \int_0^{T_n} \cos\left(2\pi\left(2f_0 + \frac{i+j}{T_n}\right)t + \phi_i + \phi_j\right) dt = \\ & \quad \frac{1}{4\pi(2f_0T_n + i + j)} \left[\sin\left(2\pi\left(2f_0 + \frac{i+j}{T_n}\right)T_n + \phi_i + \phi_j\right) - \sin(\phi_i + \phi_j) \right] \end{aligned} \quad (3.3)$$

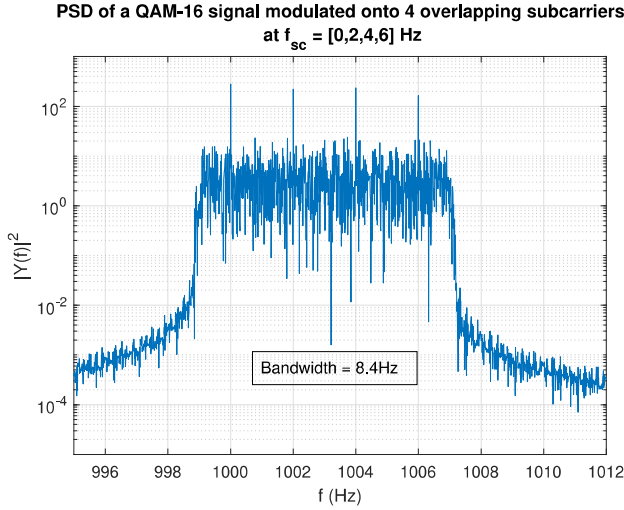


Figure 3.4: PSD of an orthogonal multicarrier signal transmitted over 4 subcarriers with a baseband sampling rate of $f_s = 8\text{Hz}$

For $f_0 T_n \gg 1$, or the ideal case where $\phi_i = \phi_j = 0$, we see that the second term in Equation 3.2 approaches zero. Thus we may approximate Equation 3.2 to

$$\begin{aligned} & \frac{1}{T_n} \int_0^{T_n} \cos \left(2\pi \left(f_0 + \frac{i}{T_n} \right) t + \phi_i \right) \cos \left(2\pi \left(f_0 + \frac{j}{T_n} \right) t + \phi_j \right) dt \\ & \approx \frac{1}{2T_n} \int_0^{T_n} \cos \left(2\pi \frac{(i-j)t}{T_n} + \phi_i - \phi_j \right) dt \\ & = \frac{1}{2} \delta(i-j) \end{aligned} \quad (3.4)$$

where $\delta(\cdot)$ is the Kronecker delta which equals 1 when $i = j$, or 0 otherwise, satisfying the orthogonality condition. Therefore, frequency separation to achieve orthogonal subcarriers is $1/T_n = f_n$.

Given that each subchannel has bandwidth $B_n = f_n(\alpha + 1)$ and the subcarriers are spaced by $1/T_n = f_n$, then the total system bandwidth can be reasoned geometrically, as in Figure 3.5, yielding

$$B = f_n(N - 1) + 2 \left(\frac{f_n(1 + \alpha)}{2} \right) = f_n(N + \alpha) \quad (3.5)$$

In systems where $N > 64$, this may be approximated, $B \approx N/T_n$ since a reasonable value for α is $0.2 \ll N$. An example PSD of a multi-carrier system with overlapping subchannels is shown in Figure 3.4, in which we can see the signal has bandwidth of 8.4Hz, less than that of the single-carrier system. Given the orthogonality of this set of basis functions, despite overlapping in the frequency domain, each subchannel can be separated out at the receiver provided correct sampling at multiples of $1/T_n$.

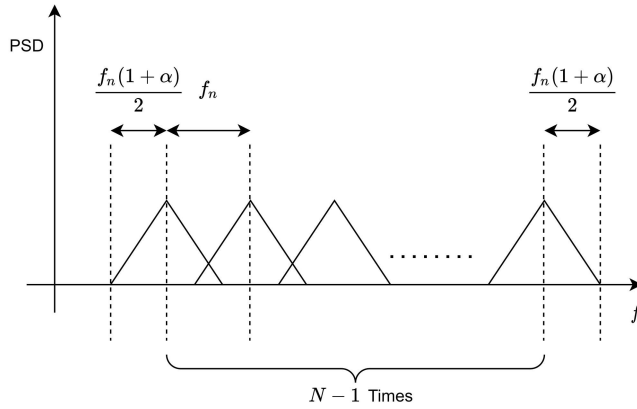


Figure 3.5: PSD of an arbitrary orthogonal MC system with subcarriers spaced by $f_n = 1/T_n$ and symbol bandwidth $f_n(1 + \alpha)$.

3.1.3 Multi-carrier Detection With Overlapping Subchannels

We will now show that the orthogonal system can be demodulated using simple multiplication operations, despite overlapping in the frequency domain, which is easier to realise on a chip in terms of complexity and size. In the absence of fading and noise, the received MC signal is given as,

$$y(t) = \sum_{j=0}^{N-1} s_j \cdot g(t) \cdot \cos(2\pi f_j t + \phi_j)$$

assuming, $\{\phi_j\}$ is known, we may demodulate the received signal as,

$$\hat{s}_i = \int_0^{T_s} y(t)g(t) \cos(2\pi f_i t + \phi_i) dt \quad (3.6)$$

$$\begin{aligned} &= \sum_{j=0}^{N-1} s_j \int_0^{T_s} g^2(t) \cos\left(2\pi\left(f_0 + \frac{j}{T_s}\right)t + \phi_j\right) \\ &\quad \cos\left(2\pi\left(f_0 + \frac{i}{T_s}\right)t + \phi_i\right) dt \end{aligned} \quad (3.7)$$

$$\approx \sum_{j=0}^{N-1} s_j \delta(j - i) = s_i \quad (3.8)$$

which follows from the previous orthogonality condition for the set of functions $\{\cos(2\pi(f_0 + i/T_s)t + \phi_i)\}$ presented in section 3.2.1. As a result we can see, $\hat{s}_i = s_i$ for $i = 0, 1, \dots, N - 1$ which shows perfect detection of the transmitted symbols.

3.2 Multi-Carrier Modulation Using the FFT

Previous discussion has shown the feasibility of orthogonal multi-carrier systems in the continuous time domain under the assumption of no noise and no fading. We

now proceed with a discrete-in-time model of transmission incorporating the idea of a discrete-in-time, finite length, CIR $\mathbf{h} = [h_0, h_1, \dots, h_L]$ (adopting the notation $\mathbf{h}[n] = h_n$ and dropping the time dependency for notational simplicity), and discrete-in-time noise vector $\mathbf{v} = [v_0, v_1, \dots, v_{N-1}]$, based upon the discussion in chapter 2. Furthermore we will also show how the fast fourier transform (FFT) can be used as a tool for efficiently carrying out multi-carrier modulation, vastly reducing the hardware requirements over the previous schemes.

3.2.1 OFDM Modulation

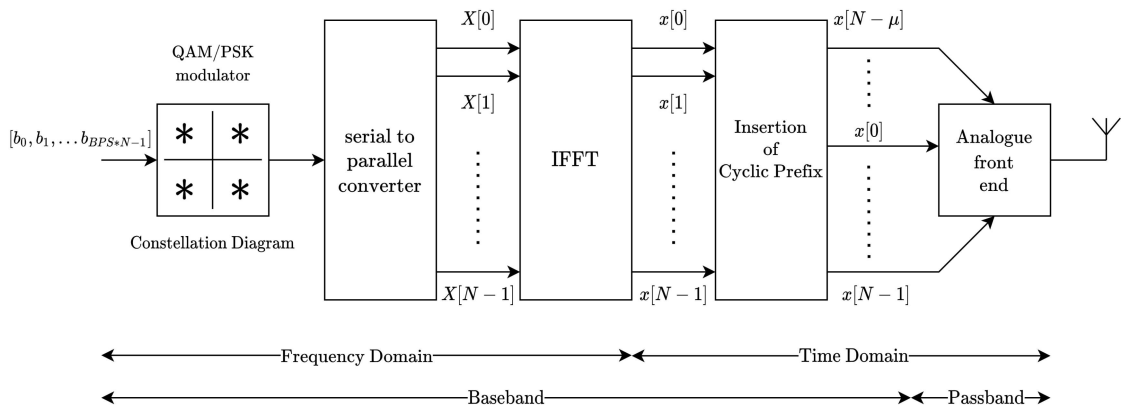


Figure 3.6: OFDM modulator block diagram

Figure 3.6 shows the block diagram of the OFDM modulator. The input bit vector is modulated by a complex constellation alphabet, \mathcal{M} , such as QAM- M or M -PSK, at a symbol rate f_s resulting in the discrete time sequence of frequency-domain symbols $\mathbf{X} = [X_0, X_1, \dots, X_{N-1}]$ with $X_j \in \mathcal{M}$ for $j = 0, 1, \dots, N - 1$. The frequency-domain symbols are then converted into the time-domain by performing an Inverse FFT, resulting in the sequence $\mathbf{x} = [x_0, x_1, \dots, x_{N-1}]$, where

$$\mathbf{x}[n] = \frac{1}{\sqrt{N}} \sum_{i=0}^{N-1} \mathbf{X}[i] e^{\frac{j2\pi ni}{N}} \quad n = 0, 1, \dots, N - 1 \quad (3.9)$$

A ‘cyclic-prefix’ is then appended to the start of the sequence by taking the last $\mu = L + 1$ symbols of \mathbf{x} and appending them to the start to form $\tilde{\mathbf{x}} = [x_{N-\mu}, \dots, x_0, \dots, x_{N-1}]$. This cyclic-prefix is key to mathematically satisfying the necessary conditions to permit one-tap equalisation at the receiver. This can be observed by first supposing a complex time-domain sequence, $\mathbf{x} = [x_0, x_1, \dots, x_{N-1}]$, is subject to a channel with impulse response, $\mathbf{h} = [h_0, h_1, \dots, h_L]$ of length $L + 1 = T_d/T_s \approx 8$. Each received symbol, $\mathbf{y}[n]$ is equal to the convolution of the transmitted symbol $\mathbf{x}[n]$ with the CIR, written

$$\mathbf{y}[n] = \mathbf{h}[n] * \mathbf{x}[n] + \mathbf{v}[n] = \sum_{k=0}^L \mathbf{h}[k] \mathbf{x}[n-k] + \mathbf{v}[n] \quad (3.10)$$

This presents a problem since each $\mathbf{y}[n]$ is equal to the sum of $L + 1$ $\mathbf{x}[n - k]$ terms, each subject to a complex path gain, $\mathbf{h}[n - k]$, meaning there is no easy way to recover $\mathbf{x}[n]$ from $\mathbf{y}[n]$. However, if instead our linear convolution was turned into a circular convolution such that

$$\mathbf{y}[n] = \mathbf{h}[n] \circledast \mathbf{x}[n] + \mathbf{v}[n] = \sum_{k=0}^L \mathbf{h}[k] \mathbf{x}[n - k]_N + \mathbf{v}[n] \quad (3.11)$$

(where $\mathbf{x}[n - k]_N \triangleq \mathbf{x}[n - k \bmod N]$) then we could take advantage of the fact that $\text{DFT}\{\mathbf{x}[n] \circledast \mathbf{h}[n]\} = \mathbf{X}[i]\mathbf{H}[i]$, where $\mathbf{H} = [H_0, H_1, \dots, H_{N-1}]$ is the discrete channel-frequency-response, and $\text{DFT}\cdot$ denotes the discrete-fourier-transform. Under such conditions we could therefore write

$$\begin{aligned} \mathbf{Y}[i] &= \text{DFT}\{\mathbf{h}[n] \circledast \mathbf{x}[n] + \mathbf{v}[n]\} \\ &= \mathbf{X}[i]\mathbf{H}[i] + \mathbf{V}[i] \quad i = 0, 1, \dots, N - 1 \end{aligned} \quad (3.12)$$

where $\mathbf{V} = [V_0, V_1, \dots, V_{N-1}]$ is the fourier transformed noise vector - a zero mean circularly-symmetric gaussian variable. We can then detect each of the frequency-domain symbols through one-tap-equalisation (OTE), as follows

$$\tilde{\mathbf{X}}[i] = \frac{\mathbf{Y}[i]}{\mathbf{H}[i]} = \mathbf{X}[i] + \frac{\mathbf{V}[i]}{\mathbf{H}[i]} \quad i = 0, 1, \dots, N - 1 \quad (3.13)$$

Fortunately, this exact effect is what is achieved by appending the cyclic-prefix. We notice that for each element in the CP-extended transmit vector $\tilde{\mathbf{x}}[n] = \mathbf{x}[n]_N$ for $-\mu \leq n \leq N - 1$, which implies $\tilde{\mathbf{x}}[n - k] = \mathbf{x}[n - k]_N$ for $-\mu \leq n - k \leq N - 1$. Therefore, as a result of applying the cyclic-prefix, when convolving the input sequence with the channel impulse response (CIR) we see the following effect,

$$\mathbf{y}[n] = \mathbf{h}[n] * \tilde{\mathbf{x}}[n] \quad (3.14)$$

$$= \sum_{k=0}^L \mathbf{h}[k] \tilde{\mathbf{x}}[n - k] \quad (3.15)$$

$$= \sum_{k=0}^L \mathbf{h}[k] \mathbf{x}[n - k]_N = \mathbf{x}[n] \circledast \mathbf{h}[n] \quad (3.16)$$

That is, the linear convolution of the CP-extended input sequence and the CIR is exactly equivalent to the circular convolution of the non-CP extended sequence and the CIR. Therefore, since the constellation modulation results in a complex *frequency-domain* symbol vector $\mathbf{X} = [X_0, X_1, \dots, X_{N-1}]$, the IFFT is employed at the transmitter to form the time domain transmit sequence, \mathbf{x} , which can then be cyclically extended to form $\tilde{\mathbf{x}}$, which is ultimately subject to the channel with the desired effects.

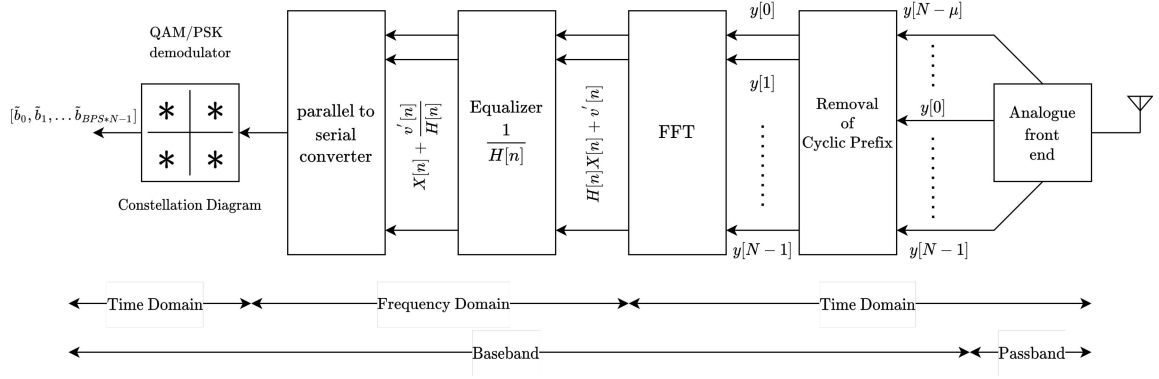


Figure 3.7: OFDM demodulator block diagram

3.2.2 OFDM Demodulation

Figure 3.7 shows the block diagram for how the OFDM demodulator. The received signal, \mathbf{y} , has length $N + \mu$, yet the first μ samples are not needed to recover \mathbf{x} , owing to the redundancy associated with the cyclic-prefix. Thus, we begin demodulation by discarding the first μ samples of \mathbf{y} . Demodulation then proceeds by fourier transforming \mathbf{y} to realise Equation 3.12, yielding

$$\mathbf{Y}[i] = \text{DFT} \{ \mathbf{y}[n] \} = \text{DFT} \{ \mathbf{h}[n] \otimes \mathbf{x}[n] + \mathbf{v}[n] \} \quad (3.17)$$

$$= \mathbf{H}[i] \mathbf{X}[i] + \mathbf{V}[i] \quad i = 0, 1, \dots, N - 1 \quad (3.18)$$

We then subject each $\mathbf{Y}[i]$ to the one-tap equaliser with value $1/\mathbf{H}[i]$, $i = 0, 1, \dots, N - 1$ to generate the N decision variables, $\tilde{\mathbf{X}}[i] = [\tilde{X}_0, \tilde{X}_1, \dots, \tilde{X}_{N-1}]$. The length N vector of M -Ary symbols are then serialised and constellation demodulated to form the demodulated bit vector, $\tilde{\mathbf{b}}$. For a more rigorous treatment of why in particular the (I)FFT and cyclic-prefix results in frequency flat fading, Appendix C details a matrix representation of OFDM that explores these ideas thoroughly.

3.3 Performance of OFDM

3.3.1 Bit Error Rate

Figure 3.8 shows the BER curve of OFDM for various constellation modulation schemes over a rayleigh fading channel with additive white gaussian noise. We observe that the BER of the simulation aligns exactly with the expected result which can be derived analytically [22] and plotted using MATLAB's `berfading()` function. This shows us that OFDM does not offer performance gains over single carrier modulation but rather equal performance at a reduced complexity. Furthermore, we have labelled each curve with its spectral efficiency η , defined as the bits per subcarrier. For OFDM

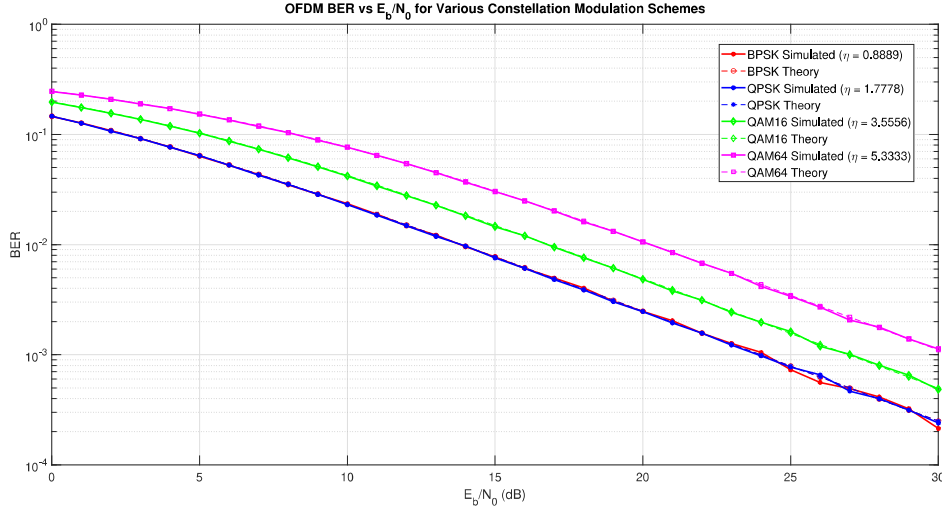


Figure 3.8: OFDM BER vs Bit-to-noise power ratio, $N = 64$, $\mu = 8$, $L = 8$.

this is simply

$$\eta_{OFDM} = \frac{N}{N + \mu} \log_2(M) \quad (3.19)$$

for modulation order M , cyclic-prefix length μ , and N subcarriers. Figure 3.8 will be the reference with which we compare the performance of the forthcoming index-modulation schemes investigated in section 4.1.1.

3.3.2 Peak to Average Power Ratio

One considerable drawback of OFDM in comparison to single carrier schemes is its power requirements [16, 12.5.1]. To understand why this is the case, we may analyse the PAPR of an OFDM signal analytically, beginning with the general equation for PAPR which states

$$\text{PAPR} \triangleq \frac{\text{Peak signal power}}{\text{Average signal power}} \quad (3.20)$$

In the case of a square constellation of order M , following the derivation laid out in Appendix E, the *maximum* PAPR of an OFDM signal is given by

$$PAPR_{OFDM} = \frac{N_a^2(\sqrt{M}-1)^2}{\frac{N_a}{3}(M-1)} = \frac{3N_a(\sqrt{M}-1)}{\sqrt{M}+1} \quad (3.21)$$

which varies linearly with the number of active subcarriers N_a (Conventional OFDM operates with $N_a = N$).

In reality however, the PAPR of an arbitrary OFDM symbol varies depending on the data being modulated as this dictates the phase of the subcarriers and subsequently whether they add constructively or destructively. Therefore, we must quantify the PAPR statistically in order to compare it to single-carrier modulation schemes. One

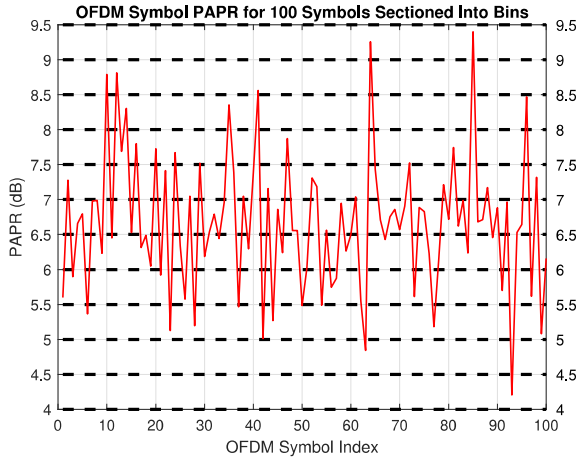


Figure 3.9: PAPR of 100 OFDM symbols sorted into value bins

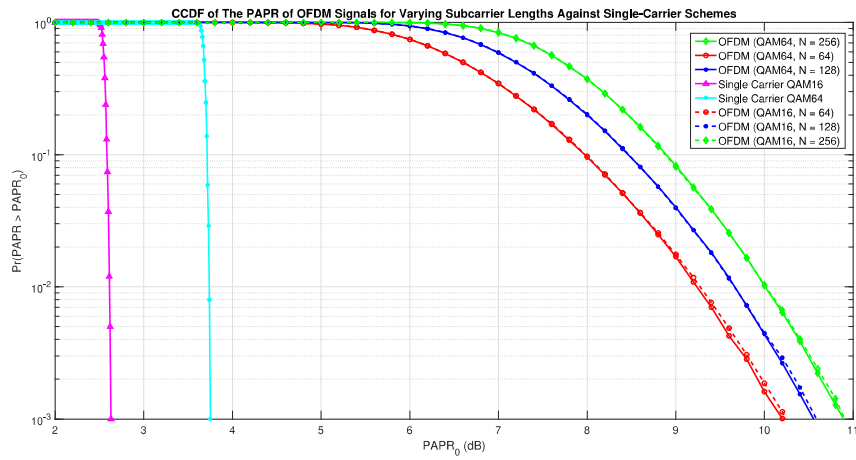


Figure 3.10: CCDF of the PAPR of OFDM compared against single carrier QAM-16 and QAM-64 for various values of N

approach is to measure the power of an OFDM symbol as a function of time and quantise the value at each time step into a bin, as shown in Figure 3.9.

Repeating this process over a large number of OFDM symbols we can then approximate the probability that the signal power reaches a given power level. What we call the complementary cumulative distribution function (CCDF) of the PAPR of an OFDM symbol is the plot of $P(PAPR > PAPR_0)$ against $PAPR_0$, where $PAPR_0$ is a threshold power level. Figure 3.10 shows the CCDF of OFDM against that of single-carrier QAM-16 and QAM-64 which clearly indicates a greater PAPR on behalf of OFDM.

Having a high PAPR forces the transmit power amplifier to have a large *backoff* [16] - this is the power level below the saturation point at which the amplifier must be biased to ensure operation in the linear region in the event of an increase in input power. It ensures the amplification process does not introduce non-linear distortions

which would compromise the orthogonality of the subcarriers. This results in the requirement of an amplifier with a characteristic that is linear over a large dynamic range, which can be expensive to realise. Additionally, a high PAPR requires an ADC with a large dynamic range at the receiver, requiring well matched components which may not be attainable to the required accuracy [23].

4 | Index Modulation Aided OFDM

Since the OFDM PAPR scales linearly with N_a we are motivated to reduce N in order to minimise PAPR. However, this increases the proportional of symbols which carry the redundant cyclic-prefix, leading to a reduction in data-rate. Furthermore, with fewer subcarriers the channel is split into fewer, and thus larger bandwidth, subchannels such that our assumption of flat fading over each subcarrier becomes less valid. IM aided OFDM (IM-OFDM) is a family of techniques which aim to resolve this issue by fixing N and instead using a subset of the available subcarriers, transmitting implicit binary data through the subcarrier activation pattern to mitigate throughput losses. IM-OFDM can be categorised into ‘single mode’ techniques, which we shall look into first, such as Subcarrier-Index-Modulated OFDM (SIM-OFDM), Enhanced SIM-OFDM (ESIM-OFDM) and Generalised SIM-OFDM (GSIM-OFDM) or ‘multi-mode’ schemes, such as Dual-Mode IM-OFDM (DM-OFDM), which we shall cover second.

4.1 Single Mode Index Modulation

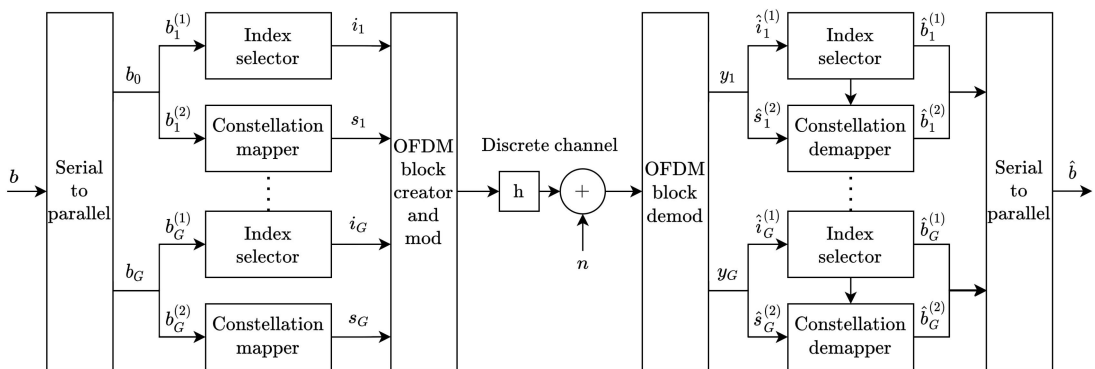


Figure 4.1: General Single mode IM-OFDM block diagram [24]

Our investigation into single mode techniques will begin with GSIM-OFDM as ESIM-OFDM and SIM-OFDM are considered special cases of this approach.

4.1.1 GSIM-OFDM (IM-OFDM)

Unlike traditional modulation schemes, index modulation transmits data on the premise that given an enumerable resource, such as the set of OFDM subcarriers, each of which has a state, such as active or inactive, then information can be transmitted by encoding our message signal into the state of the active subcarriers. The greater we can parameterise our system, the more number of states our system has; the more states we have the greater the number of bits are required to encode the state, and so the greater amount of data transmitted implicitly via index modulation.

To formulate this more rigorously, Figure 4.1 portrays a block diagram of the GSIM-OFDM transceiver [24]. We see that an input bitstream, \mathbf{b} , of length m is split into G groups $\{\mathbf{b}_1, \dots, \mathbf{b}_G\}$, each with p bits such that $m = G \cdot p$. Each group of p bits maps to L subcarriers in the OFDM symbol, where $L = N/G$. The g th subgroup, \mathbf{b}_g , is then further split into two subgroups, $\mathbf{b}_g^{(1)}$ and $\mathbf{b}_g^{(2)}$, $g = 1, \dots, G$, which represent the index-bits and the data bits respectively. We can thus deduce $\lfloor \log_2(C_k^L) \rfloor$ bits from the subcarrier activation pattern (where C_k^L is the binomial coefficient function ‘ L choose k ’), while $k \log_2(M)$ data bits are transmitted on the k active subcarriers per block. Therefore, $\mathbf{b}_g^{(2)}$ is chosen to have length, p_2 , where

$$p_2 = k \log_2(M) \quad (4.1)$$

while, $\mathbf{b}_g^{(1)}$ has length p_1 , where

$$p_1 = \lfloor \log_2(C_k^L) \rfloor \quad (4.2)$$

One of the aims of IM-OFDM is to make up for the loss in throughput which using a subset of the available subcarriers entails. Therefore an important performance metric is the spectral efficiency, η , a measure of the bits conveyed per subcarrier. For GSIM-OFDM the spectral-efficiency is [25]

$$\eta_{GSIM-OFDM} = G \cdot \frac{k \log_2(M) + \lfloor \log_2(C_k^L) \rfloor}{N + \mu} \quad (4.3)$$

4.1.1.1 Modulation

With the previous considerations in mind, the modulation policy is as follows. Using $\mathbf{b}_g^{(1)}$, a selection procedure is employed to select k out of L subcarriers per block as active. Selection procedures, such as that described in Appendix F, can vary as long as it is a one-to-one mapping of p_1 bits to a set of k active subcarriers which we denote

$$\mathbf{I}_g = [i_1, i_2, \dots, i_k] \quad (4.4)$$

for $g = 1, 2, \dots, G$, with $i_\gamma \in \{1, 2, \dots, L\}$ for $\gamma = 1, 2, \dots, k$. In general, for p_1 index bits there are $N_I = 2^{p_1}$ possible realisations of \mathbf{I}_g , therefore, the set of all possible

index patters is defined as

$$\mathcal{I} = \{\mathbf{I}_g^{(1)}, \mathbf{I}_g^{(2)}, \dots, \mathbf{I}_g^{(N_I)}\} \quad (4.5)$$

The p_2 bits of $\mathbf{b}_g^{(2)}$ are then modulated using a constellation modulator of order M to produce k M -ary symbols. The resulting symbol-vector corresponding to the g th sub-block is denoted

$$\mathbf{S}_g = [s_1, s_2, \dots, s_k] \quad (4.6)$$

with $s_j \in \mathcal{M}$ for $j = 1, 2, \dots, k$. If each symbol can take one of M complex values then there are $N_S = M^k$ possible realisations of \mathbf{S}_g , which we can group together as the set of transmissible data-symbol-vectors given by

$$\mathcal{S} = \{\mathbf{S}_g^{(1)}, \mathbf{S}_g^{(2)}, \dots, \mathbf{S}_g^{(N_S)}\} \quad (4.7)$$

Therefore, for the g th sub-block there are $N_s N_I = 2^{p_1} M^k$ transmissible index modulated symbol-vectors. Following decision of the active subcarriers we construct the g th transmitted sub-block as $\mathbf{X}_g(\mathbf{I}_g) = \mathbf{S}_g$. Repeating this for the G sub-blocks and concatenating each vector yields $\mathbf{X} = [\mathbf{X}_1, \mathbf{X}_2, \dots, \mathbf{X}_g]$, a fully formed index-modulated frequency-domain symbol vector which can then be subject to the IFFT, as in conventional OFDM.

4.1.1.2 Detection

[26] presents both an ML and LLR method of detection for GSIM-OFDM. Since there are $N_S N_I = 2^{p_1} M^k$ possible realisation of the index modulated symbol vector the computational complexity of the ML detector would require $\mathcal{O}(G2^{p_1} M^k)$ complex multiplications per OFDM symbol. This is unfeasible to compute in real time, so only the reduced complexity LLR detector shall be considered.

Log-Likelihood-Ratio (LLR) detection is a probabilistic approach to detection. Given that each subcarrier can either be zero (inactive) or non-zero (active), we denote the LLR of each subcarrier, λ_α , for $\alpha = 1, 2, \dots, N$, as the ratio of the posterior probabilities of the frequency domain symbols occupying either states, i.e.

$$\lambda_\alpha = \ln \left(\frac{\sum_{\chi=1}^M P(\mathbf{X}(\alpha) = s_\chi \mid \mathbf{Y}(\alpha))}{P(\mathbf{X}(\alpha) = 0 \mid \mathbf{Y}(\alpha))} \right) \quad (4.8)$$

Together, these form the LLR-Vector for the OFDM symbol $\boldsymbol{\lambda} = [\lambda_1, \lambda_2, \dots, \lambda_N]$. A value $\lambda_\alpha > 0$ indicates that the subcarrier is likely to have been selected as active during modulation, while $\lambda < 0$ indicates inactivity.

Following the derivation provided in Appendix E, Equation 4.8 has a closed form given by

$$\lambda_\alpha = \ln \left(\frac{k}{M(L-k)} \right) + \ln \left(\sum_{\chi=1}^M \exp \left(-\frac{1}{N_{0,F}} |\mathbf{Y}(\alpha) - \mathbf{H}(\alpha)s_\chi|^2 \right) \right) + \frac{|\mathbf{Y}(\alpha)|^2}{N_{0,F}} \quad (4.9)$$

Using this method we can select the active subcarriers indices, $\hat{\mathbf{I}}_g$ as those indices with positive LLR values while those with negative LLRs are considered inactive. In some cases the number of positive LLRs per sub-block, \hat{k} , may be greater than k , which will lead to incorrect detection of both index and data bits. We therefore employ an error correction algorithm, described rigorously in Appendix G, which yields the most optimal \hat{k} -element activation pattern, $\hat{\mathbf{I}}_g$, given the initial \hat{k} -element decoded activation pattern. For each of the L subcarriers per block, Equation 4.9 entails M complex multiplications (one per LSE term), such that the complexity per sub-block is $\mathcal{O}(ML)$.

Furthermore, once we have decided on $\hat{\mathbf{I}}_g$, we are then presented with two options for detection of the symbols at such indices. One option is to perform OTE on the received symbol vector and selecting the data symbols as those symbols at the indices $\hat{\mathbf{I}}_g$ in $\hat{\mathbf{Y}} = \mathbf{Y}/\mathbf{H}$. This is computationally cheap as we are already required to compute \mathbf{H} (via an FFT) for the LLR calculations so the only overhead is N complex multiplications per symbol yielding an overall complexity of $\mathcal{O}(GML + N) = \mathcal{O}(N(M + 1))$. Alternatively, we can carry out an ML detection procedure over the deduced set of active subcarrier indices. In such a scenario, the g th sub-block's data symbols are given by

$$\hat{\mathbf{S}}_g = \arg \min_{\mathbf{S}_g \in \mathcal{S}} \sum_{\gamma=1}^k |\mathbf{Y}_g(\hat{\mathbf{I}}_g(\gamma)) - \mathbf{H}_g(\hat{\mathbf{I}}_g(\gamma))\mathbf{S}_g(\gamma)|^2 \quad (4.10)$$

for $g = 1, 2, \dots, G$. Given there are k active subcarriers, for each we trial M^k possible M -Ary symbol vector, such that the complexity is $\mathcal{O}(M^k)$, yielding an overall complexity of $\mathcal{O}(GM(L + M^{k-1}))$ per symbol.

4.1.1.3 Performance

We begin this analysis by looking at the two special cases of GSIM-OFDM, originally presented as SIM-OFDM [27] and ESIM-OFDM [25]. These two cases are considered the extremities of GSIM-OFDM such that they will help to formulate an argument for the optimal block-length and number of active subcarriers per block. In the following analysis, assume a power reallocation policy in which the power saved from utilising a subset of the available carrier is reallocated to the activated subcarriers, unless stated otherwise.

Special Case - SIM-OFDM ($L = N$, $k = N/2$)

SIM-OFDM is the original formulation of IM-OFDM presented in [27]. It considers the case where there is only one sub-block, with half the subcarriers chosen as active. Unlike what is presented in Appendix F, the original formulation did not use the combinadics approach to subcarrier mapping, which enabled a low complexity

threshold detection strategy [27], however it was shown to be susceptible to errors and so will not be considered.

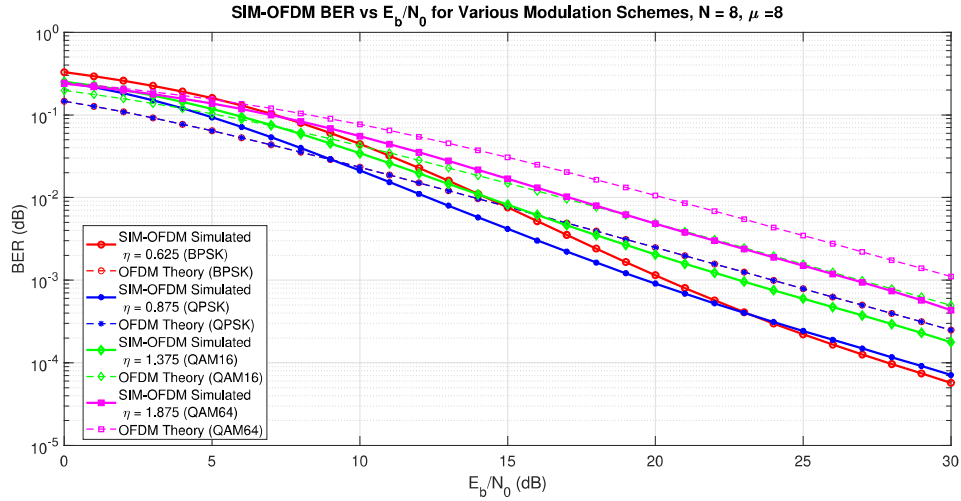


Figure 4.2: BER of SIM-OFDM using the LLR detector of GSIM-OFDM

Figure 4.2 shows the BER performance of SIM-OFDM using the LLR detector and one-tap-equalisation. In this case, we chose $N = L = 8$ and $k = 4$ which yields a relatively poor spectral efficiency in comparison to the other schemes we shall discuss since $\mu = N$, however this was necessary to ensure that the index-mapping look-up-tables (of size C_k^L) did not grow obscenely large, preventing excess memory utilisation during simulation. SIM-OFDM+QPSK first out performs its conventional OFDM counterpart after $E_b/N_0 = 9$ dB while for BPSK this occurs after 15db. In comparison, QAM-64 has better performance than its OFDM counterpart for all values of E_b/N_0 while QAM-16 offers better performance for $E_b/N_0 > 7.5$ dB. As the E_b/N_0 grows we see SIM-OFDM+BPSK decreases in BER at a greater rate than other curves such that for E_b/N_0 greater than 24dB SIM-OFDM+BPSK out performs all other schemes. Furthermore we see the SIM-OFDM+QAM-64 performance approach that of conventional OFDM+QAM-16 for $E_b/N_0 > 20$ dB, with SIM-OFDM+QAM-16 approaching the performance of OFDM+BPSK for $E_b/N_0 > 15$ dB.

Special Case - ESIM-OFDM ($L = 2, k = 1$)

On the other hand, ESIM-OFDM [25] considers the scenario in which we minimise the sub-block length, setting it to 2 with 1 active subcarrier. One drawback of SIM-OFDM is its ability to propagate errors, arising from the fact that if the activation pattern is incorrectly deduced then the subcarriers chosen for constellation demodulation will be wrong across the whole OFDM symbol. By limiting the sub-block length to 2, an incorrect subcarrier activation pattern (which will be of the form $\hat{\mathbf{I}}_g = [i_1]$ with $i_1 \in \{1, 2\}$) will lead to incorrect detection of only the single symbol within the corresponding sub-block, preventing any error propagation. This prevention of error

propagation comes at the cost to spectral efficiency, given by

$$\eta_{ESIM-OFDM} = \frac{N}{N + \mu} \left(\frac{\log_2(M)}{2} + \frac{1}{2} \right) \quad (4.11)$$

While the LLR detector may be employed, ESIM-OFDM also presents a viable reduced complexity detection strategy. Since each of the $N/2$ sub-block contains only two subcarriers, a simply way to detect which is active is by measuring which one has more power. Naturally, the one with more power we can expect to be active, such that we may write

$$\hat{I}_g = \begin{cases} 1 & \text{when } |\hat{\mathbf{X}}_g(1)|^2 > |\hat{\mathbf{X}}_g(2)|^2 \\ 2 & \text{otherwise} \end{cases} \quad g = 1, 2, \dots, \frac{N}{2} \quad (4.12)$$

Where $\hat{\mathbf{X}}_g$ is the g th one-tap-equalised received symbol vector, following OFDM demodulation. This process requires 2 complex multiplications per sub-block, in addition to N complex multiplications for OTE, such that the complexity is $\mathcal{O}(2 \cdot \frac{N}{2} + N) = \mathcal{O}(2N)$ complex multiplications per symbol.

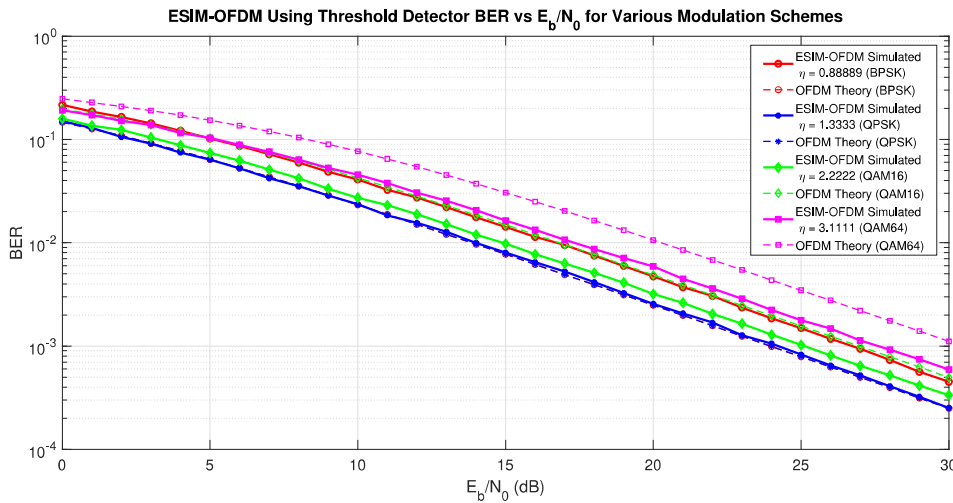


Figure 4.3: BER of ESIM-OFDM over a Rayleigh fading channel using the threshold detector

Figure 4.3 shows the BER vs. E_b/N_0 curve of ESIM-OFDM for various modulation types using the simple threshold detector contrasted against the analytical performance of conventional OFDM. We can see that for the case of BPSK, ESIM-OFDM performs significantly worse than conventional OFDM over the entire range of E_b/N_0 . However, as the constellation order grows, the BER improves significantly relative to the corresponding OFDM schemes, such that in the case of ESIM-OFDM+QAM-64 we see performance gains over all E_b/N_0 values. However, at such constellation orders the spectral efficiency falls greatly behind that of conventional OFDM since each data symbol conveys proportionally more information.

To improve upon the performance for lower order constellations, we may turn our attention to the performance of the LLR detector with one-tap-equalisation, shown in Figure 4.4. In the case of both BPSK and QPSK, the LLR detector outperforms the threshold detector for all values of the E_b/N_0 , however, as the modulation order grows the threshold detector approaches equivalent performance, particularly at low values of the E_b/N_0 . Compared to conventional OFDM, QPSK, QAM-16 and QAM-64 are able to outperform their corresponding conventional OFDM schemes for all E_b/N_0 values, while for BPSK this is only the case for $E_b/N_0 > 14$ dB.

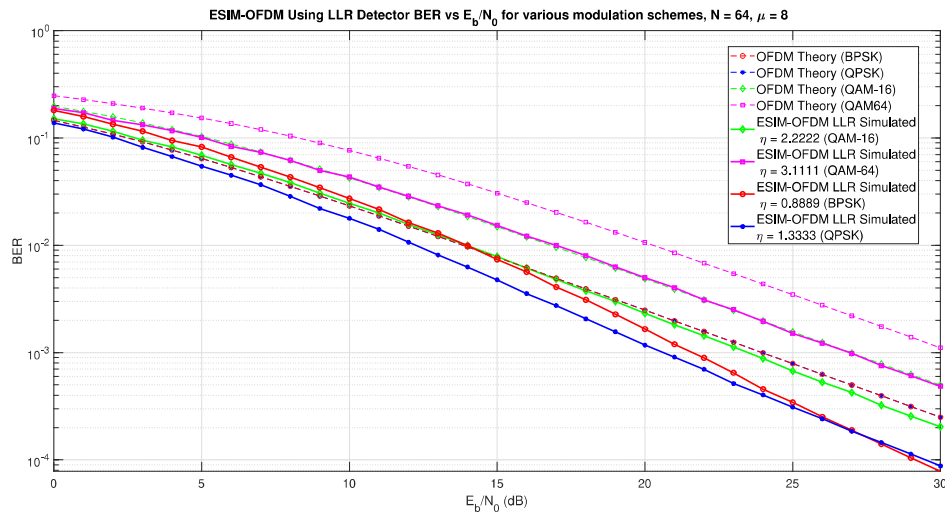


Figure 4.4: BER of ESIM-OFDM using the LLR detector over a Rayleigh fading channel

Comparing the ESIM-OFDM LLR performance to that of SIM-OFDM, we see that the QAM-16 and QAM-64 schemes marginally favour SIM-OFDM for high values of E_b/N_0 , however at lower values ESIM-OFDM considerably outperforms. In the case of BPSK and QPSK, we see that the ESIM-OFDM curves decay more gradually yielding better performance than the corresponding SIM-OFDM schemes at low values of E_b/N_0 , worse performance throughout the 10 – 20dB region, and marginally so at higher values.

These observations may be reasoned as follows. For low order constellations, the index bits proportionally carry a lot of weight, which is maximised by having a long sub-block length. Therefore, when the E_b/N_0 is high and the LLR detectors ability to distinguish active versus inactive subcarriers is at its highest, the low order schemes with long sub-blocks, such as SIM-OFDM+BPSK, will see BER gains over the ESIM-OFDM counterparts. When an error occurs for SIM-OFDM at these noise levels it is catastrophic to the symbol, but it occurs so infrequently that it is outweighed by the gain in BER achieved via repeated correct detection of the index bits. As the modulation order grows the index bits carry proportionally much less information

than the data bits such that BER is minimised by preventing error propagation of incorrect activation patterns. Therefore, when the E_b/N_0 is low and low the ability of the LLR to detect active subcarriers is poor, schemes with long sub-block lengths are heavily penalised causing favourable performance for GSIM-OFDM.

General Case - GSIM-OFDM ($L = 8, k = 4$)

We have seen from ESIM-OFDM preventing error propagation is important, but this comes at the cost of spectral efficiency, which is maximised with a long sub-block length. Therefore, to compromise we realise our GSIM-OFDM scheme with $L = 8$, such that for $N = 64$ we have $G = 8$ independent sub-blocks. Furthermore, to maximise spectral efficiency, we must maximise C_k^L which is achieved when $k = L/2 = 4$. The BER performance of this configuration of GSIM-OFDM over a range of modulation schemes can be seen in Figure 4.5. In comparison to the ESIM-OFDM scheme shown in Figure 4.3, at low values of E_b/N_0 we see GSIM-OFDM displaying favourable performance, with GSIM-OFDM achieving a BER slightly below that of SIM-OFDM across all modulation types. However, as the E_b/N_0 increases the GSIM-OFDM performance begins to approach ESIM-OFDM. For $E_b/N_0 > 20$ dB all of the modulation schemes under review perform better than their conventional OFDM counterparts. This suggests GSIM-OFDM with LLR detection should be employed in environments where the signal power is considerably greater than that of the noise. Under harsher channel conditions, ESIM-OFDM is favourable which achieves performance gains at the cost spectral efficiency.

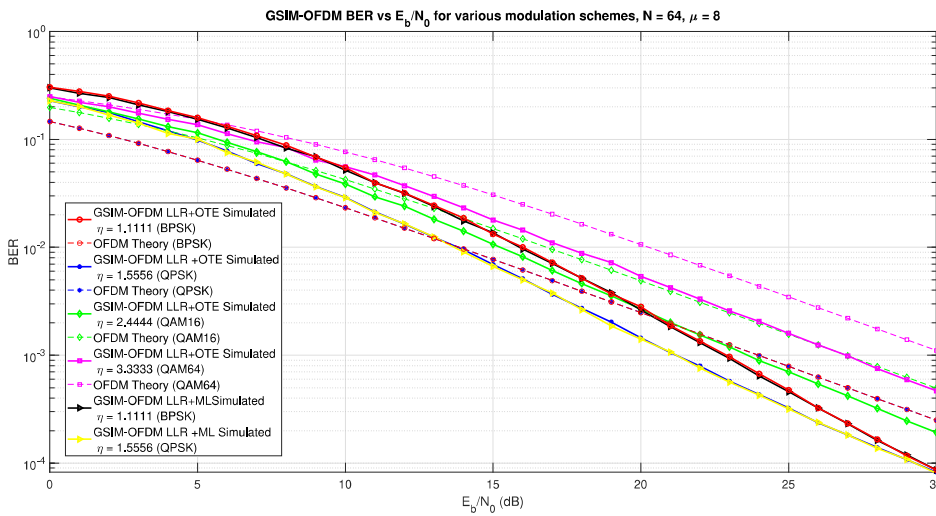


Figure 4.5: BER of GSIM-OFDM using an LLR Detector compared against conventional OFDM and against the choice of an ML vs. OTE output stage.

Also contrasted on Figure 4.5 is the performance of GSIM-OFDM when using the LLR detector followed by ML detection versus one-tap-equalisation. It is clear to see that the ML approach achieves performance equal to that of LLR detection followed

by one-tap-equalisation, despite the former's considerably higher complexity, making OTE a better approach.

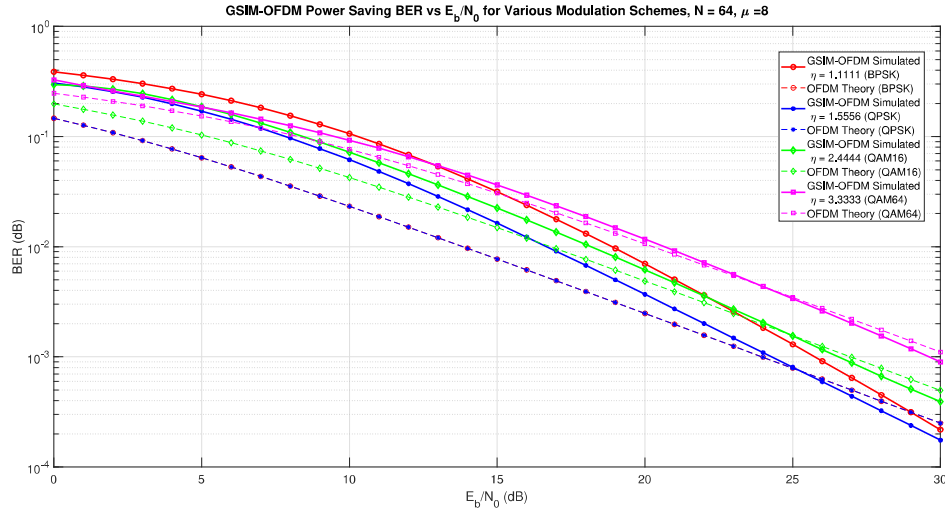


Figure 4.6: GSIM-OFDM BER performance over a rayleigh fading channel using a power saving policy (Curve fit)

Finally, Figure 4.6 shows the BER performance of GSIM-OFDM using a power saving policy in which the activated subcarriers are allocated equal power to as if they were part of a conventional OFDM scheme. While this does not change the PAPR of the signal (since both the peak and average power are scaled equally), it reduces the average power of the signal, which may be more beneficial in low power scenarios, or devices which can only afford power amplifiers with a small dynamic range. As we might expect, the performance is considerably worse than the power reallocation policy shown in Figure 4.5, yet for E_b/N_0 values beyond 25dB the power saving scheme achieves better performance in the case of QPSK, QAM-16 and QAM-64, than their conventional OFDM counterparts. For BPSK the crossover is achieved slightly delayed at 29dB, such that this scheme is still viable provided sufficiently good channel conditions.

Power Considerations

Now considering power, the CCDF of IM-OFDM can be seen in Figure 4.7. As expected since both ESIM-OFDM and GSIM-OFDM utilise half of the available subcarriers, they have a similar CCDF, which is shifted left to that of conventional OFDM, representing a lower average PAPR. Measuring the PAPR at the 10% line for $N = 64$, we see that 10% of index modulated symbols have PAPR greater than 7.9dB, down from 8dB in conventional OFDM.

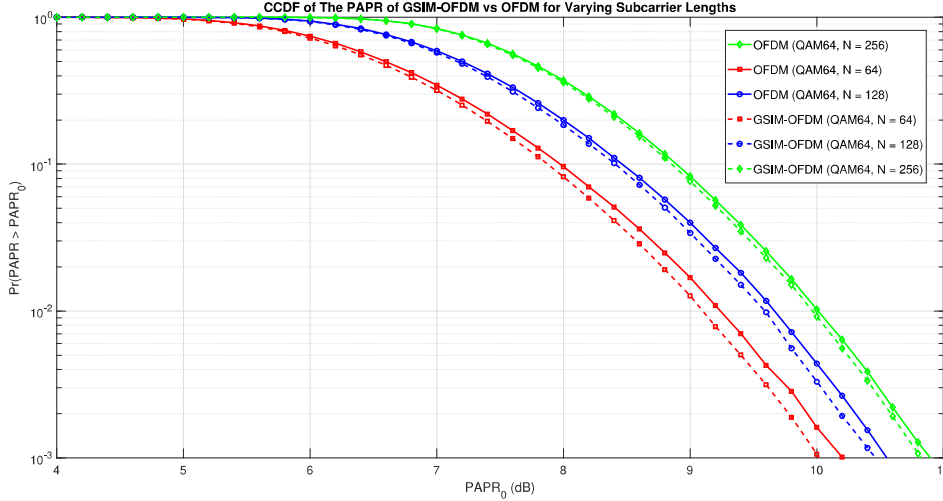


Figure 4.7: CCDF of GSIM-OFDM vs conventional OFDM for $N = \{64, 128, 256\}$

4.1.2 EGSIM-OFDM

We have now presented a generalised theory of IM-OFDM, however, if we are to plot the spectral efficiency of each scheme we see Figure 4.8. It is clear to see that beyond

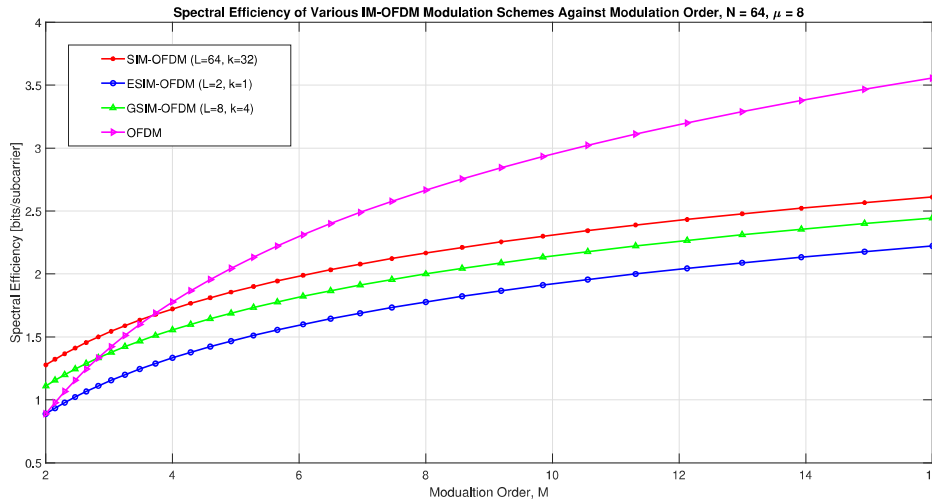


Figure 4.8: Spectral efficiency of the previous IM-OFDM schemes

BPSK ($M = 2$) the spectral efficiency gains of GSIM-OFDM are lost. EGSIM-OFDM aims to counteract this through further parameterisation of our IM-OFDM system to increase the number of permutations of each sub-block, requiring more index bits to encode.

4.1.2.1 Modulation

The approach to EGSIM-OFDM [28] generalises upon GSIM-OFDM by defining an activation *set* of $R \leq L + 1$ activation counts $\mathbf{K} = \{k_1, k_2, \dots, k_R\}$ with $k_r \in$

$\{0, \dots, L\}$. With each sub-block we select an element $k_r \in \mathbf{K}$ as the number of active subcarriers, from which we denote the corresponding set of active subcarrier indices for the g th sub-block corresponding to the r th activation count, $\mathbf{I}_r^{(g)}$, to be

$$\mathbf{I}_r^{(g)} = [i_1, i_2, \dots, i_{k_r}] \quad (4.13)$$

where, $i_\gamma \in \{1, 2, \dots, L\}$ for $\gamma = 1, 2, \dots, k_r$ and $g = 1, 2, \dots, G$. What's key to note is that the value of k_r used by a sub-block for any given symbol period varies from one symbol period to the next. Recalling that the incoming p bits allocated to the sub-block are divided into two sets of bits of lengths p_1 and p_2 , in EGSIM-OFDM the value of p_1 and p_2 vary from symbol-to-symbol, depending on the contents of \mathbf{b}_g , however, $p = p_1 + p_2$ remains constant. Heuristically, we can see that a gain in spectral efficiency is achievable by encoding additional data in terms of the additional permutations which arise from varying ratio with which p bits are split into p_1 and p_2 bits. Corresponding to each k_r there are $N_S^{(r)} = M^{k_r}$ valid transmissible M -Ary symbol vectors, each denoted $\mathbf{S}_r = [s_1, s_2, \dots, s_{k_r}]$ with $s_i \in \mathcal{M}$, leading to the set of possible symbol vectors corresponding to the r th activation count $\mathcal{S}_r = \{\mathbf{S}_r^{(1)}, \mathbf{S}_r^{(2)}, \dots, \mathbf{S}_r^{N_S^{(r)}}\}$. Therefore, considering all R activation counts, the set of all possible transmissible symbol vectors is

$$\mathcal{S} = \{\mathcal{S}_1, \mathcal{S}_2, \dots, \mathcal{S}_R\} \quad (4.14)$$

With this formulation, the total number of bits that can be transmitted by all $k_r \in \mathbf{K}$ per sub-block, p , is given by [28]

$$p = \left\lfloor \log_2 \left(\sum_{k_r \in \mathbf{K}} M^{k_r} \cdot C(L, k_r) \right) \right\rfloor \quad (4.15)$$

It follows that $\mathbf{K} = \{0, 1, \dots, L\}$ yields the best spectral efficiency [28] (for BPSK) - each sub-block has $L + 1$ possible subcarrier activation patterns and therefore, this leads to $L + 1$ different ways in which p can be divided. In a similar way to how a constellation can increase throughput by having more constellation points, the EGSIM-OFDM modulator increases throughput by having more states for the lengths of p_1 and p_2 . We may thus write the EGSIM-OFDM spectral efficiency as

$$\eta_{EGSIM-OFDM} = G \cdot \frac{\lfloor \log_2 (\sum_{k_r \in \mathbf{K}} M^{k_r} \cdot C(L, k_r)) \rfloor}{N + \mu} \quad (4.16)$$

By varying the number of active subcarriers per sub-block, the mapping policy is not as simple as that of GSIM-OFDM. First we must map the of index bits to a value of p_2 , from which p_1 may be deduced, and then for each k_r we must generate a unique index-mapping LUT which maps the p_1 index bits to a length k_r activation pattern, $\mathbf{I}_r^{(g)}$. A detailed example of how this is achieved is discussed in Appendix H.

4.1.2.2 Detection

In the case of EGSIM-OFDM, ML Detection has a complexity of $\mathcal{O}(G \sum_{r=1}^R 2^{p_1^{(r)}} M^{k_r})$ per symbol, where $p_1^{(r)}$ is the number of index bits corresponding to the r th activation count, which is entirely unfeasible. Therefore, only LLR detection will be considered as it provides suitable accuracy while approaching a sufficient complexity for real-time operation.

We therefore proceed by reforming Equation 4.9 into one which depends on $k_r \in \mathbf{K}$, such that for the g th sub-block, in consideration of the r th activation pattern, the LLR at subcarrier α is given

$$\lambda_{r,\alpha}^{(g)} = \ln \left(\frac{k_r}{L - k_r} \right) + \ln \left(\sum_{\chi=1}^M \exp \left(- \frac{1}{N_{0,F}} |\mathbf{Y}_g(\alpha) - \mathbf{H}_g(\alpha)s_\chi|^2 \right) \right) + \frac{|\mathbf{Y}_g(\alpha)|^2}{\sigma_n^2} \quad (4.17)$$

for $\alpha = 1, 2, \dots, L$. The complexity of this computation is $\mathcal{O}(RML)$ complex multiplications per sub-block, since we generate R LLR-vectors, corresponding to each k_r .

For each of the G sub-blocks we then consider each $k_r \in \mathbf{K}$ and select the subcarriers with $\lambda_{r,\alpha}^{(g)} > 0$ and assemble them into $\tilde{\mathbf{I}}_r^{(g)}$, applying the error correction procedures discussed in Appendix G to ensure a valid index pattern. This yields a set of possible activation patterns for the g th sub-block given by $\tilde{\mathcal{I}}_g = \{\tilde{\mathbf{I}}_1^{(g)}, \tilde{\mathbf{I}}_2^{(g)}, \dots, \tilde{\mathbf{I}}_R^{(g)}\}$. We proceed with an ML detection strategy, which for each $\tilde{\mathbf{I}}_\gamma^{(g)} \in \tilde{\mathcal{I}}_g$, $\gamma = 1, 2, \dots, R$, computes a distance metric over all possible transmissible symbol vectors. $(\hat{\mathbf{I}}_r^{(g)}, \hat{\mathbf{S}}_r^{(g)})$ are therefore the optimal LLR decoded activated subcarriers and data symbols which minimise the metric

$$(\hat{\mathbf{I}}_r^{(g)}, \hat{\mathbf{S}}_r^{(g)}) = \arg \min_{\tilde{\mathbf{I}}_r^{(g)} \in \tilde{\mathcal{I}}_g, \tilde{\mathbf{S}}_r^{(g)}(\gamma) \in \mathcal{S}_r} \left(\sum_{\xi \notin \tilde{\mathbf{I}}_r^{(g)}} |\mathbf{Y}_g(\xi)|^2 + \sum_{\gamma=1}^{k_r} |\mathbf{Y}_g(\tilde{\mathbf{I}}_r^{(g)}(\gamma)) - \mathbf{H}_g(\tilde{\mathbf{I}}_r^{(g)}(\gamma)) \tilde{\mathbf{S}}_r^{(g)}(\gamma)|^2 \right) \quad (4.18)$$

for $g = 1, 2, \dots, G$. The first sum in this metric is the power of the supposed inactive subcarriers - ideally this is zero, but otherwise it should be minimised which is why it is included in Equation 4.18. Given that for each realisation of the activation pattern, there are k_r active subcarriers, each of which can take one of M possible values, the complexity of the second term in Equation 4.18 is $\mathcal{O}(\sum_{r=1}^R M^{k_r})$. Equally, the first term requires $L - k_r$ complex multiplications for each $k_r \in \mathbf{K}$, yielding a complexity of $\mathcal{O}(\sum_{r=1}^R (L - k_r))$. Therefore, for the entire LLR base detector we have a complexity of $\mathcal{O}(G(RML + \sum_{r=1}^R (M^{k_r} + (L - k_r))))$ per symbol.

Once the index pattern and corresponding symbol vector have been deduced, $\hat{\mathbf{S}}_r^{(g)}$ is constellation demodulated to yield that data bits of the g th sub-block, while a $\hat{\mathbf{I}}_r^{(g)}$

is input to a reverse look-up operation on the previously generated index-mapping LUT corresponding to k_r , carrying out the inverse of the operations in Appendix H to deduce the index bits.

4.1.2.3 Performance

In the EGSIM-OFDM mapping scheme the $p \rightarrow p_2$ map has 2^p keys, where p is given by Equation 4.15. Therefore, for $M = 16$, $L = 8$ and $\mathbf{K} = \{1, 3, 5\}$, the table would have 33554432 elements, which was unfeasible to realise in a MATLAB simulation. We can combat this by using lower order modulation schemes, and therefore only BPSK and QPSK will be considered in this analysis. None the less, the resulting BER curve seen is shown in Figure 4.9 contrasted against the performance of ESIM-OFDM and GSIM-OFDM using LLR detection. The dashed line shows the baseline performance achieved by conventional OFDM with BPSK.

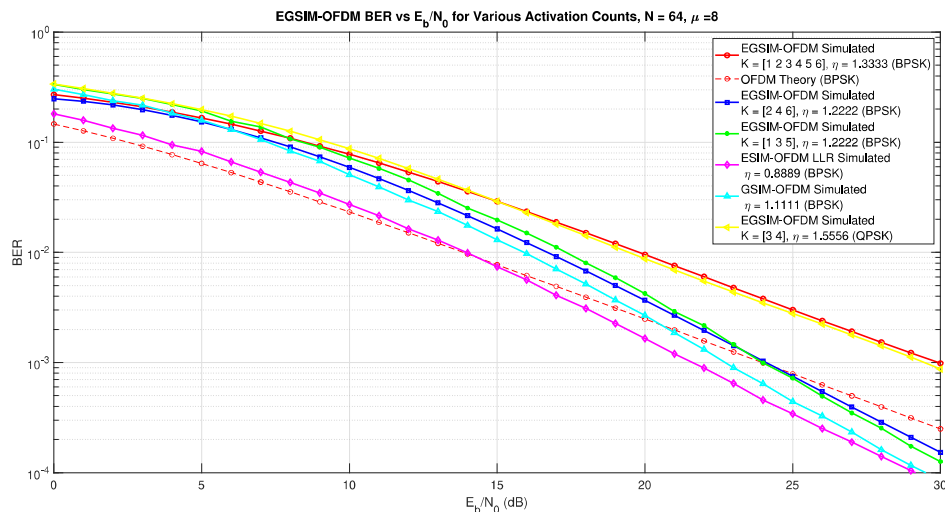


Figure 4.9: BER of EGSIM-OFDM for various realisations of \mathbf{K} compared against other IM-OFDM schemes and conventional OFDM

We can see that the BER performance of EGSIM-OFDM varies with the choice of \mathbf{K} and with the constellation type. For $E_b/N_0 < 25$ dB, the EGSIM-OFDM scheme performs worse than conventional OFDM, after which the EGSIM-OFDM+BPSK schemes with three element activation sets start to see BER gains. However, When $K = \{1, 2, 3, 4, 5, 6\}$, the performance is considerably degraded since the LLR detector must distinguish between a greater number of activation states, which incurs more frequent errors. When a QPSK based EGSIM-OFDM scheme with $\mathbf{K} = \{3, 4\}$ is employed, the performance roughly matches that of BPSK with $\mathbf{K} = \{1, 2, 3, 4, 5, 6\}$, giving it a worse BER across all E_b/N_0 values in comparison to conventional OFDM+QPSK. The $\mathbf{K} = \{1, 3, 5\}$ and $\mathbf{K} = \{2, 4, 6\}$ schemes offer a 0.1111 [bits/subcarrier] increase in spectral-efficiency over GSIM-OFDM, and 0.333 [bits/subcarrier] increase over

both ESIM-OFDM and conventional OFDM with BPSK. For $N = 64$ this equates to 7.1 and 21.3 additional bits per OFDM symbol respectively, which is a considerable increase in throughput.

Table I.1 of Appendix I shows numerical values for the complexity of each IM scheme in terms of the number of complex multiplications per OFDM symbol. These results can be contrasted against Appendix K which derives a figure for the number of complex multiplications permitted per symbol in order to realise a bit-rate of 20Mbps, as a function of M . The general trend shows that LLR detection with one-tap-equalisation is the lowest complexity approach, except for the case of ESIM-OFDM where the use of a threshold detector enables a very efficient operation which has complexity $\mathcal{O}(128)$ independent of M . Each of the (E/G)SIM-OFDM schemes which employed LLR+OTE have equal complexity, some of which are less feasible due to the size of index-mapping LUT which must be realised. Finally, in all cases EGSIM-OFDM required a greater number of computations than GSIM-OFDM which means its use depends on whether the gain in spectral efficiency is sufficient to offset the greater power and delay. We notice the LLR detectors have complexity slightly above the limits derived in Appendix K, therefore, future approaches may wish to consider low-complexity LLR detectors, such as that of [29].

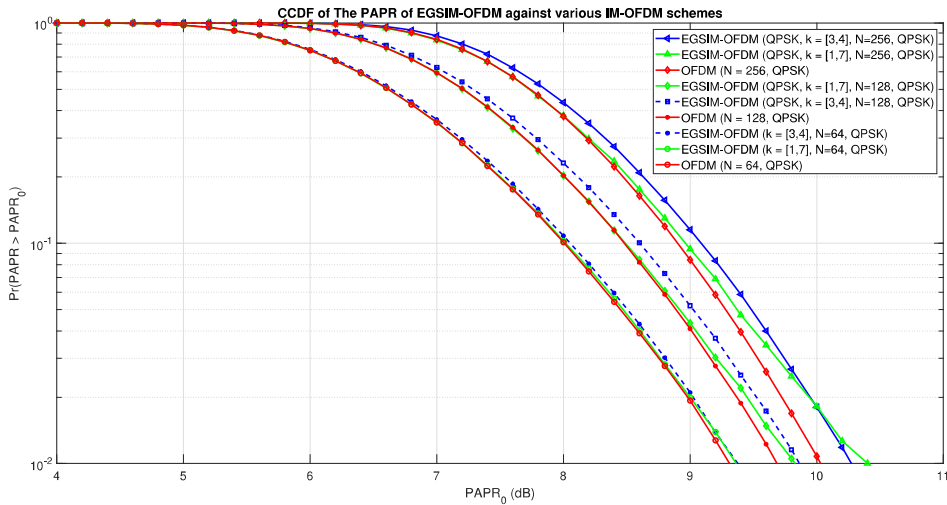


Figure 4.10: CCDF of the PAPR of EGSIM-OFDM for various realisations of \mathbf{K} with $L = 8$, $N = 64$

Figure 4.10 shows the CCDF of the PAPR of EGSIM-OFDM compared against GSIM-OFDM and conventional OFDM for various realisations of \mathbf{K} . We observe that the $\mathbf{K} = \{1, 7\}$ scheme has a PAPR worse than that of conventional OFDM. We can deduce that this arises as a result of having two activation counts which are vastly different in magnitude, leading to large variations in power from symbol-to-symbol, and thus a large PAPR. The $\mathbf{K} = \{3, 4\}$ scheme improves upon the $\mathbf{K} = \{1, 7\}$ scheme, but remains higher than the PAPR achieved by conventional OFDM.

4.2 Multi Mode Index Modulation

We have previously shown that we can use single-mode IM to reduce the PAPR of OFDM while also achieving similar BER performance over fading channels, with varying success of throughput loss mitigation. However, for higher order constellations the bits conveyed by each symbol greatly outweighs the additional data inferred through the subcarrier mapping leading to a spectral efficiency loss. The multi-mode family of index modulation schemes aims to provide a solution here by utilising all of the OFDM subcarriers in a way which employs multiple different constellation alphabets such that index bits may be inferred not by whether a subcarrier is active or inactive, but instead based on which constellation the received symbol belongs to.

4.2.1 DM-OFDM

Figure 4.11 shows the block diagram of the DM-OFDM [30] modulator-demodulator pair. We can see that in comparison to the single mode case presented in Figure 4.1, the modulator now features two constellation mappers, each of which have the corresponding alphabets \mathcal{M}_A and \mathcal{M}_B .

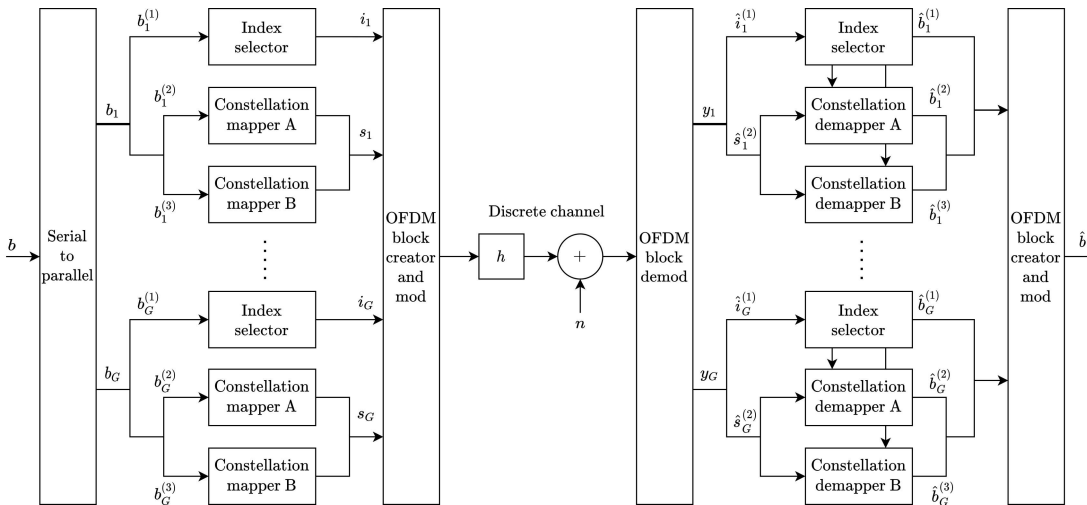


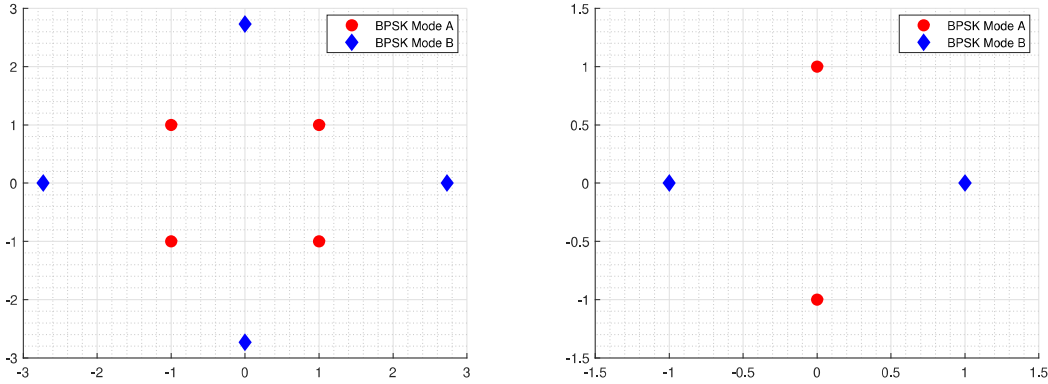
Figure 4.11: Block diagram for the dual mode index modulated system, recreated [30]

More so than single-mode OFDM, an important part of DM-OFDM is constellation design. It is important that the two constellations are differentiable at the receiver, and therefore $\mathcal{M}_A \cap \mathcal{M}_B = \emptyset$. This can be achieved by taking an M -Ary constellation and splitting it into two M_A -Ary and M_B -Ary constellations such that $M = M_A + M_B$. As an example, Figure 4.12a shows a modified 8-QAM constellation, split into two subsets where $\mathcal{M}_A = \{\pm 1 \pm j\}$ and $\mathcal{M}_B = \{1 + \sqrt{3}, (1 + \sqrt{3})j, -1 - \sqrt{3}, (-1 - \sqrt{3})j\}$. In this case average power is given by averaging the square of the euclidean distance

of a point from \mathcal{M}_A and \mathcal{M}_B to the origin.

$$P_{avg} = \frac{(\sqrt{2})^2 + (1 + \sqrt{3})^2}{2} = 3 + \sqrt{3}$$

Therefore, to make the average power unitary, we divide each complex symbol by a factor $\sqrt{3 + \sqrt{3}}$. In the case of Figure 4.12b the normalisation factor is simply 1.



(a) A modified 8-QAM constellation split into two QPSK constellations (dual-QPSK)
(b) A QPSK constellation split into two BPSK constellations (Diamond dual-BPSK)

4.2.1.1 Modulation

The modulation approach for DM-OFDM is equivalent to that of GSIM-OFDM, except now the p bits attributed to each sub-block is divided into p_1 index bits, and $p_2 + p_3$ data bits. The p_1 index bits, denoted $\mathbf{b}_g^{(1)}$, encode the C_k^L realisations of the length L sub-block with k subcarriers from mapper-A and $L - k$ subcarriers from mapper-B. Therefore, as was the case in GSIM-OFDM

$$p_1 = \lfloor \log_2(C_k^L) \rfloor$$

Equally, the k subcarriers attributed to mapper-A, can modulate

$$p_2 = k \log_2(M_A) \quad (4.19)$$

bits, while the $L - k$ subcarriers attributed to mapper-B modulate

$$p_3 = (L - k) \log_2(M_B) \quad (4.20)$$

bits. This yields a spectral efficiency improved upon that of GSIM-OFDM given by

$$\eta_{DM-OFDM} = G \cdot \frac{\lfloor \log_2(C_k^L) \rfloor + k \log_2(M_A) + (L - k) \log_2(M_B)}{N + \mu} \quad (4.21)$$

In the case where $M_A = M_B = M$, as we have shown in the example constellations, then $\eta_{DM-OFDM}$ reduces to

$$\eta_{DM-OFDM} = G \cdot \frac{\lfloor \log_2(C_k^L) \rfloor + L \log_2(M)}{N + \mu} \quad (4.22)$$

Comparing this to GSIM-OFDM we see that $\eta_{DM-OFDM} \geq \eta_{GSIM-OFDM}$ since $L > k$. Furthermore, the spectral efficiency is at maximum when $k = L/2$, as per Figure 4.13. To balance error propagation and complexity we shall once again employ a sub-block length of $L = 8$.

Index bits	I_A	Sub-block
[0, 0]	[1, 2]	$[s_A^{(1)}, s_A^{(2)}, s_B^{(1)}, s_B^{(2)}]$
[0, 1]	[2, 3]	$[s_B^{(1)}, s_A^{(1)}, s_A^{(2)}, s_B^{(2)}]$
[1, 0]	[3, 4]	$[s_B^{(1)}, s_B^{(2)}, s_A^{(1)}, s_A^{(2)}]$
[1, 1]	[1, 4]	$[s_A^{(1)}, s_B^{(1)}, s_B^{(2)}, s_A^{(2)}]$

Table 4.1: Example DM-OFDM Subcarrier index pattern LUT.

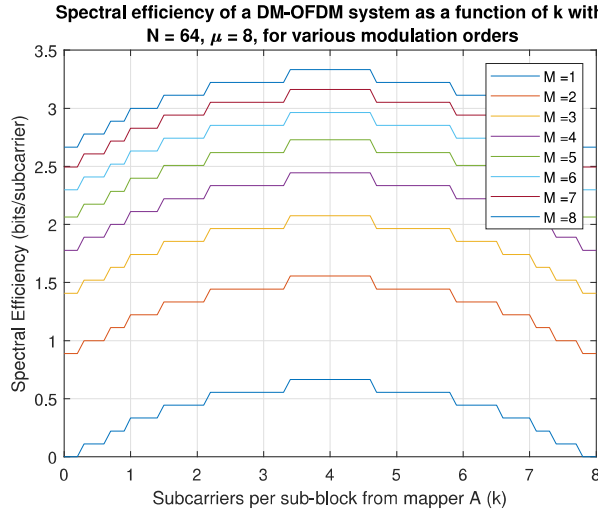


Figure 4.13: Spectral efficiency of a DM-OFDM as a function of the number of subcarrier taken from mapper-A with $N = 64$ and $\mu = 8$ over a range of modulation orders.

The index-mapping process maps the p_1 index bits to one of $N_I = 2^{p_1}$ activation patterns, $\mathbf{I}_A = [i_1, i_2, \dots, i_k]$ with $i_\gamma \in 1, 2, \dots, L$ for $\gamma = 1, 2, \dots, k$, which describes the indices of the mapper-A modulated symbols. This fully describes the sub-block's state since the mapper-B activation pattern, \mathbf{I}_B , is the complement of mapper-A's. Therefore, the set of all distinct index patterns for mapper-A is given as

$$\mathcal{I}_A = \{\mathbf{I}_A^{(1)}, \mathbf{I}_A^{(2)}, \dots, \mathbf{I}_A^{(N_I)}\} \quad (4.23)$$

As an example, Table 4.1 shows the possible values of \mathbf{I}_A in the case where $p_1 = 2$, $L = 4$, $k = 2$ and the corresponding index modulated sub-block.

The process of transforming a set of index bits to a unique subcarrier index pattern is exactly equivalent as what was discussed in Appendix F for IM-OFDM, such that the same combinadics approach is employed. In general, since there are M_A choices for the k symbols from mapper-A and M_B choices for the $L - k$ symbols from mapper-B, then there are $N_S = M_A^k M_B^{L-k}$ elements in the set of all transmissible symbol vectors corresponding to each \mathbf{I}_A . Each element of the set is an L element vector of complex symbols which we denote $\mathbf{S}_{\mathbf{I}_A} = [s_1, s_2, \dots, s_L]$ for $j = 1, 2, \dots, N_S$, with $s_\gamma \in \mathcal{M}_A$ for $\gamma = 1, 2, \dots, k$. The set of all possible transmissible symbol vector from mapper-A, given an index pattern \mathbf{I}_A , is therefore constructed as

$$\mathcal{S}_{\mathbf{I}_A} = \{\mathbf{S}_{\mathbf{I}_A}^{(1)}, \mathbf{S}_{\mathbf{I}_A}^{(2)}, \dots, \mathbf{S}_{\mathbf{I}_A}^{(N_S)}\} \quad (4.24)$$

Therefore, since each valid set of N_S symbol vectors corresponds to one of the N_I index patterns, there are $N_S N_I$ transmissible sub-blocks.

4.2.1.2 Detection

As with GSIM-OFDM an ML detection strategy is possible, however with 2^{p_1} different activation patterns, and $M_A^k M_B^{L-k}$ transmissible symbol vectors, it has a complexity of $\mathcal{O}(G2^{p_1}M_A^k M_B^{L-k})$ complex multiplications per OFDM symbol. This makes unfeasible to realise in actuality, so we shall only present an LLR detection strategy which uses a probabilistic approach to greatly reduce complexity while retaining near-ML performance [30].

In this LLR detector, the ratio of *a posteriori* probabilities, is that of whether a subcarrier belongs to \mathcal{M}_A or \mathcal{M}_B . We denote the vector of N LLR values as $\boldsymbol{\lambda} = [\lambda_1, \lambda_2, \dots, \lambda_N]^T$ with the LLR at subcarrier $\alpha = 1, 2, \dots, N$ given by

$$\lambda_\alpha = \ln \left(\frac{\sum_{j=1}^{M_A} P(\mathbf{X}(\alpha) = s_A^{(j)} | \mathbf{Y}(\alpha))}{\sum_{i=1}^{M_B} P(\mathbf{X}(\alpha) = s_B^{(i)} | \mathbf{Y}(\alpha))} \right) \quad (4.25)$$

where $\mathbf{X}(\alpha)$ is the frequency-domain complex symbol at subcarrier α , with $s_A^{(j)} \in \mathcal{M}_A$ and $s_B^{(i)} \in \mathcal{M}_B$. Based upon the full derivation provided in Appendix J, the closed form for Equation 4.25 can be stated as

$$\begin{aligned} \lambda_\alpha = & \ln \left(\frac{M_B k}{M_A (L - k)} \right) + \ln \left(\sum_{j=1}^{M_A} \exp \left(-\frac{1}{N_{0,F}} |\mathbf{Y}(\alpha) - \mathbf{H}(\alpha)s_A(j)|^2 \right) \right) - \\ & \ln \left(\sum_{i=1}^{M_B} \exp \left(-\frac{1}{N_{0,F}} |\mathbf{Y}(\alpha) - \mathbf{H}(\alpha)s_B(i)|^2 \right) \right) \end{aligned} \quad (4.26)$$

In this case $N_{0,F} = N_0$ since all subcarriers are utilised. In addition, both of the log-sum-exp terms of Equation 4.26 are susceptible to arithmetic overflow, and therefore the Jacobian exponential presented in Appendix D is employed.

We can then consider $\boldsymbol{\lambda}$ on a sub-block-by-sub-block basis by splitting it into G vectors of length L , i.e $\boldsymbol{\lambda} = [\boldsymbol{\lambda}_1, \boldsymbol{\lambda}_2, \dots, \boldsymbol{\lambda}_G]^T$ where $\boldsymbol{\lambda}_g = [\lambda_{L(g-1)+1}, \lambda_{L(g-1)+2}, \dots, \lambda_{Lg}]$ for $g = 1, 2, \dots, G$. If the LLR of a given subcarrier is positive then it is attributed to mapper-A, and if negative mapper-B. For each sub-block the index of the mapper-A attributed subcarriers are grouped together to form the trial index pattern, $\hat{\mathbf{I}}_A^{(i)}$. The same error correction technique described in Appendix G is employed to prevent selection of an invalid $\hat{\mathbf{I}}_A^{(i)}$. Once we have established an 'optimal' index pattern we still do not know the optimal M -Ary symbol at each subcarrier. In the OTE approach, given that $\hat{\mathbf{I}}_A \in \mathcal{I}_A$ and $\hat{\mathbf{I}} \in \mathcal{I}_B$ are the deduced index patterns, the symbols

$$\hat{\mathbf{S}}_{\hat{\mathbf{I}}_A} = \hat{\mathbf{X}}_g(\hat{\mathbf{I}}_A) \quad (4.27)$$

are passed to demapper-A while the remaining are passed to demapper-B, where $\hat{\mathbf{X}}_g = \mathbf{Y}_g / \mathbf{H}_g$ is the vector of one-tap equalised subcarriers for the g th sub-block. Another approach is to use an ML detector, which has reduced complexity in comparison to full-symbol ML detection since we know which mapper each subcarrier belongs to. To detect, the optimal set of symbols transmitted on the subcarriers at indices $\hat{\mathbf{I}}_A$ we minimise the metric

$$\hat{\mathbf{S}}_{\hat{\mathbf{I}}_A} = \arg \min_{\mathbf{S}_A \in \mathcal{S}_{\hat{\mathbf{I}}_A}} \sum_{\gamma=1}^k |\mathbf{Y}_g(\hat{\mathbf{I}}_A(\gamma)) - \mathbf{H}_g(\hat{\mathbf{I}}_A(\gamma)) \mathbf{S}_A(\gamma)|^2 \quad (4.28)$$

while to deduce $\hat{\mathbf{S}}_{\hat{\mathbf{I}}_B}$ we minimise

$$\hat{\mathbf{S}}_{\hat{\mathbf{I}}_B} = \arg \min_{\mathbf{S}_B \in \mathcal{S}_{\hat{\mathbf{I}}_B}} \sum_{\gamma=1}^{L-k} |\mathbf{Y}_g(\hat{\mathbf{I}}_B(\gamma)) - \mathbf{H}_g(\hat{\mathbf{I}}_B(\gamma)) \mathbf{S}_B(\gamma)|^2 \quad (4.29)$$

For each sub-block containing L subcarriers, we calculate and sum M_A LSE terms for mapper-A, and M_B terms for mapper-B, giving a complexity $\mathcal{O}(L(M_A + M_B))$ complex multiplications per sub-block. If the one-tap-equalisation approach is used the symbol complexity therefore becomes $\mathcal{O}(GL(M_A + M_B) + N) = \mathcal{O}(N(M_A + M_B + 1))$. Conversely, If we proceed ML detection with the knowledge of the index pattern, mapper-A (Equation 4.28) gives rise to M_A^k complex multiplications while the $L - k$ subcarriers attributed to mapper-B give rise to $M_B^{(L-k)}$ complex multiplications (Equation 4.29). Therefore, the complexity is $\mathcal{O}(G(L(M_A + M_B) + M_A^k + M_B^{(L-k)}))$ per OFDM symbol.

4.2.1.3 Performance

In comparison to the other schemes shown in Figure 4.14, DM-OFDM performs worse over most of the E_b/N_0 values. It is only at $E_b/N_0 = 25$ dB that dual-BPSK DM-OFDM overtakes conventional OFDM+QPSK. Once we approach 27dB we see that the dual-QPSK schemes overtake OFDM+QAM-8 and the dual-BPSK scheme overtakes GSIM-OFDM+QAM-16.

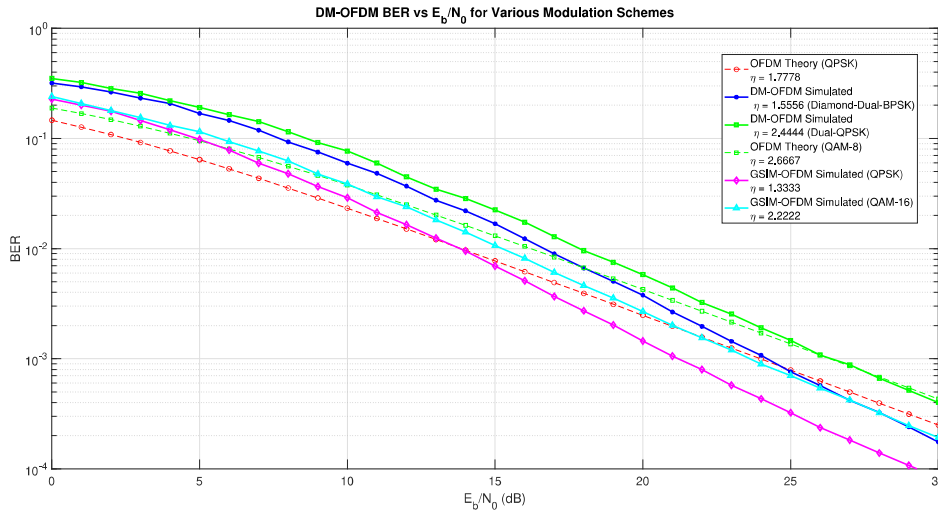


Figure 4.14: BER of DM-OFDM using LLR Detection with ML detector contrasted against GSIM-OFDM

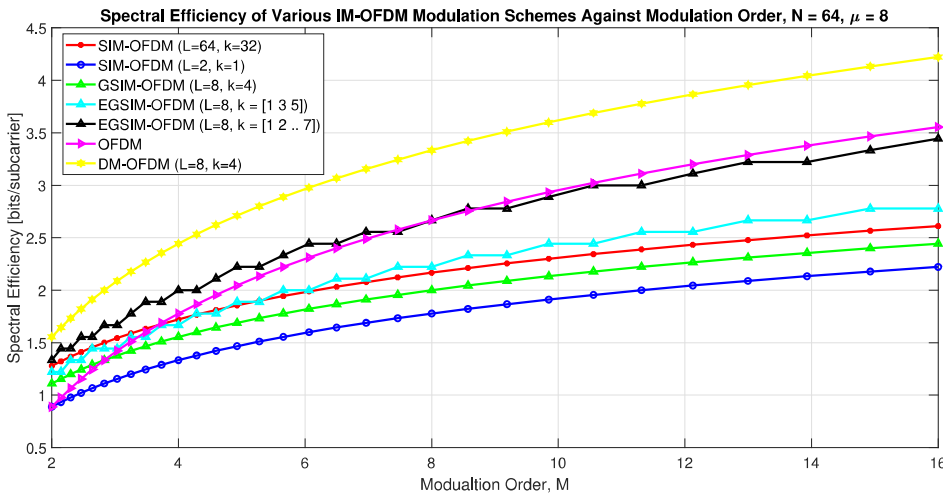


Figure 4.15: Spectral efficiency comparison of all the investigated index modulation schemes

Comparing the spectral efficiencies, in Figure 4.15 we see that DM-OFDM yields improved throughput than all other schemes considered. Furthermore, unlike the single-mode IM schemes the spectral efficiency gains of DM-OFDM are retained as the constellation order grows, asymptotically approaching that of conventional OFDM in the limiting case.

Table 4.2 shows the complexity analysis for the investigated DM-OFDM schemes. Because the constellations we looked at had $M_A = M_B$ the complexity of DM-OFDM matches that of GSIM-OFDM, therefore, when choosing between the two schemes it should be based on whether PAPR or spectral efficiency are more valuable for the given scenario. For example, DM-OFDM may be employed on the downlink where

PAPR is not so important, while the uplink may employ a more power efficient IM-OFDM scheme with better BER.

Scheme	Dual-BPSK	Dual-QPSK
DM-OFDM (ML)	$\mathcal{O}(131072)$	$\mathcal{O}(33554432)$
DM-OFDM (LLR+OTE)	$\mathcal{O}(320)$	$\mathcal{O}(576)$
DM-OFDM (LLR+ML)	$\mathcal{O}(512)$	$\mathcal{O}(4608)$

Table 4.2: Complexity comparison of the LLR and ML detector for DM-OFDM with the two constellations considered for $N = 64$, $G = 8$, $L = 8$, $k = 4$

Finally, Figure 4.16 shows the CCDF of DM-OFDM. Since we are now using all the available subcarriers, the PAPR of the various DM-OFDM schemes closely matches that of conventional OFDM. In the case of $N = 64$, at the 1% probability line dual-QPSK DM-OFDM are closely matched, with an increase in power of 0.05dB over conventional OFDM, while dual-BPSK sees an increase of 0.08dB respectively. This illustrates the ability of DM-OFDM to increase data-rate with minimal overhead.

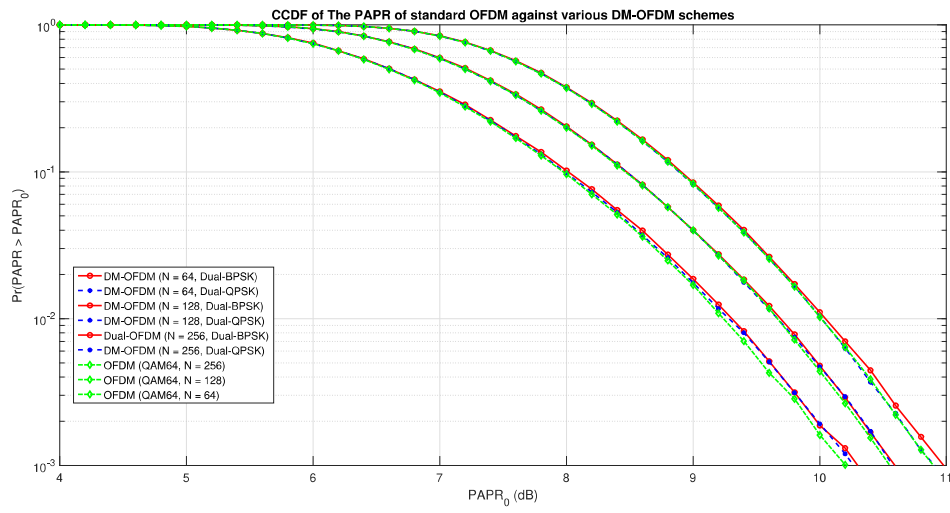


Figure 4.16: CCDF of the PAPR of DM-OFDM using dual-BPSK and dual-QPSK constellations, contrasted against conventional OFDM.

5 | Conclusions

5.1 Review of Findings

In this report we have developed from first principles a model of the wireless channel, and investigated the effect it has on a wirelessly transmitted signal. Based on the effects imposed by the channel we motivated the use of a multi-carrier modulation system which divides the channel into parallel subchannels to mitigate frequency-selective fading caused by inter-symbol-interference. The multi-carrier system was then developed using a discrete-in-time implementation which took advantage of the FFT to effectively carry out OFDM at a reduced complexity in the digital domain. This enabled the use of a low complexity one-tap-equalisation method of detection, at the cost of increased PAPR versus traditional single-carrier schemes. Metrics such as bit-error-rate, bandwidth, PAPR CCDF and spectral efficiency were simulated for the OFDM system using MATLAB, serving as a baseline reference for our investigation into methods of PAPR reduction.

Theoretical analysis showed that the PAPR of OFDM signals scales linearly with the number of active subcarriers, which motivated use of index modulation. We began by presenting a derivation of GSIM-OFDM coupled with an LLR Detector, from which we investigated the special case of SIM-OFDM. This scheme achieved spectral efficiency gains up to QPSK and showed promising BER performance at high E_b/N_0 values, however was unrealisable as its long block lengths became computational unfeasible. Therefore, we investigate ESIM-OFDM which improved upon the BER performance of SIM-OFDM by dividing the OFDM symbol into $N/2$ pairs of subcarriers whose power could easily be compared at the receiver to deduce the activation pattern, at the cost of spectral-efficiency. Subsequently, we looked at GSIM-OFDM and found sub-blocks of length $L = 8$ presented a compromise which limited error propagation and achieved considerable BER gains over conventional OFDM at high E_b/N_0 values, with a complexity that was feasible to realise in real time. Furthermore, upon simulating the CCDF of GSIM-OFDM we saw a reduction in PAPR for 10% of symbols, and limited the peak-PAPR by half. EGSIM-OFDM generalised further upon GSIM-OFDM, letting the number of active subcarriers vary from one sub-block to the next in order to achieve further spectral efficiency gains. The benefits here were outweighed by the

worse BER performance and an increase in complexity which grew with the number of activation patterns.

Finally, we investigated DM-OFDM which applied the idea of index-modulation to a system with two constellation modulators, to achieve spectral efficiency beyond that of OFDM, irrespective of constellation size. Upon implementing DM-OFDM we saw performance which was worse than GSIM-OFDM but was able to match traditional OFDM at high E_b/N_0 values. This was achieved at a complexity exactly equal to that of GSIM-OFDM and a minimal PAPR overhead compared to OFDM. Ultimately, the range of configurations presented should be employed based upon a consideration of performance, data rate requirements, power budget, and complexity budget.

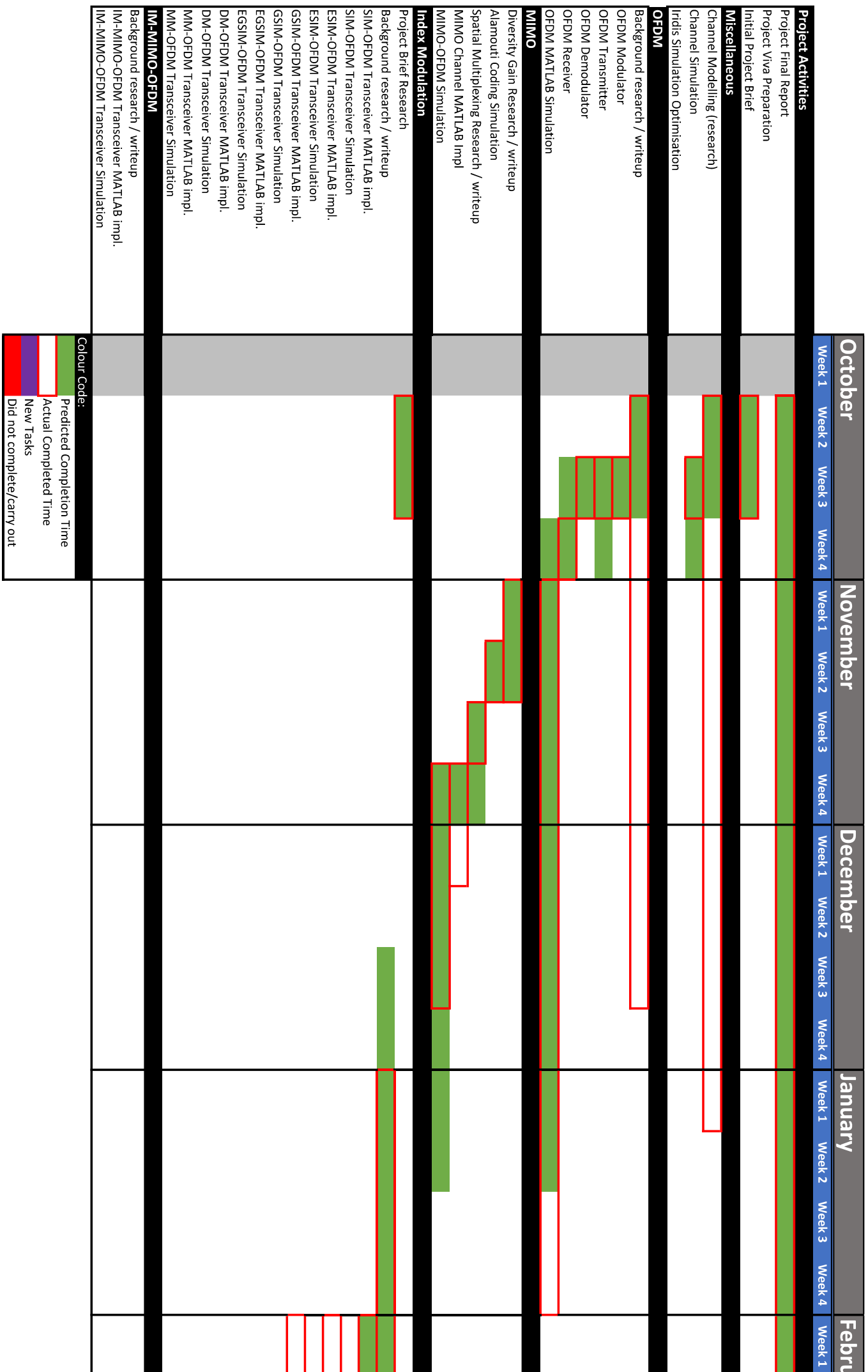
This was achieved in the time periods described by the gantt charts shown in the upcoming pages. Notably, the initial work breakdown structure included investigation into MIMO-OFDM with the intention of combining this with our work on IM to achieve MIMO-IM-OFDM, however in order to limit the scope of the report, work on MIMO was discontinued following the initial progress report. Furthermore, we were not able to realise multi-mode index modulation, as charted, which arose from an underestimation of the time required to carry out the necessary simulations, and a decision to instead investigate EGSIM-OFDM. Furthermore, use of the IRIDIS computing cluster was not necessary since all simulations could be realised to sufficient accuracy on my local device.

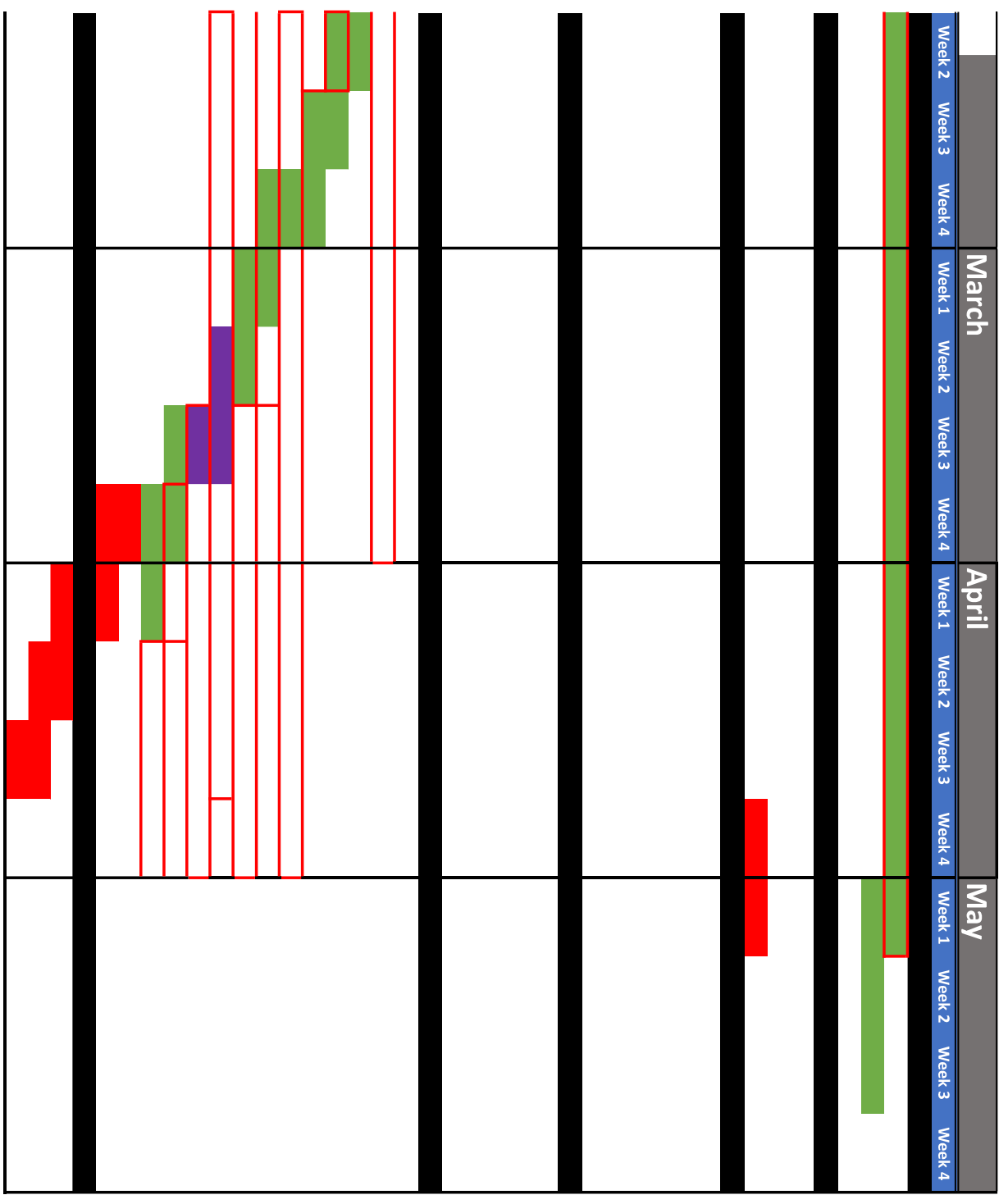
5.2 Future Work

In recent years, index modulation has presented itself as a technique which should be considered as candidate for future wireless standards. It is clear that there are problems which arise in its use; at low values of E_b/N_0 its performance with the LLR detector cannot match conventional OFDM, and as modulation order grows the single-mode schemes' spectral efficiency gains disappear. While DM-OFDM solves the latter, we are then presented with same PAPR problem that initially plagued OFDM. Future work here may therefore wish to consider the feasibility of the higher performance ML detectors at low E_b/N_0 values. Furthermore, implementation and evaluation of the reduced complexity LLR detector presented in [29] should be considered as the lower complexity approach may enable use of IM schemes with longer block length, which maximises spectral efficiency.

In addition, [24] presents a more generalised form of DM-OFDM called multi-mode OFDM in which n_{MM} distinct constellation alphabets are employed to achieve considerable throughput gains via further diversifying the index bits. We may also wish to apply the techniques seen in EGSIM-OFDM to that of DM-OFDM where the number of active subcarriers may vary in each sub-block for further system parameterisation.

It is clear also that the balance of parameters is yet to be perfected; sub-block length and constellation design both will play important roles in implementation feasibility such that a rigorous characterisation of the trade-offs may need to be carried out before index modulation is fit for standardisation. Finally, to enhance our analysis further, we should subject IM-OFDM to more rigorous channel models, such as those which consider doppler shift, frequency and phase offsets, and slow-fading effects.





Bibliography

- [1] “Ieee standard for information technology–telecommunications and information exchange between systems local and metropolitan area networks–specific requirements part 11: Wireless lan medium access control (mac) and physical layer (phy) specifications amendment 1: Enhancements for high-efficiency wlan,” *IEEE Std 802.11ax-2021 (Amendment to IEEE Std 802.11-2020)*, pp. 1–767, 2021.
- [2] “Ieee standard for air interface for broadband wireless access systems,” *IEEE Std 802.16-2017 (Revision of IEEE Std 802.16-2012)*, pp. 1–2726, 2018.
- [3] 3GPP, “Evolved universal terrestrial radio access (e-utra); physical channels and modulation (3gpp ts 36.211 version 14.2.0 release 14),” https://www.etsi.org/deliver/etsi_ts/136200_136299/136211/14.02.00_60/ts_136211v140200p.pdf.
- [4] ——, “5g nr physical channels and modulation(3gpp ts 38.211 version 15.2.0 release 15),” https://www.etsi.org/deliver/etsi_ts/138200_138299/138211/15.02.00_60/ts_138211v150200p.pdf.
- [5] S. Chen, “Elec3203 digital coding and transmission – modem,” <https://www.southampton.ac.uk/~sqc/ELEC3203/MODEM-L5.pdf>, 2021, accessed: 09-04-2022.
- [6] R. W. Chang, “Synthesis of band-limited orthogonal signals for multichannel data transmission,” *The Bell System Technical Journal*, vol. 45, no. 10, pp. 1775–1796, 1966.
- [7] S. Weinstein and P. Ebert, “Data transmission by frequency-division multiplexing using the discrete fourier transform,” *IEEE Transactions on Communication Technology*, vol. 19, no. 5, pp. 628–634, 1971.
- [8] M. Zimmerman and A. Kirsch, “The an/gsc-10 (kathryn) variable rate data modem for hf radio,” *IEEE Transactions on Communication Technology*, vol. 15, no. 2, pp. 197–204, 1967.
- [9] Y. Rahmatallah and S. Mohan, “Peak-to-average power ratio reduction in ofdm systems: A survey and taxonomy,” *IEEE Communications Surveys Tutorials*, vol. 15, no. 4, pp. 1567–1592, 2013.

- [10] R. Mesleh, H. Haas, C. W. Ahn, and S. Yun, "Spatial modulation - a new low complexity spectral efficiency enhancing technique," in *2006 First International Conference on Communications and Networking in China*, 2006, pp. 1–5.
- [11] S. Ganesan, R. Mesleh, H. Ho, C. W. Ahn, and S. Yun, "On the performance of spatial modulation ofdm," in *2006 Fortieth Asilomar Conference on Signals, Systems and Computers*, 2006, pp. 1825–1829.
- [12] L. Hanzo, "Digital transmission - part 2," <https://secure.ecs.soton.ac.uk/notes/elec3203/hanzo1-4up.pdf>, 2021, accessed: 08-04-2022.
- [13] C. Xu, "Wireless channel modelling, wireless systems, space-time processing and performance," <https://secure.ecs.soton.ac.uk/notes/elec3204/cx/Slides2021.pdf>, 2022, accessed: 20-03-2022.
- [14] D. Tse and P. Viswanath, *The wireless channel*. Cambridge University Press, 2005.
- [15] G. Matz and F. Hlawatsch, "Chapter 1 - fundamentals of time-varying communication channels," in *Wireless Communications Over Rapidly Time-Varying Channels*, F. Hlawatsch and G. Matz, Eds. Oxford: Academic Press, 2011, pp. 1–63. [Online]. Available: <https://www.sciencedirect.com/science/article/pii/B9780123744838000017>
- [16] A. Goldsmith, *Multicarrier Modulation*. Cambridge University Press, 2005, p. 374–402.
- [17] D. Montgomery and G. Runger, *Applied Statistics and Probability for Engineers*. John Wiley & Sons, 2010. [Online]. Available: https://books.google.co.uk/books?id=_f4KrEcNAfEC
- [18] J. Bingham, "Multicarrier modulation for data transmission: an idea whose time has come," *IEEE Communications Magazine*, vol. 28, no. 5, pp. 5–14, 1990.
- [19] M. L. Doelz, E. T. Heald, and D. L. Martin, "Binary data transmission techniques for linear systems," *Proceedings of the IRE*, vol. 45, no. 5, pp. 656–661, 1957.
- [20] C. W. HELSTROM, "Iv - detection of a known signal," in *Statistical Theory of Signal Detection (Second Edition)*, second edition ed., ser. International Series of Monographs in Electronics and Instrumentation, C. W. HELSTROM, Ed. Pergamon, 1968, pp. 102–147. [Online]. Available: <https://www.sciencedirect.com/science/article/pii/B9780080132655500100>
- [21] G. Forney, "Maximum-likelihood sequence estimation of digital sequences in the presence of intersymbol interference," *IEEE Transactions on Information Theory*, vol. 18, no. 3, pp. 363–378, 1972.

- [22] M. Simon and M. Alouini, “A unified approach to the performance analysis of digital communication over generalized fading channels,” *Proceedings of the IEEE*, vol. 86, no. 9, pp. 1860–1877, 1998.
- [23] S. Wang, “Data converters - lecture 3,” <https://secure.ecs.soton.ac.uk/notes/elec3208/>, 2022, accessed: 20-04-2022.
- [24] T. Mao, Q. Wang, Z. Wang, and S. Chen, “Novel index modulation techniques: A survey,” *IEEE Communications Surveys Tutorials*, vol. 21, no. 1, pp. 315–348, 2019.
- [25] D. Tsonev, S. Sinanovic, and H. Haas, “Enhanced subcarrier index modulation (sim) ofdm,” in *2011 IEEE GLOBECOM Workshops (GC Wkshps)*, 2011, pp. 728–732.
- [26] E. Basar, U. Aygolu, E. Panayirci, and H. V. Poor, “Orthogonal frequency division multiplexing with index modulation,” in *2012 IEEE Global Communications Conference (GLOBECOM)*, 2012, pp. 4741–4746.
- [27] R. Abu-alhiga and H. Haas, “Subcarrier-index modulation ofdm,” in *2009 IEEE 20th International Symposium on Personal, Indoor and Mobile Radio Communications*, 2009, pp. 177–181.
- [28] R. Fan, Y. J. Yu, and Y. L. Guan, “Generalization of orthogonal frequency division multiplexing with index modulation,” *IEEE Transactions on Wireless Communications*, vol. 14, no. 10, pp. 5350–5359, 2015.
- [29] Z. Hu, F. Chen, M. Wen, F. Ji, and H. Yu, “Low-complexity llr calculation for ofdm with index modulation,” *IEEE Wireless Communications Letters*, vol. 7, no. 4, pp. 618–621, 2018.
- [30] T. Mao, Z. Wang, Q. Wang, S. Chen, and L. Hanzo, “Dual-mode index modulation aided ofdm,” *IEEE Access*, vol. 5, pp. 50–60, 2017.
- [31] C. E. Shannon, “A mathematical theory of communication,” *The Bell System Technical Journal*, vol. 27, no. 3, pp. 379–423, 1948.
- [32] L.-L. Yang, “Elec3204-part ii: Principles of multicarrier modulation and ofdm,” <https://secure.ecs.soton.ac.uk/notes/elec3204/lly/ELEC3204-MC-OFDM-principles-slides.pdf>, 2022, accessed: 16-04-2022.
- [33] F. Xiong, *Digital Modulation Techniques*, ser. Artech House telecommunications library. Artech House, 2000. [Online]. Available: <https://books.google.co.uk/books?id=VVSJQwAACAAJ>

- [34] W. Chu, “Abel’s lemma on summation by parts and basic hypergeometric series,” *Advances in Applied Mathematics*, vol. 39, no. 4, pp. 490–514, 2007. [Online]. Available: <https://www.sciencedirect.com/science/article/pii/S0196885807000693>
- [35] W. Koch and A. Baier, “Optimum and sub-optimum detection of coded data disturbed by time-varying intersymbol interference (applicable to digital mobile radio receivers),” in *[Proceedings] GLOBECOM ’90: IEEE Global Telecommunications Conference and Exhibition*, 1990, pp. 1679–1684 vol.3.
- [36] P. Blanchard, D. J. Higham, and N. J. Higham, “Accurately computing the log-sum-exp and softmax functions,” *IMA Journal of Numerical Analysis*, vol. 41, no. 4, pp. 2311–2330, 08 2020. [Online]. Available: <https://doi.org/10.1093/imanum/draa038>
- [37] D. E. Knuth, “The art of computer programming, pre-fascicle 3a, a draft of section 7.2. 1.3: Generating all combinations. zeroth printing (revision 7). 2004.”
- [38] Q. Technologies, “888 5g mobile platform,” https://www.qualcomm.com/content/dam/qcomm-martech/dm-assets/documents/prod_brief_qcom_sd888_5g_0.pdf, 2022, accessed: 12-04-2022.
- [39] K. Maharatna, “Elec3221 notes,” <https://secure.ecs.soton.ac.uk/notes/elec3221/KMnotes/>, 2022, accessed: 20-03-2022.

A | Baseband Discrete-in-time Channel Input-Output Relationship

The expression for the CIR described in Equation 2.21 of section 2.1.5 is one which can be applied to the signal *after* it has been up-converted onto a much higher frequency carrier and undergone sufficient transmit and receive pulse shaping to limit the signals bandwidth. We may therefore insert it into the block-level MODEM for quadrature-amplitude-modulation (QAM) as shown in Figure A.1. However, given

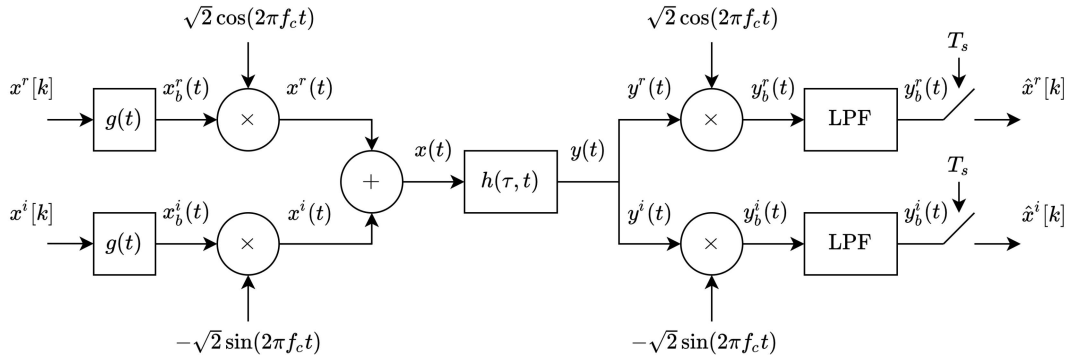


Figure A.1: Generalised wireless channel block diagram including transmit and receive filters, and modulation stages

our purpose is to simulate modulation schemes carried out at baseband frequencies (i.e. centred around 0Hz) then we are motivated to develop a baseband channel model which can be applied directly to baseband signals. This will allow us to avoid having to make considerations about the passband, such as phase and frequency offset in the carrier or sampling synchronisation while drawing the same conclusions about the efficacy of our transmission scheme.

We begin by representing the passband transmitted signal, $x(t)$ as the carrier modulated version of a baseband signal $x_b(t)$ which carries all the information within $x(t)$, only at the base band

$$x(t) = \sqrt{2} \Re e \{ x_b(t) e^{j2\pi f_c t} \} \quad (\text{A.1})$$

Correspondingly, we may write the passband received signal, $y(t)$, which has been subject to the CIR, as a function of its baseband signal which has been downconverted to 0Hz

$$y(t) = \sqrt{2}\Re\{y_b(t)e^{j2\pi f_c t}\} \quad (\text{A.2})$$

Using Equation 2.19, we may reformulate the input-output relationship for the system in terms of the baseband signals, such that for the quadrature component we have

$$\begin{aligned} \Re\{y_b(t)e^{j2\pi f_c t}\} &= \sum_i \alpha_i(t) \Re\{x_b(t - \tau_i(t))e^{j2\pi f_c(t - \tau_i(t))}\} \\ &= \sum_i \alpha_i(t) \Re\{x_b(t - \tau_i(t))e^{j2\pi f_c t} e^{j2\pi f_c \tau_i(t)}\} \\ &= \Re\left[e^{j2\pi f_c t} \sum_i \alpha_i(t) x_b(t - \tau_i(t)) e^{-j2\pi f_c \tau_i(t)}\right] \end{aligned} \quad (\text{A.3})$$

and equally for the in-phase component,

$$\Im\{y_b(t)e^{j2\pi f_c t}\} = \Im\left[e^{j2\pi f_c t} \sum_i \alpha_i(t) x_b(t - \tau_i(t)) e^{-j2\pi f_c \tau_i(t)}\right] \quad (\text{A.4})$$

Now letting $\alpha_i^b(t) = \alpha_i(t)e^{-j2\pi f_c \tau_i(t)}$ we may write

$$\Re\{y_b(t)e^{j2\pi f_c t}\} = \Re\left[e^{j2\pi f_c t} \sum_i \alpha_i^b(t) x_b(t - \tau_i(t))\right] \quad (\text{A.5})$$

$$\Im\{y_b(t)e^{j2\pi f_c t}\} = \Im\left[e^{j2\pi f_c t} \sum_i \alpha_i^b(t) x_b(t - \tau_i(t))\right] \quad (\text{A.6})$$

Therefore, in order to satisfy the two relationships above, we must have

$$y_b(t) = \sum_i \alpha_i^b(t) x_b(t - \tau_i(t)) \quad (\text{A.7})$$

Equally, we can then write the baseband CIR

$$h_b(\tau, t) = \sum_i \alpha_i^b(t) \delta(\tau - \tau_i(t)) \quad (\text{A.8})$$

From Equation A.7 we can see that the baseband output is the sum over all paths of the baseband signal subject to a delay and attenuated by the path attenuation coefficients.

Because the baseband signal is modulated onto a sinusoidal carrier, a significant change in phase of $\pi/2$ is when the path length changes by $\lambda/4 = c/(4f_c)$, such that for a body travelling at a speed, v , this occurs in $c/(4f_c v)$ seconds. Given that the Doppler shift at a frequency f is $D = fv/c$ as before, and assuming narrow-band communications then this phase change occurs in $\approx 1/(4D)$ seconds which will be an important figure in the future discussion on doppler spread. Equally, we may write

the baseband equivalent of the CFR, as $H_b(b; t)$ at a given f as $H(f + f_c; t)$, which is the passband CFR shifted (down) by the carrier frequency.

In order for our channel model to be useful to us in simulation we want it to be *discrete* in time which will suit the discrete nature of simulation tools. We can create a discrete model by now considering the transmit filter, $g(t)$ and sampling procedure following the Low-Pass-Filter (LPF) at the receiver in Figure A.1. The sampling theorem [31] states that any waveform band-limited to a bandwidth $B/2$ can be expanded in terms of the orthogonal basis $\{\text{sinc}(Bt - n)\}_n$ with coefficients given by the magnitude at the sampled points (at integer multiples of $1/B$). That is, for an arbitrary signal $f(t)$,

$$f(t) = \sum_{n=-\infty}^{\infty} f[n] \text{sinc}(Bt - n) = \sum_{n=-\infty}^{\infty} f[n] \frac{\sin(\pi(Bt - n))}{\pi(Bt - n)}$$

Therefore, the baseband transmitted signal may be represented as

$$x_b(t) = \sum_k x[k] \text{sinc}(Bt - k) \quad k = 1, 2, \dots \quad (\text{A.9})$$

where $x[k]$ is $x_b(k/B)$ for $k = 1, 2, \dots$. Using Equation A.7 we can therefore write

$$y_b(t) = \sum_i \alpha_i^b(t) \sum_k x[k] \text{sinc}(Bt - k) \quad (\text{A.10})$$

$$= \sum_k x[k] \sum_i \alpha_i^b(t) \text{sinc}(Bt - B\tau_i(t) - k) \quad (\text{A.11})$$

As per Figure A.1 we then sample the received baseband signal as integer multiples of $T_s = 1/f_s = 1/(2 \cdot f_{max}) = 1/(2 \cdot B/2) = 1/B$ to give discrete samples $y[n] = y_b(n/B)$ for $n = 0, 1, \dots$

$$y[n] = \sum_k x[k] \sum_i \alpha_i^b(n/B) \text{sinc}(n - k - B\tau_i(n/B)) \quad (\text{A.12})$$

Now, letting $l = n - k$ we have

$$y[n] = \sum_l x[n - l] \sum_i \alpha_i^b(n/B) \text{sinc}(l - B\tau_i(n/B)) \quad (\text{A.13})$$

and defining,

$$h_l[n] = \sum_i \alpha_i^b(n/B) \text{sinc}(l - B\tau_i(n/B)) \quad (\text{A.14})$$

we may write,

$$y[n] = \sum_l h_l[n] x[n - l] \quad (\text{A.15})$$

which is our discrete channel model. $h_l[n]$ is the l th tap of the discrete baseband CIR at time n . Its value depends on the sum of baseband path gains scaled by the sinc

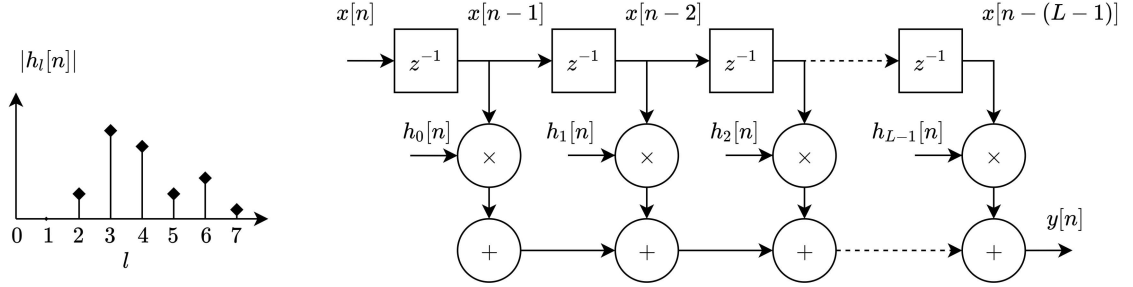


Figure A.2: Discrete baseband channel model representation as an FIR filter with L taps (right) with the characterising power-delay profile (left).

function, such that those paths with delay close to l/B contribute most significantly to tap l . The baseband channel may therefore be interpreted as an FIR filter with the l th tap weight given by $h_l[n]$, at symbol period n , as shown in Figure A.2.

Finally, our model of the channel includes the additive noise inherent to wireless communication. This noise arises from many sources, but primarily as a result of thermal noise which exists in the circuits processing the signal, as well as radiation intrinsic to the universe. With this consideration, we can assume the noise is zero-mean additive white gaussian noise, distributed over the interval $[0, 1]$ with power (variance) $N_0/2$. Our input output relation is therefore extended to

$$y(t) = \sum_i \alpha_i(t)x(t - \tau_i(t)) + v(t) \quad (\text{A.16})$$

with the discrete-in-time baseband equivalent

$$y[n] = \sum_l h_l[n]x[n - l] + v[n] \quad n = 0, 1, \dots \quad (\text{A.17})$$

where $v[n]$ is noise band-limited to $B/2$ sampled at the instant n/B . Moreover, if both real and imaginary components of $v[n]$ are distributed as $\sim \mathcal{N}(0, N_0/2)$ then $v[n]$ is said to be a complex *circularly-symmetric* gaussian random variable which has the property $e^{j\phi}v$ has the same distribution as v for all ϕ . This is denoted, $v \sim \mathcal{CN}(0, N_0/2)$.

B | Derivation of the Distribution of the Channel Path Gain

In general, for n normally distributed random constituent processes, $\alpha_i \sim \mathcal{CN}(0, \sigma_i^2)$ with means $\bar{\alpha}_i$ and variance σ^2 , the sum of their squares, $y = \sum_{i=1}^n \alpha_i^2$ has a χ^2 (chi-squared) distribution [13] with probability density function (PDF)

$$p(y) = \frac{1}{2\sigma^2} \left(\frac{y}{s^2} \right)^{\frac{n-2}{4}} \exp \left(\frac{-(s^2 + y)}{2\sigma^2} \right) \mathbf{I}_{(n/2)-1} \left(\sqrt{y} \frac{s}{\sigma^2} \right) \quad (\text{B.1})$$

where $s^2 = \sum_{i=1}^n \bar{\alpha}_i^2$ and $\mathbf{I}_k(x)$ is the modified k th-order Bessel function of the first kind. In our case, we have two components, such that $n = 2$, and $y = \alpha_i^2 + \alpha_q^2$ in which case our χ^2 reduces to the special case of a Rician distribution [13], with PDF

$$p_{rice}(y) = \frac{1}{2\sigma^2} \exp \left(\frac{-(y + s^2)}{2\sigma^2} \right) \mathbf{I}_0 \left(\sqrt{y} \frac{s}{\sigma^2} \right) \quad (\text{B.2})$$

However, we want this as a function of the magnitude, $\alpha = \sqrt{y}$. This is achieved by setting $y = \alpha^2$ and multiplying by 2α to ensure the integral of the PDF remains unitary [13].

$$p_{rice}(\alpha) = \frac{\alpha}{\sigma^2} \exp \left(\frac{-(\alpha^2 + s^2)}{2\sigma^2} \right) \mathbf{I}_0 \left(\alpha \frac{s}{\sigma^2} \right) \quad (\text{B.3})$$

We introduce a metric called the κ -factor, this is defined as the ratio of the power from the line-of-sight (LOS) path to that of the non LOS paths. Given that $\bar{\alpha}_i$ and $\bar{\alpha}_q$ are the means of α_i and α_q respectively, then $s^2 = \bar{\alpha}_i^2 + \bar{\alpha}_q^2$ is the fraction of transmit power received via the LOS path. Equally, both components have variances σ^2 , such that $2\sigma^2$ is the fraction of the transmit power received from non LOS paths [13]. Overall, we consider that fast fading does not affect the overall power of the Tx signal, such that $s^2 + 2\sigma^2 = 1$. Following from this, the ‘ κ -factor’ is therefore

$$\kappa = \frac{s^2}{2\sigma^2} \quad (\text{B.4})$$

The greater the value of κ the more deterministic the channel is, i.e., for $\kappa = 1$ the channel impulse response is the Dirac delta function. We may therefore reformulate

Equation B.3 in terms of the κ -factor introduced previously

$$p_{rice}(\alpha) = \frac{\alpha}{\sigma^2} \exp\left(\frac{-\alpha^2}{2\sigma^2}\right) e^{-\kappa} I_0\left(\sqrt{2\kappa}\frac{\alpha}{\sigma}\right) \quad (\text{B.5})$$

When there is no LOS path all of the power is transmitted through reflected paths such that $s = 0$ and $\kappa = 0$. In this case, we have the worst case Rayleigh PDF

$$p_{rice}(\alpha)|_{\kappa=0} = p_{rayleigh}(\alpha) = \frac{\alpha}{\sigma^2} \exp\left(\frac{-\alpha^2}{2\sigma^2}\right) \quad (\text{B.6})$$

Comparatively, when there is only an LOS path (such as in satellite-to-ground communications), the PDF becomes a Dirac delta with a step function cumulative distribution function. In order to achieve such a PDF, $h_l[m]$ can be modelled as [13]

$$h_l[n] = \sqrt{\frac{\kappa}{\kappa+1}} \sigma e^{j\theta} + \sqrt{\frac{1}{\kappa+1}} \mathcal{CN}(0, \sigma^2) \quad (\text{B.7})$$

where the first term denotes the LOS path arriving with uniform phase θ , while the second term denotes the reflected paths. This is often a better model for the channel, but is harder to draw comparison against the existing literature, therefore we proceed under the notion the CIR is given $\mathbf{h}[n] = [h_1[n], h_2[n], \dots, h_L[n]]$ where $h_i[n] \sim \mathcal{CN}(0, \sigma_i^2 = 1/L)$ for $i = 1, 2, \dots, L$.

C | Matrix Representation of OFDM

In order to further enhance our understanding of *why* such a cyclic prefix enables such a simple demodulation procedure, we may formulate OFDM in terms of matrix algebra. At the transmitter, we begin by constellation modulating $N \cdot \log_2(M)$ bits, to form the N frequency domain complex symbols given by (dropping the time dependence on n) $\mathbf{X} = [X_0, X_1, \dots, X_{N-1}]^T$. As per the previous reasoning of section 3.2.1, OFDM modulation is then equivalent to applying an inverse fourier transform operation, to yield the time-domain symbol vector, $\mathbf{x} = [x_0, x_1, \dots, x_{N-1}]$. In matrix terms this is equivalent to multiplication of the frequency-domain symbol vector with the IFFT matrix, \mathcal{F}^H where \mathcal{F} is the FFT matrix given by [32]

$$\mathcal{F} = \frac{1}{\sqrt{N}} \begin{bmatrix} 1 & 1 & 1 & \cdots & 1 \\ 1 & W_N & W_N^2 & \cdots & W_N^{N-1} \\ \vdots & \vdots & \vdots & \ddots & \vdots \\ 1 & W_N^{N-1} & W_N^{2(N-1)} & \cdots & W_N^{(N-1)^2} \end{bmatrix} \quad (\text{C.1})$$

where $W_N = \exp\left(\frac{-j2\pi}{N}\right)$. This FFT matrix is scaled by the factor $1/\sqrt{N}$ in order to make the transform unitary. Importantly, the FFT matrix has the property $\mathcal{F}\mathcal{F}^H = \mathcal{F}^H\mathcal{F} = I_N$, which means to say its conjugate is equal to its inverse. The resulting time-domain symbols can thus be formulated as,

$$\mathbf{x} = \frac{1}{\sqrt{N}} \mathcal{F}^H \mathbf{X} \quad (\text{C.2})$$

We then proceed by appending the cyclic prefix to \mathbf{x} , which we assume to be the last L element of \mathbf{x} , where $L + 1$ is the length of the CIR. This yields a vector $\tilde{\mathbf{x}} = [x_{-L}, \dots, x_{-1}, x_0, x_1, \dots, x_{N-1}]^T$ which is what is transmitted over the channel where it is subject to the effects of fading and additive white gaussian noise. In this discrete model, the channel fading coefficients are chosen as circularly symmetric complex Gaussian random variates distributed as $\sim \mathcal{CN}(0, \frac{1}{L+1})$ with $L + 1$ being the length of the CIR, $\mathbf{h} = [h_0, h_1, \dots, h_L]^T$. Equally the noise, $\mathbf{v} = [v_0, v_1, \dots, v_{N-1}]^T$, is distributed as $\sim \mathcal{CN}(0, \frac{N_0}{2})$, where N_0 is the noise power. Letting $\mathbf{y} = [y_0, y_1, \dots, y_{N-1}]^T$ then the input-output relationship of this system is thus given by

$$y_n = \sum_{k=0}^{L-1} h_k \tilde{x}_{n-k} + v_n, \quad n = 0, 1, \dots, N - 1 \quad (\text{C.3})$$

however, recall that with the cyclic prefix, \tilde{x}_{n-k} for $k > n$ is equivalent to $x_{N-(n-k)}$, such that we may reformulate the previous expression in a matrix-like way as follows [32]

$$\begin{array}{cccccccccc}
 x_{-L} & \dots & x_{-1} & x_0 & x_1 & x_2 & x_3 & \dots \\
 \\
 h_0 & & h_0x_0 & h_0x_1 & h_0x_2 & h_0x_3 & \dots \\
 h_1 & & h_1x_{-1} & h_1x_0 & h_1x_1 & h_1x_2 & \dots \\
 \vdots & & \vdots & \vdots & \vdots & \vdots & \ddots & \\
 h_L & & h_Lx_{-L} & h_Lx_{-L+1} & h_Lx_{-L+2} & h_Lx_{-L+3} & \dots \\
 & & \sum & \sum & \sum & \sum & \dots \\
 & & +v_0 & +v_1 & +v_2 & +v_3 & \dots \\
 & = & = & = & = & = & \dots \\
 & y_0 & y_1 & y_2 & y_3 & \dots
 \end{array} \tag{C.4}$$

From Equation C.4 we can say generally,

$$y_n = h_Lx_{n-L} + h_{L-1}x_{n-L+1} + \dots + h_1x_{n-1} + h_0x_n + v_n$$

which may be represented in matrix form as

$$\underbrace{\begin{bmatrix} y_0 \\ y_1 \\ \vdots \\ y_{N-1} \end{bmatrix}}_{\mathbf{y}} = \underbrace{\begin{bmatrix} h_L & h_{L-1} & \dots & h_0 & 0 & \dots & 0 & 0 & \dots & 0 \\ 0 & h_L & h_{L-1} & \dots & h_0 & \dots & 0 & 0 & \dots & 0 \\ \vdots & \vdots & \vdots & \ddots & \vdots & \dots & \vdots & \vdots & \dots & \vdots \\ 0 & 0 & 0 & \dots & 0 & \dots & h_L & h_{L-1} & \dots & h_0 \end{bmatrix}}_{\hat{\mathbf{H}}} \underbrace{\begin{bmatrix} x_{-L} \\ x_{-1} \\ x_0 \\ x_1 \\ \vdots \\ x_{N-1} \end{bmatrix}}_{\mathbf{x}} + \underbrace{\begin{bmatrix} v_0 \\ v_1 \\ \vdots \\ v_{N-1} \end{bmatrix}}_{\mathbf{v}} \tag{C.5}$$

Now we can notice, as a result of the cyclic prefix that we may rewrite Equation C.5 as

$$\underbrace{\begin{bmatrix} y_0 \\ y_1 \\ \vdots \\ y_{N-1} \end{bmatrix}}_{\mathbf{y}} = \underbrace{\begin{bmatrix} h_0 & 0 & \dots & 0 & \dots & 0 & \dots & h_2 & h_1 \\ h_1 & h_0 & \dots & 0 & \dots & 0 & \ddots & \vdots & \vdots \\ \vdots & \vdots & \ddots & \vdots & \ddots & 0 & \dots & 0 & h_L \\ h_L & h_{L-1} & \dots & h_0 & \dots & 0 & 0 & \dots & 0 \\ \vdots & \vdots & \ddots & \vdots & \ddots & \vdots & \ddots & \vdots & \vdots \\ 0 & 0 & \dots & 0 & \dots & h_0 & 0 & \dots & 0 \\ \vdots & \vdots & \ddots & \vdots & \ddots & \vdots & \ddots & \vdots & \vdots \\ 0 & 0 & \dots & 0 & \dots & h_{L-1} & \dots & h_0 & 0 \\ 0 & 0 & \dots & 0 & \dots & h_L & \dots & h_1 & h_0 \end{bmatrix}}_{\mathbf{H}} \underbrace{\begin{bmatrix} x_0 \\ x_1 \\ \vdots \\ x_{N-1} \end{bmatrix}}_{\mathbf{x}} + \underbrace{\begin{bmatrix} v_0 \\ v_1 \\ \vdots \\ v_{N-1} \end{bmatrix}}_{\mathbf{v}} \tag{C.6}$$

where each column contains a copy of the CIR shifted down one element, and circling back to the top. As a result of this property, \mathbf{H} is a circulant channel matrix which can be decomposed into $\mathbf{H} = \mathcal{F}^H \boldsymbol{\Lambda} \mathcal{F}$, where $\boldsymbol{\Lambda} = \text{diag}\{H_0, H_1, \dots, H_{N-1}\}$, which is an $N \times N$ diagonal matrix and H_n is the channel frequency response (or the fading gain) of the n th subcarrier [32]. Additionally note, \mathcal{F} is the FFT matrix described previously. With the knowledge that $\mathbf{x} = \mathcal{F}^H \mathbf{X}$ we may therefore write an equation for the received time domain symbol vector, \mathbf{y}

$$\mathbf{y} = \mathbf{H} \mathcal{F}^H \mathbf{X} + \mathbf{v} = \mathcal{F}^H \boldsymbol{\Lambda} \mathcal{F} \mathcal{F}^H \mathbf{X} + \mathbf{v} = \mathcal{F}^H \boldsymbol{\Lambda} \mathbf{X} + \mathbf{v} \quad (\text{C.7})$$

Carrying out the FFT on \mathbf{y} as motivated in section 3.2.1 yields

$$\mathbf{Y} = \mathcal{F} \mathbf{y} = \mathcal{F} \mathcal{F}^H \boldsymbol{\Lambda} \mathbf{X} + \mathcal{F} \mathbf{v} = \boldsymbol{\Lambda} \mathbf{X} + \mathbf{V}$$

or in matrix representation

$$\begin{bmatrix} Y_0 \\ Y_1 \\ \vdots \\ Y_{N-1} \end{bmatrix} = \begin{bmatrix} H_0 & 0 & \dots & 0 \\ 0 & H_1 & 0 & \vdots \\ \vdots & 0 & \ddots & 0 \\ 0 & \dots & 0 & H_{N-1} \end{bmatrix} \begin{bmatrix} X_0 \\ X_1 \\ \vdots \\ X_{N-1} \end{bmatrix} + \begin{bmatrix} V_0 \\ V_1 \\ \vdots \\ V_{N-1} \end{bmatrix} \quad (\text{C.8})$$

Therefore, equalisation may proceed on a subcarrier-by-subcarrier basis, where for $n = 0, 1, \dots, N - 1$

$$Y_n = H_n X_n + V_n \quad (\text{C.9})$$

$$\implies X_n = \frac{Y_n}{H_n} + \frac{V_n}{H_n} \quad (\text{C.10})$$

We can then deduce the transmitted bits by demodulating using the constellation diagram for the modulations scheme used at the transmitter. Note that there is an error term V_n/H_n which arises as a result of the AWGN. For a larger SNRs this term becomes increasingly insignificant, however for lower SNRs, measures such as error correcting channel codes are required to combat its effect.

D | OFDM PAPR Derivation

This section follows a derivation presented in [33], however we shall generalise this, akin to [25], which considers the case of N_a out of N subcarriers as ‘active’, with $N - N_a$ subcarriers inactive, transmitting a 0 amplitude signal. This approach will favour our discussion about index modulation in subsection 4.1.1. Recalling Equation 3.1, the total power of multi-carrier signal can be written as

$$P_{total} = \frac{1}{T_s} \int_0^{T_s} \left[\sum_{i=0}^{N-1} s_i \cdot g(t) \cdot \cos(2\pi f_i t + \phi_i) \right]^2 dt \quad (\text{D.1})$$

$$\begin{aligned} &= \frac{1}{T_s} \int_0^{T_s} \left[\sum_{i=0}^{N-1} s_i^2 \cdot g^2(t) \cdot \cos^2(2\pi f_i t + \phi_i) \right. \\ &\quad \left. + \sum_{i \neq j} s_i s_j g^2(t) \cos(2\pi f_i t + \phi_i) \cos(2\pi f_j t + \phi_j) \right] dt \end{aligned} \quad (\text{D.2})$$

$$\begin{aligned} &= \frac{1}{T_s} \left\{ \int_0^{T_s} \left[\sum_{i=0}^{N-1} s_i^2 \cdot g^2(t) \cdot \cos^2(2\pi f_i t + \phi_i) \right] dt \right. \\ &\quad \left. + \int_0^{T_s} \left[\sum_{i \neq j} s_i s_j g^2(t) \cos(2\pi f_i t + \phi_i) \cos(2\pi f_j t + \phi_j) \right] dt \right\} \end{aligned} \quad (\text{D.3})$$

We have stated previously that a requirement of OFDM is that the subcarriers are orthogonally spaced such that $f_i = f_0 + i/T_n$, and that the pulse shaping filter, $g(t)$, is designed such that $g^2(t) = 1$. Therefore, the second integral term of Equation D.3 is equivalent to

$$\begin{aligned} &\int_0^{T_s} \left[\sum_{i \neq j} s_i s_j g^2(t) \cos(2\pi f_i t + \phi_i) \cos(2\pi f_j t + \phi_j) \right] dt \\ &= \sum_{i \neq j} s_i s_j \underbrace{\int_0^{T_s} \left[g^2(t) \cos(2\pi f_i t + \phi_i) \cos(2\pi f_j t + \phi_j) \right] dt}_{=0} \\ &= 0 \end{aligned} \quad (\text{D.4})$$

Therefore, the total power may now be written

$$P_{total} = \frac{1}{T_s} \sum_{i=0}^{N-1} s_i^2 \int_0^{T_s} \left[\cos^2(2\pi f_i t + \phi_i) \right] dt \quad (\text{D.5})$$

$$= \frac{1}{2T_s} \sum_{i=0}^{N-1} s_i^2 \int_0^{T_s} \left[1 + \cos(4\pi f_i t + 2\phi_i) \right] dt \quad (\text{D.6})$$

$$= \frac{1}{2T_s} \sum_{i=0}^{N-1} s_i^2 \left\{ T_s + \underbrace{\left[\frac{1}{4\pi(f_0 + \frac{i}{T_s})} \left(\sin(4\pi(f_0 + i/T_s)T_s + 2\phi_i) - \sin(2\phi_i) \right) \right]}_{=0 \text{ when } f_0 T_s >> 1} \right\} \quad (\text{D.7})$$

As was the case in Equation 3.3, the second term of Equation D.3 reduces to zero under the assumption $f_0 T_s \gg 1$ or when the phase offset is 0 (i.e. under ideal conditions), such that we arrive at the final expression for the total power

$$P_{total} = \frac{1}{2} \sum_{i=0}^{N-1} s_i^2 \quad (\text{D.8})$$

However, recalling that only N_a subcarriers are active then more generally if $\mathbf{I} = [i_1, i_2, \dots, i_{N_a}]$, $i_k \in [0, N-1]$ for $k = 1, 2, \dots, N_a$, is the vector of active subcarrier indices, then

$$P_{total} = \frac{1}{2} \sum_{k=1}^{N_a} s_{i_k}^2 = \sum_{k=1}^{N_a} P_{i_k} \quad (\text{D.9})$$

where P_{i_k} is the power of the symbol at the subcarrier index given by the k th element of \mathbf{I} . In the case of $N_a = N$, then $\mathbf{I} = [1, 2, 3, \dots, N]$, such that Equation D.9 reduces to Equation D.8. Therefore, the power of the OFDM symbol is simply the sum of the power of the active M -Ary complex symbols being modulated. We can then formulate the average power of an OFDM signal as

$$P_{avg}^{OFDM} = \mathcal{E}(P_{total}) \quad (\text{D.10})$$

$$= \sum_{i=0}^{N_a-1} \mathcal{E}(P_{i_k}) = \sum_{i=0}^{N_a-1} P_{avg} \quad (\text{D.11})$$

where \mathcal{E} is the expectation operator and P_{avg} is the average M -Ary symbol power. It can be shown [33, Chapter 9, 9.25] that for a square QAM constellation

$$P_{avg} = \frac{P_0}{3}(M-1) \quad (\text{D.12})$$

where P_0 is the power of the symbol closest to the origin. Given that the outermost point in our arbitrary QAM constellation is of the form $(\sqrt{M}-1) + j(\sqrt{M}-1)$, which has amplitude $\sqrt{2}(\sqrt{M}-1)$, and that the symbol closest to the origin will always be a point from a 4-Ary QAM constellation, then P_0 is given by

$$P_0 = \frac{(\sqrt{2}(\sqrt{4}-1))^2}{2} = 1 \quad (\text{D.13})$$

Therefore, we arrive at an expression for the average power of an OFDM symbol with N_a active subcarriers

$$P_{avg}^{OFDM} = \sum_{i=0}^{N_a-1} \frac{1}{3}(M-1) = \frac{N_a}{3}(M-1) \quad (\text{D.14})$$

On the contrary, the peak amplitude of the OFDM signal is when all N_a active subcarriers add coherently with a maximum-amplitude M -Ary symbol that has equal phase at all subcarriers. Thus the peak amplitude is

$$A_{peak}^{OFDM} = N_a \sqrt{2}(\sqrt{M} - 1) \quad (\text{D.15})$$

such that the peak power is

$$P_{peak}^{OFDM} = \frac{(A_{peak}^{OFDM})^2}{2} = \frac{(N_a \sqrt{2}(\sqrt{M} - 1))^2}{2} = N_a^2(\sqrt{M} - 1)^2 \quad (\text{D.16})$$

We may therefore write an equation for the maximum PAPR of an OFDM signal modulated by a square QAM constellation with $N_a \leq N$ active subcarriers as

$$PAPR_{OFDM} = \frac{N_a^2(\sqrt{M} - 1)^2}{\frac{N_a}{3}(M-1)} = \frac{3N_a(\sqrt{M} - 1)}{\sqrt{M} + 1} \quad (\text{D.17})$$

E | GSIM-OFDM LLR Closed Form Derivation

We denote the LLR of each subcarrier, λ_α , for $\alpha = 1, 2, \dots, N$, as the natural logarithm ratio of the posterior probability that a given frequency domain symbol is either active or inactive, i.e.

$$\lambda_\alpha = \ln \left(\frac{\sum_{\chi=1}^M P(\mathbf{X}(\alpha) = s_\chi \mid \mathbf{Y}(\alpha))}{P(\mathbf{X}(\alpha) = 0 \mid \mathbf{Y}(\alpha))} \right) \quad (\text{E.1})$$

If we then consider Bayes' theorem which states $P(A|B) = P(B|A) \cdot P(A)/P(B)$, then the numerator Equation E.1 may be written as

$$\begin{aligned} & \sum_{\chi=1}^M P(\mathbf{X}(\alpha) = s_\chi \mid \mathbf{Y}(\alpha)) \\ &= \sum_{\chi=1}^M \frac{P(\mathbf{Y}(\alpha) \mid \mathbf{X}(\alpha) = s_\chi) \cdot P(\mathbf{X}(\alpha) = s_\chi)}{P(\mathbf{Y}(\alpha))} \end{aligned} \quad (\text{E.2})$$

The numerator of Equation E.2 may be expanded using the summation by parts formula [34] which states

$$\sum_{k=m}^n a_k b_k = [S_n b_n - S_{m-1} b_m] + \sum_{k=m}^{n-1} [S_k (b_k - b_{k+1})] \quad (\text{E.3})$$

where $S_N = \sum_{n=1}^N a_n$. In our case, $m = 1$, $n = M$, $a_k = P(\mathbf{Y}(\alpha) \mid \mathbf{X}(\alpha) = s_k)$ and $b_k = P(\mathbf{X}(\alpha) = s_k)$. We notice that since all symbols are equiprobable, based on the uniform distribution of the input bits, $b_k - b_{k+1} = 0$. Furthermore, we have $S_0 = \sum_{n=1}^0 a_n = 0$, such that the summation by parts formula reduces to

$$\begin{aligned} & \sum_{\chi=1}^M P(\mathbf{Y}(\alpha) \mid \mathbf{X}(\alpha) = s_\chi) \cdot P(\mathbf{X}(\alpha) = s_\chi) \\ &= P(\mathbf{X}(\alpha) = s_M) \sum_{\chi=1}^M P(\mathbf{Y}(\alpha) \mid \mathbf{X}(\alpha) = s_\chi) \end{aligned} \quad (\text{E.4})$$

We then note

$$\begin{aligned} P(\mathbf{X}(\alpha) = s_M) &= P(\text{Active}) \cdot P(s_M) \\ &= \frac{k}{L} \cdot \frac{1}{M} \end{aligned} \quad (\text{E.5})$$

such that Equation E.2 may finally be written

$$\begin{aligned} \sum_{\chi=1}^M P(\mathbf{X}(\alpha) = s_\chi | \mathbf{Y}(\alpha)) \\ = \left(\frac{k}{ML} \right) \sum_{\chi=1}^M \frac{P(\mathbf{Y}(\alpha) | \mathbf{X}(\alpha) = s_\chi)}{P(\mathbf{Y}(\alpha))} \end{aligned} \quad (\text{E.6})$$

Equally, applying Bayes law to the denominator yields the equivalent expression

$$\begin{aligned} P(\mathbf{X}(\alpha) = 0 | \mathbf{Y}(\alpha)) \\ = \frac{P(\mathbf{Y}(\alpha) | \mathbf{X}(\alpha) = 0) \cdot P(\mathbf{X}(\alpha) = 0)}{P(\mathbf{Y}(\alpha))} \\ = \left(\frac{L-k}{L} \right) \frac{P(\mathbf{Y}(\alpha) | \mathbf{X}(\alpha) = 0)}{P(\mathbf{Y}(\alpha))} \end{aligned} \quad (\text{E.7})$$

Now, substituting Equation E.7 and Equation E.6 back into Equation E.1 yields

$$\lambda_\alpha = \ln \left(\frac{\frac{k}{ML} \cdot \sum_{\chi=1}^M P(\mathbf{Y}(\alpha) | \mathbf{X}(\alpha) = s_\chi)}{\frac{L-k}{L} \cdot P(\mathbf{Y}(\alpha) | \mathbf{X}(\alpha) = 0)} \right) \quad (\text{E.8})$$

which, utilising the laws of logarithms may be written

$$\begin{aligned} \lambda_\alpha = \ln \left(\frac{k}{M(L-k)} \right) + \ln \left(\sum_{\chi=1}^M P(\mathbf{Y}(\alpha) | \mathbf{X}(\alpha) = s_\chi) \right) - \\ \ln \left(P(\mathbf{Y}(\alpha) | \mathbf{X}(\alpha) = 0) \right) \end{aligned} \quad (\text{E.9})$$

Now, given generally that

$$P(\mathbf{Y}(\alpha) | \mathbf{X}(\alpha) = s_\chi) = \exp \left(-\frac{1}{N_{0,F}} |\mathbf{Y}(\alpha) - \mathbf{H}(\alpha)s_\chi|^2 \right) \quad (\text{E.10})$$

then

$$\ln \left(P(\mathbf{Y}(\alpha) | \mathbf{X}(\alpha) = 0) \right) = \ln \left(\exp \left(-\frac{1}{N_{0,F}} |\mathbf{Y}(\alpha)|^2 \right) \right) \quad (\text{E.11})$$

$$= -\frac{|\mathbf{Y}(\alpha)|^2}{N_{0,F}} \quad (\text{E.12})$$

where $N_{0,F}$ is the frequency domain noise power given by $N_{0,F} = N_0(k/L)$. Therefore, we may finally write

$$\lambda_\alpha = \ln \left(\frac{k}{L-k} \right) + \ln \left(\sum_{\chi=1}^M \exp \left(-\frac{1}{N_{0,F}} |\mathbf{Y}(\alpha) - \mathbf{H}(\alpha)s_\chi|^2 \right) \right) + \frac{|\mathbf{Y}(\alpha)|^2}{N_{0,F}} \quad (\text{E.13})$$

Also of note, the $\ln \left(\sum_{\chi=1}^M \exp \left(-\frac{1}{N_{0,F}} |\mathbf{Y}(\alpha) - \mathbf{H}(\alpha)s_\chi|^2 \right) \right)$ term of Equation 4.9 is susceptible to arithmetic overflow as a result of summing many exponential terms. This becomes a particular problem when simulating high values of E_b/N_0 , leading to incorrect results. To overcome this, we employ the Jacobian logarithm [35, 36], also known as the ‘log-sum-exp’ expression. We begin by letting $\gamma_\chi = -\frac{1}{N_{0,F}} |\mathbf{Y}(\alpha) - \mathbf{H}(\alpha)s_\chi|^2$ for $\chi = 1, 2, \dots, M$, and then defining

$$f_{max}(\gamma_1, \gamma_2) = \ln(e^{\gamma_1} + e^{\gamma_2}) = \max\{\gamma_1, \gamma_2\} + \ln(1 + e^{-|\gamma_1 - \gamma_2|}) \quad (\text{E.14})$$

Then given that $\Delta_1 = \ln(e^{\gamma_1} + e^{\gamma_2} + \dots + e^{\gamma_{M-1}})$ we may write

$$\begin{aligned} \Delta_0 &= \ln(e^{\gamma_1} + e^{\gamma_2} + \dots + e^{\gamma_M}) \\ &= \ln(e^{\Delta_1} + e^{\gamma_M}) \\ &= \max\{\Delta_1, \gamma_M\} + \ln(1 + e^{-|\gamma_M - \Delta_1|}) \\ &= \max\{\Delta_1, \gamma_M\} + f(|\Delta_1 - \gamma_M|) \end{aligned} \quad (\text{E.15})$$

We can iteratively apply this procedure, forming a new expression for Δ_1 in terms of $\Delta_2 = \ln(e^{\gamma_1} + e^{\gamma_2} + \dots + e^{\gamma_{M-2}})$ and so on up to $\Delta_{M-1} = \ln(e^{\gamma_1}) = \gamma_1$ yielding the identity

$$\begin{aligned} \ln(e^{\gamma_1} + e^{\gamma_2} + \dots + e^{\gamma_M}) &= \\ f_{max}(f_{max}(\dots f_{max}(f_{max}(\gamma_1, \gamma_2), \gamma_3), \dots), \gamma_M) \end{aligned} \quad (\text{E.16})$$

This identity, iteratively computed using algorithm 1 [30], can then be used to calculate a value for the Log-Sum-Exp term of Equation 4.9 free from arithmetic overflow.

Algorithm 1 Algorithm for iteratively calculating Log-Sum-Exp terms free from arithmetic overflow.

Require: \mathbf{Y} is the fourier transform of the received symbol vector, \mathbf{y} , and \mathbf{H} is the CFR. $s_i \in \mathcal{M}$.

Ensure: $\gamma_1 = \ln \left(\sum_{\chi=1}^M \exp \left(-\frac{1}{N_{0,F}} |\mathbf{Y}(\alpha) - \mathbf{H}(\alpha)s_\chi|^2 \right) \right)$

- 1: $\gamma_1 = -\frac{1}{N_{0,F}} |\mathbf{Y}(\alpha) - \mathbf{H}(\alpha)s_0|^2$
 - 2: **for** ($i = 2$; $i < M$; $i + +$) **do**
 - 3: $\gamma_2 = -\frac{1}{N_{0,F}} |\mathbf{Y}(\alpha) - \mathbf{H}(\alpha)s_i|^2$
 - 4: $LSE = \max\{\gamma_1, \gamma_2\} + \log(1 + e^{(-|\gamma_1 - \gamma_2|)})$
 - 5: $\gamma_1 = LSE$
 - 6: **end for**
-

F | GSIM-OFDM Subcarrier Mapping Policy

[26] presents two methods of mapping the set of length $\lfloor \log_2(C_k^L) \rfloor$ index bit-vectors to a set of activation indices, \mathcal{I} , of which we shall present the ‘combinadics’ approach. Combinadics [37] is a number system which provides a one-to-one mapping of the

Index bits	Z	$\mathbf{I}_g = \mathbf{J} + 1$	Sub-block
[0, 0, 0, 0, 0, 0]	0	[1, 2, 3, 4]	$[s_1, s_2, s_3, s_4, 0, 0, 0, 0]$
[0, 0, 0, 0, 0, 1]	1	[1, 2, 4, 5]	$[s_1, s_2, 0, s_3, s_4, 0, 0, 0]$
\vdots	\vdots	\vdots	\vdots
[1, 0, 1, 1, 0, 1]	45	[1, 2, 6, 8]	$[s_1, s_2, 0, 0, 0, s_3, 0, s_4]$
\vdots	\vdots	\vdots	\vdots
[1, 1, 1, 1, 1, 0]	63	[3, 5, 7, 8]	$[0, 0, s_1, 0, s_2, 0, s_3, s_4]$
[1, 1, 1, 1, 1, 1]	63	[4, 5, 7, 8]	$[0, 0, 0, s_1, s_2, 0, s_3, s_4]$

Table F.1: The first 64 entries into the index-mapping LUT generated for $\{L, k\} = \{8, 4\}$ using algorithm 2.

natural numbers to a strictly decreasing sequence $\mathbf{J} = \{c_k, \dots, c_1\}$ where $c_k > \dots > c_1 \geq 0$, such that each Z can be constructed from the corresponding \mathbf{J} as

$$Z = \sum_{i=1}^k C_i^{c_i} \quad (\text{F.1})$$

provided that we chose c_i correctly, and we assume $C_k^n = 0$ when $k > n$. Algorithm 2 describes a process which uses a combinadics approach to generate a LUT such as Table F.1 which maps integers in the range $[0, C_k^L - 1]$ to activation patterns, \mathbf{I}_g containing unique elements in the range $[1, L]$. For each sub-block the activation pattern can therefore be deduced by converting the p_1 index bits to an integer and subjecting them to the aforementioned LUT.

At the receiver, the index-mapping LUT is used in reverse. After deducing the active subcarriers, we thus obtain $\hat{\mathbf{I}}_g$ which we subject to a reverse LUT search on,

Algorithm 2 Algorithm for determining the index mapping table utilising a combinatorics approach

Require: k is number of the active subcarriers per sub-block, L is the number of subcarriers per sub-block, \mathbf{I} is a length k vector which begins empty.

Ensure: \mathbf{M} is a LUT which maps integers in the range 0 to C_k^L to a unique set of k decreasing integers in the range $[1, L]$

```

1: for  $j = 0; j < C_k^L - 1; j++ \text{ do}$ 
2:    $x = j;$ 
3:    $t = k;$ 
4:   for  $i = 1; i < k; i++ \text{ do}$ 
5:      $n = 0;$ 
6:     while  $C_t^n \leq x \text{ do}$ 
7:        $n = n + 1;$ 
8:     end while
9:      $\mathbf{I}(i) = n + 1;$ 
10:     $x = x - C_t^n;$ 
11:     $t = t - 1;$ 
12:  end for
13:   $\mathbf{M}(j) = \mathbf{I};$ 
14: end for

```

for example Table F.1, generating the corresponding \hat{Z} . We can then deduce the index, $\hat{\mathbf{b}}_g^{(1)}$, by converting \hat{Z} into binary. The dynamic nature of this method enables simulation of different block lengths more easily, which is preferable when comparing schemes.

G | LLR Error Correction Algorithm

We noted in section 4.1.1.2 that upon calculation of the L LLR values for a given sub-block, we chose those that are positive as the active subcarrier indices. In some cases however the number of positive LLRs, \hat{k} may be greater than k . This will lead to multiple errors; first, the reverse look-up table operation will fail since $\hat{\mathbf{I}}_g$ is the wrong length, and second, the decoded bits per sub-block would be greater than at the transmitter, which will offset the subsequent sub-blocks leading to a propagation of bit errors.

As an example suppose there are $L = 8$ subcarrier per sub-block, of which $k = 4$ are supposedly active. Then suppose we carry out LLR detection to produce the following vector of LLR values for the g th sub-block

$$\boldsymbol{\lambda}_g = [0.59, -2.04, -3.74, 1.78, -0.65, 1.70, 2.97, 2.61] \quad (\text{G.1})$$

We can see the active indices would be detected as $\hat{\mathbf{I}}_g = [1, 4, 6, 7, 8]$ which has length $5 > k = 4$. The natural way to resolve this is to flip the sign of the LLR which the lowest value greater than zero, in this case 0.5931 at index $\hat{\mathbf{I}}_g(1)$ to yield a new $\hat{\mathbf{I}}_g = [4, 6, 7, 8]$. Naturally, if this does not produce a valid index pattern (which can be checked by subjecting the new to a reverse search on the index-mapping LUT) then we can proceed by resetting $\hat{\mathbf{I}}_g$ and flipping the sign of the second smallest LLR greater than zero, i.e. $\hat{\mathbf{I}}_g(6)$, which yields $\hat{\mathbf{I}}_g = [1, 4, 7, 8]$. This is repeated until either a valid pattern is found, or all negative LLRs have been subjected tested, in which case the activation pattern can be chosen randomly.

Extending this notion further we may consider the cases where \hat{k} is greater than k by more than one. I.e., consider again a case with $\{L, k\} = \{8, 4\}$ and an LLR vector of

$$\boldsymbol{\lambda}_g = [0.59, -2.04, -3.74, 1.78, 0.65, 1.70, 2.97, 2.61] \quad (\text{G.2})$$

such that $\hat{\mathbf{I}}_g$ is detected as $\hat{\mathbf{I}}_g = [1, 4, 5, 6, 7, 8]$. This time we flip the two LLRs at a time, such that the first modified activation pattern is $\hat{\mathbf{I}}_g = [4, 6, 7, 8]$, flipping indices 1 and 4 as they are the positions of the least positive LLRs in Equation G.2. If this pattern is invalid, we would then try flipping the next two least positive LLRs yielding

the trial pattern $\hat{\mathbf{I}}_g = [1, 4, 7, 8]$. This is implemented by first sorting the indices of $\boldsymbol{\lambda}_g$ in ascending order of their corresponding LLR values, to create a vector $\boldsymbol{\omega}_g$. Then we construct a new vector, $\boldsymbol{\delta}_g^{(i)}$, for the i th iteration of the correction algorithm which has a 0 at the index where the LLR is negative and a 1 where the LLR is positive. For the case of Equation G.1 we'd have

$$\begin{aligned}\boldsymbol{\lambda}_g &= [-3.74 \quad -2.04 \quad -0.65 \quad 0.59 \quad 1.70 \quad 1.78 \quad 2.61 \quad 2.97] \\ \boldsymbol{\omega}_g &= [3 \quad 2 \quad 5 \quad 1 \quad 6 \quad 4 \quad 8 \quad 7] \\ \boldsymbol{\delta}_g^{(0)} &= [0 \quad 0 \quad 0 \quad 1 \quad 1 \quad 1 \quad 1 \quad 1]\end{aligned}\quad (\text{G.3})$$

On the i th iteration of the error correcting detection scheme we generate a new $\boldsymbol{\delta}_g^{(i)}$ from which we generate a new trial activation pattern, $\hat{\mathbf{I}}_g$, given by the non-zero elements of the vector formed from the element-wise multiplication of $\boldsymbol{\delta}_g^{(i)}$ and $\boldsymbol{\omega}_g$. The detection method can be represented by the state progression of $\boldsymbol{\omega}_g$, which for the case of Equation G.1 would be

$$\begin{array}{cccccc}[00001111] & \rightarrow & [0010111] & \rightarrow & [00011011] & \rightarrow [00011101] & \rightarrow [00011110] \\ \boldsymbol{\delta}_g^{(1)} & & \boldsymbol{\delta}_g^{(2)} & & \boldsymbol{\delta}_g^{(3)} & & \boldsymbol{\delta}_g^{(4)} & & \boldsymbol{\delta}_g^{(5)}\end{array}\quad (\text{G.4})$$

The algorithm is concluded when we have either found an index pattern which is valid or all possible valid combinations have been tried in which case we choose a random, valid, index pattern.

In terms of implementation, if we write $\boldsymbol{\delta}_g^{(0)}$ generally as

$$\boldsymbol{\delta}_g^{(0)} = [0, 0, \dots, 0, 1, 1, \dots, 1] \quad (\text{G.5})$$

then we may define n_0 and n_1 as the number of zeros and number of ones in $\boldsymbol{\delta}_g^{(0)}$ respectively. Equally, let n_e be the number of errors per sub-block given by $n_e = n_1 - k$. If we overestimate the number of active subcarriers, $n_e > 0$, whereas if we underestimate, $n_e < 0$. Thus, on the i th iteration of the error correction loop if $n_e > 0$ we flip the indices from index $n_0 + i + 1$ up to index $n_0 + |n_e| + i$ of $\boldsymbol{\delta}_g^{(0)}$ to produce $\boldsymbol{\delta}_g^{(i)}$. Otherwise, if $n_e < 0$ we flip the indices from index $L - n_1 - i$ down to index $L - n_1 - |n_e| - i + 1$ of $\boldsymbol{\delta}_g^{(0)}$ to produce $\boldsymbol{\delta}_g^{(i)}$ (assuming a base index of 1, as is the case in MATLAB).

H | EGSIM-OFDM Subcarrier Mapping Policy

Modulation begins by choosing the set \mathbf{K} , for example $\mathbf{K} = \{1, 3, 5\}$. We then a modulation scheme, in this example we shall use BPSK, and sub-block length, $L = 8$. From this we use Equation 4.15 to deduce the number of bits per sub-block

$$p = \lfloor \log_2 (2^1 \cdot C(8, 1) + 2^3 \cdot C(8, 3) + 2^5 \cdot C(8, 5)) \rfloor \quad (\text{H.1})$$

$$= 11 \quad [\text{bits}/\text{sub-block}] \quad (\text{H.2})$$

Our first goal is to subdivide the set of 11-bit input vectors into three groups, to which we can assign a value of $k_r \in \mathbf{K}$ to each. Once achieved, we can set $p_2 = k_r \log_2(M)$, for $r = 1, 2, \dots, R$, following from the fact there are $\log_2(M)$ bits per activated subcarrier. In doing so, each 11-bit input vector considered will map to a value of p_2 , from which we can deduce the number of index bits, p_1 using $p_1 = p - p_2$.

In general, for each k_r active subcarriers, a constellation of order M and a sub-block of length L , then there are $M^{k_1} C_{k_1}^L$ possible permutations of the sub-block. Therefore, if we let Z_p be the p -bit input bit vector in base-10 then the general mapping of $Z_p \rightarrow p_2$ is as follows

$$p_2 = \begin{cases} k_1 \log_2(M), & Z_p \in [0, M^{k_1} C_{k_1}^L - 1] \\ k_2 \log_2(M), & Z_p \in [M^{k_1} C_{k_1}^L, \sum_{i=1}^2 M^{k_i} C_{k_i}^L - 1] \\ \vdots & \vdots \\ k_R \log_2(M), & Z_p \in [\sum_{i=1}^{R-1} M^{k_i} C_{k_i}^L, \sum_{i=1}^R M^{k_i} C_{k_i}^L - 1] \end{cases} \quad (\text{H.3})$$

For example, when $p = 11$ as before, then $0 \leq Z_p \leq 2^{11} - 1 = 2047$, and the corresponding mapping is shown in Equation H.4.

$$p_2 = \begin{cases} 1, & Z_p \in [0, 15] \\ 3, & Z_p \in [16, 463] \\ 5, & Z_p \in [464, 2047] \end{cases} \quad (\text{H.4})$$

To deduce p_2 we simply convert the p input bits to a decimal and subject the result to Equation H.4. In the GSIM-OFDM case, we would then submit the p_1

index bits of each sub-block to the index-mapping LUT, however this requires more consideration for EGSIM-OFDM. This is because the index-mapping LUT used will change depending on the sub-block's value of k_r . Furthermore, as we can observe in Table H.2, the p_1 index bits of the input may not start from zero. When $Z_p \in [16, 463]$ the p_1 index bits start from $00000010_2 = 2_{10}$ which is not suitable for the combinadics approach presented in section 4.1.1 which assumes the input bits start from 0 and monotonically increase. To overcome this, we shall not change the combinadics algorithm, such that for each sub-block with k_r active carriers, an index-mapping LUT with $C_{k_r}^L$ entries will be created; Instead we shall create a mapping scheme which maps each Z_p to a value $Z'_p \in [0, C_{k_r}^L - 1]$ which is the legitimate value to subject to the index-mapping LUT.

Z_p	p_1 bits	p_2 bits
0	0000000000*	0
1	0000000000	1
2	0000000001	0
\vdots	\vdots	\vdots
14	000000111	0
15	000000111	1

Z_p	p_1 bits	p_2 bits
16	00000010*	000
17	00000010	001
18	00000010	010
\vdots	\vdots	\vdots
462	00111001	110
463	00111001	111

Table H.1: Bit mappings for $Z_p = [0, 15]$. Table H.2: Bit mappings for $Z_p = [16, 463]$.

$$*Z_p^1 = 0$$

$$*Z_p^2 = 16$$

This is achieved by first observing H.1 and H.2 and noticing that in addition to the offset of each table we also see a repetition of the p_1 index bits. In general, the length of number of repetitions is 2^{p_2} which is 1 for Table H.1 and 8 for Table H.2. Despite belonging to a unique Z_p , each of these repeated length p_1 bit vectors should map to the same activation pattern, such that the resulting sub-block is distinguished only by the data it modulates. From these considerations, we first define Z_p^r as

$$Z_p^r = \begin{cases} 0 & \text{when } r = 1 \\ M_{r-1}^k C_{k_{r-1}}^L & \text{otherwise} \end{cases} \quad (\text{H.5})$$

which for $K = \{1, 3, 5\}$ yields $Z_p^r = \{0, 16, 464\}$, which is the offset value of the tables (the table for $k_r = 5$ has been excluded here for brevity). Subsequently, the value which is subject to the index-mapping LUT, Z'_p is given by

$$Z'_p = Z_{p_1} - (Z_p^r \gg k_r) \quad (\text{H.6})$$

where Z_{p_1} is the p_1 index bits of input bit vector, $b_g^{(1)}$, as an integer, and (\gg) denotes the logical right shift operation. For example, consider the input $Z_p = 18$, which would get mapped to $k_2 = 3$. From Table H.2 we see that $Z_p^2 = 16$ and $Z_{p_1} = 00000010_2 = 2_{10}$, therefore Z'_p is given by $Z'_p = 2 - (16 \gg 3) = 0$. At the other

extreme consider $Z_p = 463$, which is also mapped to $k_2 = 3$. Again $Z_p^2 = 16$ but now $Z_{p1} = 00111001_2 = 25_{10}$, therefore Z'_p is given by $Z'_p = 57 - (16 \gg 3) = 55$. This is exactly equal to $C_3^8 - 1$ which is the maximum input value which the index-mapping LUT corresponding to $k_2 = 3$ would cover, as expected.

One final consequence of this approach is that when considering the mapping for $k_3 = 5$, there are $2^5 C_5^8 = 1792$ permutations of the activated subcarriers and data symbols. However, there are only $1048 - 448 - 16 = 1584$ bit vectors remaining to map. This means there are $1792 - 1584 = 208$ unused permutations, which represents a slight inefficiency in the approach.

I | Single Mode IM-OFDM Complexity Comparison

Scheme	BPSK	QPSK	QAM-16	QAM-64
SIM-OFDM (LLR+OTE)	$\mathcal{O}(192)$	$\mathcal{O}(320)$	$\mathcal{O}(1088)$	$\mathcal{O}(4160)$
SIM-OFDM (LLR+ML)	$\mathcal{O}(4.29 \times 10^9)$	$\mathcal{O}(1.84 \times 10^{19})$	$\mathcal{O}(8.51 \times 10^{37})$	$\mathcal{O}(6.28 \times 10^{57})$
ESIM-OFDM (Threshold)	$\mathcal{O}(128)$	$\mathcal{O}(128)$	$\mathcal{O}(128)$	$\mathcal{O}(128)$
ESIM-OFDM (LLR+OTE)	$\mathcal{O}(192)$	$\mathcal{O}(320)$	$\mathcal{O}(1088)$	$\mathcal{O}(4160)$
ESIM-OFDM (LLR+ML)	$\mathcal{O}(192)$	$\mathcal{O}(384)$	$\mathcal{O}(1536)$	$\mathcal{O}(6144)$
GSIM-OFDM (ML)	$\mathcal{O}(8192)$	$\mathcal{O}(131072)$	$\mathcal{O}(33554432)$	$\mathcal{O}(8.59 \times 10^9)$
GSIM-OFDM (LLR+OTE)	$\mathcal{O}(192)$	$\mathcal{O}(320)$	$\mathcal{O}(1088)$	$\mathcal{O}(4160)$
GSIM-OFDM (LLR+ML)	$\mathcal{O}(192)$	$\mathcal{O}(2176)$	$\mathcal{O}(524800)$	$\mathcal{O}(1.34 \times 10^8)$
EGSIM- OFDM (ML)	$\mathcal{O}(21504)$	$\mathcal{O}(559104)$	$\mathcal{O}(5.39 \times 10^8)$	$\mathcal{O}(5.50 \times 10^{11})$
EGSIM- OFDM (LLR+ML)	$\mathcal{O}(840)$	$\mathcal{O}(9624)$	$\mathcal{O}(8424696)$	$\mathcal{O}(8.59 \times 10^9)$

Table I.1: Complexity comparison of the LLR, ML and threshold detectors for various IM-OFDM schemes with $N = 64$. In the case of SIM-OFDM above we show results for $\{L, k\} = \{64, 32\}$.

J | DM-OFDM LLR Closed Form Derivation

We denote the LLR of each subcarrier, λ_α , for $\alpha = 1, 2, \dots, N$, as the natural logarithm ratio of the posterior probability that a given frequency domain symbol is either from \mathcal{M}_A or \mathcal{M}_B , i.e.

$$\lambda_\alpha = \ln \left(\frac{\sum_{j=1}^{M_A} P(\mathbf{X}(\alpha) = s_A^{(j)} | \mathbf{Y}(\alpha))}{\sum_{i=1}^{M_B} P(\mathbf{X}(\alpha) = s_B^{(i)} | \mathbf{Y}(\alpha))} \right) \quad (\text{J.1})$$

where $s_A^{(j)} \in \mathcal{M}_A$ and $s_B^{(i)} \in \mathcal{M}_B$. If we then consider Bayes' theorem which states $P(A|B) = P(B|A) \cdot P(A)/P(B)$, then the numerator Equation J.1 may be written as

$$\begin{aligned} & \sum_{j=1}^{M_A} P(\mathbf{X}(\alpha) = s_A^{(j)} | \mathbf{Y}(\alpha)) \\ &= \sum_{j=1}^{M_A} \frac{P(\mathbf{Y}(\alpha) | \mathbf{X}(\alpha) = s_A^{(j)}) \cdot P(\mathbf{X}(\alpha) = s_A^{(j)})}{P(\mathbf{Y}(\alpha))} \end{aligned} \quad (\text{J.2})$$

The numerator of Equation J.2 may be expanded using the summation by parts formula [34] which states

$$\sum_{k=m}^n a_k b_k = [S_n b_n - S_{m-1} b_m] + \sum_{k=m}^{n-1} [S_k (b_k - b_{k+1})] \quad (\text{J.3})$$

where $S_N = \sum_{n=1}^N a_n$. In our case, $m = 1$, $n = M_A$, $a_k = P(\mathbf{Y}(\alpha) | \mathbf{X}(\alpha) = s_A^{(k)})$ and $b_k = P(\mathbf{X}(\alpha) = s_A^{(k)})$. We notice that since all symbols are equiprobable, based on the uniform distribution of the input bits, $b_k - b_{k+1} = 0$. Furthermore, we have $S_0 = \sum_{n=1}^0 a_n = 0$, such that the summation by parts formula reduces to

$$\begin{aligned} & \sum_{j=1}^{M_A} P(\mathbf{Y}(\alpha) | \mathbf{X}(\alpha) = s_A^{(j)}) \cdot P(\mathbf{X}(\alpha) = s_A^{(j)}) \\ &= P(\mathbf{X}(\alpha) = s_A^{(M_A)}) \sum_{j=1}^{M_A} P(\mathbf{Y}(\alpha) | \mathbf{X}(\alpha) = s_A^{(j)}) \end{aligned} \quad (\text{J.4})$$

We then note

$$\begin{aligned} P(\mathbf{X}(\alpha) = s_A^{(M_A)}) &= P(\text{Active}) \cdot P(s_A^{(M_A)}) \\ &= \frac{k}{L} \cdot \frac{1}{M_A} \end{aligned} \quad (\text{J.5})$$

such that Equation E.2 may finally be written

$$\begin{aligned} \sum_{j=1}^{M_A} P(\mathbf{X}(\alpha) = s_A^{(j)} | \mathbf{Y}(\alpha)) \\ = \left(\frac{k}{M_A L} \right) \sum_{j=1}^{M_A} \frac{P(\mathbf{Y}(\alpha) | \mathbf{X}(\alpha) = s_A^{(j)})}{P(\mathbf{Y}(\alpha))} \end{aligned} \quad (\text{J.6})$$

Equally, applying Bayes law to the denominator yields the equivalent expression

$$\begin{aligned} \sum_{i=1}^{M_B} P(\mathbf{X}(\alpha) = s_B^{(i)} | \mathbf{Y}(\alpha)) \\ = \left(\frac{L-k}{M_B L} \right) \sum_{i=1}^{M_B} \frac{P(\mathbf{Y}(\alpha) | \mathbf{X}(\alpha) = s_B^{(i)})}{P(\mathbf{Y}(\alpha))} \end{aligned} \quad (\text{J.7})$$

Now, substituting Equation J.7 and Equation J.6 back into Equation J.1 yields

$$\lambda_\alpha = \ln \left(\frac{\frac{k}{M_A L} \cdot \sum_{j=1}^{M_A} P(\mathbf{Y}(\alpha) | \mathbf{X}(\alpha) = s_A^{(j)})}{\frac{L-k}{M_B L} \cdot \sum_{i=1}^{M_B} P(\mathbf{Y}(\alpha) | \mathbf{X}(\alpha) = s_B^{(i)})} \right) \quad (\text{J.8})$$

which, utilising the laws of logarithms may be written

$$\begin{aligned} \lambda_\alpha = \ln \left(\frac{M_B k}{M_A (L-k)} \right) + \ln \left(\sum_{j=1}^{M_A} P(\mathbf{Y}(\alpha) | \mathbf{X}(\alpha) = s_A^{(j)}) \right) - \\ \ln \left(\sum_{i=1}^{M_B} P(\mathbf{Y}(\alpha) | \mathbf{X}(\alpha) = s_B^{(i)}) \right) \end{aligned} \quad (\text{J.9})$$

Now, given generally that

$$P(\mathbf{Y}(\alpha) | \mathbf{X}(\alpha) = s_\chi) = \exp \left(-\frac{1}{N_{0,F}} |\mathbf{Y}(\alpha) - \mathbf{H}(\alpha)s_\chi|^2 \right) \quad (\text{J.10})$$

where $N_{0,F}$ is the frequency domain noise power, then we may finally write a close form for Equation J.1

$$\begin{aligned} \lambda_\alpha = \ln \left(\frac{M_B k}{M_A (L-k)} \right) + \ln \left(\sum_{j=1}^{M_A} \exp \left(-\frac{1}{N_{0,F}} |\mathbf{Y}(\alpha) - \mathbf{H}(\alpha)s_A(j)|^2 \right) \right) - \\ \ln \left(\sum_{i=1}^{M_B} \exp \left(-\frac{1}{N_{0,F}} |\mathbf{Y}(\alpha) - \mathbf{H}(\alpha)s_B(i)|^2 \right) \right) \end{aligned} \quad (\text{J.11})$$

K | Complexity Analysis

Here we shall derive an (order of magnitude) metric for the feasible number of computations per OFDM symbol for real time use. We shall begin by assuming that for ‘real-time’ computation, the processor must be able to perform the desired number of multiplications to achieve a bit-rate of $f_b = 20 \times 10^6$. Furthermore, we shall assume a mobile setting, utilising the most advanced processor commercially available, the Snapdragon 888, which has a clock frequency, f_{clk} on the order of 2.5GHz [38]. Furthermore we shall assume that one n -bit complex multiplication is comprised of 4 real n -bit multiplications, which requires $2n$ clock-cycles to compute (which are done in parallel), and two $2n$ -bit additions, which also require $2n$ clock-cycles to compute [39] (but can also be done in parallel). Furthermore, we shall assume 64-bit arithmetic (such that $n = 64$), which aligns with modern mobile operating systems, and an OFDM symbol length of 64 subcarriers, as this aligns with the simulations presented in this report.

Based on these assumptions, given that there are $N = 2n + 2n$ clock cycles per complex multiplication, then the number of complex multiplications which can be computed per second, f_m , is given by

$$\begin{aligned} f_m &= \frac{f_{clk}}{N} \\ &= \frac{2.5 \times 10^9}{2 \cdot 64 + 2 \cdot 64} \\ &\approx 9.8 \times 10^6 \quad [\text{complex multiplications/second}] \end{aligned} \tag{K.1}$$

We can proceed by defining the symbol rate, f_s , in terms of the number of complex multiplications per OFDM symbol, C , and f_m , i.e.

$$\begin{aligned} f_s &= \frac{f_m}{C} \\ &= \frac{9.8 \times 10^6}{C} \quad [\text{symbols/second}] \end{aligned} \tag{K.2}$$

Now recalling we assumed a desirable bit-rate, f_b , of 20×10^6 bits per second, and an OFDM symbol length of 64 subcarriers, then the bits per OFDM symbol is $64M$, where M is the constellation order. Therefore, the desired symbol rate

is $f_s = (20 \times 10^6)/(64M) \approx (3.1 \times 10^5)/M$. Substituting this into Equation K.2 yields

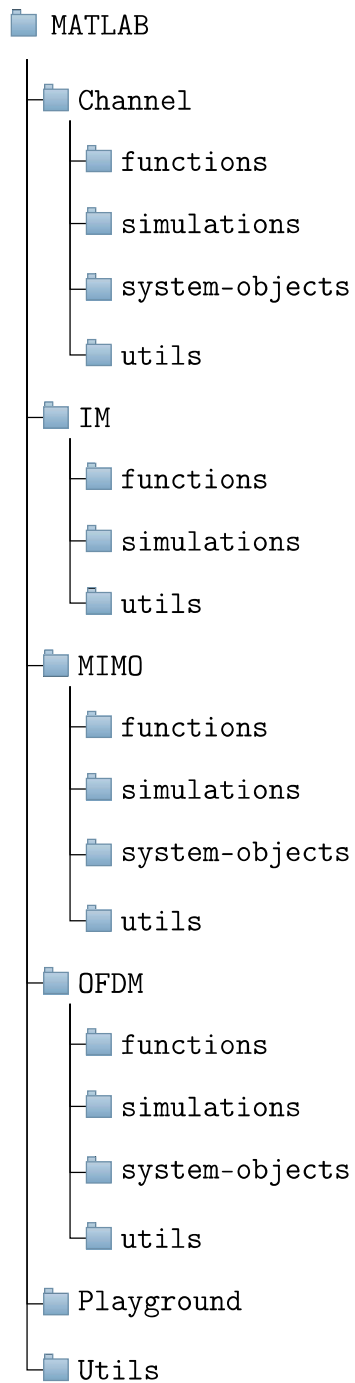
$$\frac{3.1 \times 10^5}{M} = \frac{9.8e6}{C} \quad (\text{K.3})$$

which we can re-arrange to give

$$\begin{aligned} C &= \frac{M \cdot 9.8 \times 10^6}{3.1 \times 10^5} \\ &\approx 32M \end{aligned} \quad (\text{K.4})$$

Therefore, for $M = \{2, 4, 16, 64\}$ the worst case limit in complexity is given by $C = \{64, 128, 512, 2048\}$ complex multiplications per symbol respectively.

L | Project Directory Structure



The project code directory is subdivided into folders `Channel`, `IM`, `MIMO` and `OFDM`, each of which contain sub-folders `functions`, `simulations`, `utils` and in some cases `system-objects`. Each of these sub-folders are code directories. The `function` directories contain functions which are used directly in the main simulation files located in the `simulations` folders. This includes function which carry out modulation, apply the channel, carry out the index-mapping process or calculate the log-likelihood-ratio for LLR detection. The `simulations` folders contain the main simulation scripts which can be executed to produce a numerical result, such as a BER vs. E_b/N_0 curve. The `system-objects` folders, where present, contain class-like constructs for objects used frequently throughout the project, such as the OFDM modulator and demodulator. These were implemented using MATLAB's system object types which can be used to module a simulation loop programmatically. This was an idea explored early on in the project, however a functional approach was favoured in the latter stages. Finally, the `utils` folder contains functions which aren't used directly in a simulation, such as those functions to compute a specific value, or implement an equation which is used frequently.

Additionally, the `Playground` folder in the parent director contains a set of MATLAB scripts, which were considered blank canvases for testing out ideas and running small simulations which I felt did not require their own file. Furthermore, the `Utils` folder in the parent directory contains utility functions used across all simulations, such as functions for reading and writing simulation results to excel files.

M | Risk Assessment & Project Brief

The risk factors outlined in Table M.1 are each listed in terms of a likelihood, which denotes the probability that the event will occur, and severity, which denotes the impact on the project if the described risk were to occur (without mitigation), on a scale of 1 to 10.

Risk	Likelihood	Severity	Resolution
Loss of code/diagrams due to file corruption or accidental deletion	2	8	This project utilised the university's GitLab service as a code repository which ensured there exists back-ups of the code base which can be easily reverted to in case of an error.
Loss of code/diagrams due to incorrect use of GitLab	3	6	At regular monthly intervals the code base will be manually duplicated to a folder on my local device.
Loss of project report documents due to file corruption or accidental deletion	2	8	The project report is written using Overleaf which automatically backs up your documents to the cloud.
Loss of functionality of local device due to damage, or loss of property	3	9	With the code base being synchronised to GitLab, and project notes written on Overleaf an external university computer could be used to complete the rest of the project

Table M.1: Project Risk Assessment

Jonah Foley

Implementation, Evaluation and Simulation of OFDM for Dual-Mode Index Modulated Systems in Multi-Path Fading Channels

Supervised by Prof. Sheng Chen

Problem

Due to the presence of reflective surfaces within a wireless channel, transmitted signals can travel multiple paths towards a receiver. As a result, the receiver experiences the superposition of multiple copies of the transmitted symbol. Due to the differing path lengths and variations in surface material, each copy of the transmitted signal may have a different amplitude, phase, and delay. This presents the possibility of both constructive and destructive interference at the receiver which may lead to the incorrect detection of the transmitted symbols due to severe drops in signal-to-noise ratio.

In order to overcome the effects of a fading channel, signal diversity is used. By introducing diversity in time, frequency, and space, we can reduce the probability of a fade occurring by exploiting the fact that component channels within a diverse wireless link do not share common characteristics. In particular, this study investigates OFDM, a method which achieves frequency diversity through signal transmission on multiple carrier frequencies in order to combat frequency-selective fading. Going further, we will investigate index modulation as a technique for increasing data rates by exploiting physical properties of the transceiver. Finally, state-of-the-art dual-mode index modulation will be analysed as a technique for further enhancing throughput and increasing energy efficiency.

Goals

- Development and simulation of a model of a multi-path wireless channel with Additive-White-Gaussian-Noise.
- Modelling and simulation of an OFDM transmitter and receiver.
- Evaluation of the advantages and disadvantages of OFDM using appropriate simulation results.
- Implementation and simulation of techniques such as channel estimation and channel equalisation to combat the effects of fading.
- Theoretical analysis and simulation of standard and dual-mode index modulation aided OFDM.
- A discussion of the physical limitations and considerations for the implementation of index-modulation based solutions.

Scope

If we categorised development of communications systems into; (1) Theoretical analysis (2) Simulation (3) Hardware Implementation (Micro-controller/FPGA/Antenna) and (4) System Integration, this project will cover categories (1) and (2). Mathematical analysis will be used to provide a theoretical foundation of the techniques being used, while the MATLAB programming language will be used to produce quantitative graphs which provide a rigorous outline of the advantages and disadvantages of each technique.

The limiting factor in the effectiveness of this study will be the ability to accurately model a wireless channel as a result of the complexity of a realistic multi-path propagation environment. Therefore, statistical approximations will be utilised in order to minimise the computational complexity, but also there will be a diversity in the channel models used - each of which will provide a different view of the simulated system.